UNIVERSIDADE ESTADUAL PAULISTA
"JÚLIO DE MESQUITA FILHO"
Faculdade de Ciências Farmacêuticas - Câmpus de Araraquara
Programa de Pós-Graduação em Ciências Farmacêuticas

Estudo *in vitro* do potencial da piperina encapsulada em *metal-organic frameworks* e com modificação de superfície para o tratamento do câncer de mama

CHRISTIAN RAFAEL QUIJIA QUEZADA

Araraquara-SP

2023

UNIVERSIDADE ESTADUAL PAULISTA
"JÚLIO DE MESQUITA FILHO"
Faculdade de Ciências Farmacêuticas - Câmpus de Araraquara
Programa de Pós-Graduação em Ciências Farmacêuticas

Estudo *in vitro* do potencial da piperina encapsulada em *metal-organic frameworks* e com modificação de superfície para o tratamento do câncer de mama

CHRISTIAN RAFAEL QUIJIA QUEZADA

Tese apresentada ao Programa de Pós-Graduação em Ciências Farmacêuticas, Área de Pesquisa e Desenvolvimento de Medicamentos, para obtenção do título de Doutor em Ciências Farmacêuticas**.**

Orientador: Prof. Dr. Marlus Chorilli

Coorientadora: Profa. Dra. Regina Célia Galvão Frem

Araraquara-SP

2023

Quijia Quezada, Christian Rafael.

Q36e Estudo *in vitro* do potencial da piperina encapsulada em *metal-organic frameworks* e com modificação de superfície para o tratamento do câncer de mama / Christian Rafael Quijia Quezada. – Araraquara: [S.n.], 2023.

122 f. : il.

Tese (Doutorado) – Universidade Estadual Paulista. "Júlio de Mesquita Filho". Faculdade de Ciências Farmacêuticas. Programa de Pós Graduação em Ciências Farmacêuticas. Área de Pesquisa e Desenvolvimento de Fármacos e Medicamentos.

Orientador: Marlus Chorilli.
Coorientadora: Regina Célia Galvão Frem.

1. Câncer de mama. 2. *Metal-organic frameworks*. 3. MIL-100 (Fe). 4. Piperina. 5. Membrana celular. 6. Quitosana. I. Chorilli, Marlus, orient. II. Frem, Regina Célia Galvão, coorient. III. Título.

Diretoria do Serviço Técnico de Biblioteca e Documentação - Faculdade de Ciências Farmacêuticas
UNESP - Campus de Araraquara

CAPES: 33004030078P6
Esta ficha não pode ser modificada

UNIVERSIDADE ESTADUAL PAULISTA

Câmpus de Araraquara

CERTIFICADO DE APROVAÇÃO

TÍTULO DA TESE: Avaliação do potencial da piperina encapsulada em *metal-organic frameworks* e com modificação de superfície para o tratamento do câncer de mama

AUTOR: CHRISTIAN RAFAEL QUIJIA QUEZADA

ORIENTADOR: MARLUS CHORILLI

COORIENTADORA: REGINA CÉLIA GALVÃO FREM

Aprovado como parte das exigências para obtenção do Título de Doutor em Ciências, área: Pesquisa e Desenvolvimento de Fármacos e Medicamentos pela Comissão Examinadora:

Prof. Dr. MARLUS CHORILLI (Participaçao Virtual)
Departamento de Farmacos e Medicamentos / Faculdade de Ciencias Farmaceuticas do Campus de Araraquara da Unesp

Prof. Dr. SEVERINO ALVES JUNIOR (Participaçao Virtual)
Departamento de Química Fundamental / Centro de Ciências Exatas e da Natureza da Universidade Federal de Pernambuco

Prof. Dr. ADLEY ANTONINI NEVES DE LIMA (Participaçao Virtual)
Departamento de Farmácia / Centro de Ciências da Saúde da Universidade Federal do Rio Grande do Norte

Profa. Dra. RENATA VIDOR CONTRI (Participaçao Virtual)
Departamento de Produção de Matéria-Prima / Faculdade de Farmácia da Universidade Federal do Rio Grande do Sul

Profa. Dra. PATRICIA SEVERINO (Participaçao Virtual)
Centro de Ciências Biológicas e da Saúde / Universidade Tiradentes

Araraquara, 11 de julho de 2023

Impacto esperado: Os resultados desta tese podem levar a uma terapia mais eficaz e segura para o tratamento do câncer de mama, que é uma das principais causas de morte entre mulheres portadoras de câncer no mundo. A utilização de nanoestruturas como MOFs revestidos com membranas de macrófagos ou quitosana pode melhorar as propriedades biofarmacêuticas da piperina, reduzindo sua toxicidade e aumentando sua eficácia contra as células cancerígenas. Portanto, o benefício potencial desta pesquisa para a sociedade é a possibilidade de oferecer um tratamento mais eficaz e seguro para o câncer de mama, melhorando a qualidade de vida das mulheres afetadas por essa doença.

Expected impact: The results of this these can lead to a more effective and safer therapy for the treatment of breast cancer, which is one of the leading causes of cancer-related death among women worldwide. The use of nanostructures such as MOFs coated with macrophage membranes or chitosan can improve the bio-pharmaceutical properties of piperine, reducing its toxicity and increasing its effectiveness against cancerous cells. Therefore, the potential benefit of this research to society is the possibility of offering a more effective and safer treatment for breast cancer, improving the quality of life of women affected by this disease.

DEDICATÓRIA

A mis padres (Delfida Quezada Rodríguez y Miguel Quijia Gualoto) por todo su esfuerzo y mis hermanos en especial a Angela Quijia por siempre alentarme en mis sueños y objetivos.

AGRADECIMENTO

Inicialmente, gostaria de expressar minha gratidão à minha família e amigos, em particular, aos meus pais, por todo o amor e apoio incondicional que sempre me deram.

Também gostaria de agradecer ao grupo de MOFs do laboratório de Química-UNESP, em especial a Caroline e Renata, pelo valioso conhecimento científico em MOFs que compartilharam comigo. A todos do grupo, muito obrigado.

Do mesmo modo, gostaria de agradecer ao grupo de Farmacotecnia, especialmente a Kaio, Marcelle e Camila, e a todo o pessoal, pelo auxílio fundamental na realização dos ensaios de citotoxicidade. Sem a ajuda deles, esse trabalho não seria possível.

Sou grato aos técnicos que sempre me auxiliaram, em particular ao técnico Rafael Romano, por toda a paciência e rapidez nas análises.

Gostaria de reconhecer o apoio financeiro da Coordenação de Aperfeiçoamento de Pessoal de Nível Superior (CAPES) - Código de Financiamento 001

À Fundação de Amparo de Pesquisa do Estado de São Paulo (FAPESP) (Nº processo: 2018/21119-0) e Bolsa Estágio de Pesquisa no Exterior (BEPE) (Nº processo: 2021/07281-1) que concederam bolsas e suporte financeiro para este projeto.

Aos professores que fizeram parte da minha banca de qualificação do doutorado, agradeço por aceitarem participar e por compartilharem seus conhecimentos e experiências comigo.

Expresso minha gratidão ao meu orientador, professor Dr. Marlus Chorilli, por sua dedicação permanente e sugestões valiosas que foram fundamentais para o sucesso deste trabalho de investigação. Agradeço também sua amizade e respeito.

Por fim, gostaria de agradecer minha coorientadora de teses, a professora Regina Frem, do laboratório de MOFs, por todas as suas dicas científicas e por compartilhar seus vastos conhecimentos comigo. Sou grato e em dívida com ela por todas as inúmeras horas que passamos trabalhando juntos.

Ever tried. Ever failed. No matter. Try Again. Fail again. Fail better.

Samuel Beckett

RESUMO

O câncer de mama é uma das principais causas de morte entre mulheres com câncer em todo o mundo, levando à busca por tratamentos quimioterápicos mais eficazes. Entre os compostos com potencial quimioterapêutico, destaca-se a piperina (PIP), que demonstrou atividade antitumoral em linhagens de câncer de mama. No entanto, a utilização desse composto em estudos pré-clínicos tem sido limitada devido à sua toxicidade. Uma abordagem promissora para melhorar as propriedades biofarmacêuticas da piperina é o uso de redes metalo-orgânicas (MOFs), como o MIL-100 (Fe), como sistemas de liberação de fármacos. Além disso, a modificação de nanoestruturas com materiais naturais, como as membranas de macrófagos (MM) ou quitosana (QUI), pode proporcionar uma camuflagem contra o sistema imunitário, resistência à degradação e liberação controlada. Inspirado por esses avanços científicos e tecnológicos, este trabalho tem como objetivo avaliar o potencial da piperina encapsulada em MOFs revestidos com MM ou QUI para o tratamento do câncer de mama. Neste estudo, foram sintetizados com sucesso os nanosistemas baseados no MIL-100(Fe) contendo piperina revestida com MM (MM@PIP@MIL-100(Fe)) ou com QUI (QUI@PIP@MIL-100(Fe)) por meio de síntese hidrotermal assistida por micro-ondas e método de impregnação. As análises por difração de raios-X de MIL-100(Fe) e PIP@MIL-100(Fe) revelaram a cristalinidade dos materiais e tamanhos de partícula de 18,32 nm e 76,18 nm, respectivamente. A presença de proteínas na superfície das vesículas de MM@PIP@MIL-100(Fe) foi confirmada por eletroforese (SDS-PAGE), enquanto o revestimento de quitosana (QUI) no MOF foi sugerido por espectroscopia de infravermelho. A quantificação da piperina nos MOFs foi realizada por cromatografia líquida de alta eficiência (CLAE), mostrando uma eficiência de encapsulamento de 95 ± 3%. Os ensaios de citotoxicidade em células de câncer de mama, como MCF-7, SKBR3, MDA-MB-231 e BT549, utilizando os materiais PIP@MIL-100(Fe), MM@PIP@MIL-100(Fe) e QUI@PIP@MIL-100(Fe), revelaram um índice de citotoxicidade maior em comparação com a piperina livre, com uma concentração inibitória média (IC_{50}) entre duas e dezessete vezes maior. Em conclusão, este trabalho sugere potencial aplicação da piperina nessas nanoestruturas no tratamento do câncer de mama.

Palavras chave: câncer de mama, *metal-organic frameworks*, MIL-100 (Fe), piperina, membrana celular, quitosana.

ABSTRACT

Breast cancer is one of the leading causes of death among women with cancer worldwide, triggering the search for more effective chemotherapy treatments. Among the compounds with chemotherapeutic potential, piperine (PIP) stands out as promising due to its antitumor activity in breast cancer cell lines. However, the introduction of this compound in preclinical studies has been limited due to its toxicity. Metal-organic frameworks (MOFs), including MIL-100 (Fe), represent an attractive platform as drug delivery systems and can be employed to improve the bio-pharmaceutical properties of this molecule. Additionally, one engineering strategy is the modification of nanostructures with natural materials, such as macrophage membranes (MM) or chitosan (CHI), which are used as a camouflage system against the immune system within the body, providing resistance to degradation and controlled release. Inspired by these scientific and technological advancements, the present study aims to evaluate the potential of PIP encapsulated in MOFs coated with MM or CHI for-breast cancer treatment. In this research, we report the successful synthesis of nanosystems based on MIL-100(Fe) containing piperine coated with MM (MM@PIP@MIL-100(Fe)) or with CHI (CHI@PIP@MIL-100(Fe)) via microwave-assisted hydrothermal synthesis and impregnation method. X-ray diffraction analysis of MIL-100(Fe) and PIP@MIL-100(Fe) revealed the crystallinity of the materials, with particle sizes of 18.32 nm and 76.18 nm, respectively. Coating of vesicles for MM@PIP@MIL-100(Fe) was confirmed by electrophoresis (SDS-PAGE), demonstrating the presence of proteins on its surface. Chitosan coating on the MOF was confirmed by infrared spectroscopy. High-performance liquid chromatography (HPLC) was used to quantify PIP in the MOFs, showing an encapsulation efficiency of 95 ± 3%. Cytotoxicity assays on breast cancer cells such as MCF-7, SKBR3, MDA-MB-231, and BT549, using the materials PIP@MIL-100(Fe), MM@PIP@MIL-100(Fe), and CHII@PIP@MIL-100(Fe), revealed a higher cytotoxicity index compared to free piperine, with two to seventeen times higher median inhibitory concentration (IC_{50}). In conclusion, this work undeniably demonstrates that these nanostructures hold promise for PIP-based therapies for breast cancer.

Key words: Breast cancer, metal–organic framework, MIL-100 (Fe), Piperine, cell membrane, chitosan.

RIGHTS AND PERMISSIONS

The permissions to re-use texts, figures, and tables from previously published articles from the author were secured from:

Publisher: Elsevier

Paper 1: QUIJIA, Christian Rafael et al. In situ synthesis of piperine-loaded MIL-100 (Fe) in microwave for breast cancer treatment. Journal of Drug Delivery Science and Technology, v. 75, p. 103718, 2022.

DOI: 10.1016/j.jddst.2022.103718

Elsevier have copyright policies that grant automatic permission for re-use the paper in your thesis if you are the author: (…) as the author of this Elsevier article, you retain the right to include it in a thesis or dissertation, provided it is not published commercially. Permission is not required, but please ensure that you reference the journal as the original source (…)

Publisher: MDPI

Paper 2: QUIJIA, Christian Rafael et al. Macrophage Cell Membrane Coating on Piperine-Loaded MIL-100 (Fe) Nanoparticles for Breast Cancer Treatment. Journal of Functional Biomaterials, v. 14, n. 6, p. 319, 2023.

DOI: 10.3390/jfb14060319

MDPI: Permissions, no special permission is required to reuse all or part of article published by MDPI, including figures and tables. For articles published under an open access Creative Common CC BY license, any part of the article may be reused without permission provided that the original article is clearly cited. Reuse of an article does not imply endorsement by the authors or MDPI.

SUMÁRIO

1 CAPÍTULO 1: INTRODUÇÃO

1.1 Câncer de mama

O câncer de mama é o segundo tipo de câncer mais frequente e a maior causa de morte entre mulheres portadoras de câncer no mundo. De acordo com os dados da Organização Mundial da Saúde (OMS), está previsto que em 2030 haverá 30 milhões de casos novos e 13 milhões de mortes relacionadas com este câncer, devido à sua elevada capacidade metastática. De acordo com as estimativas realizadas pelo INCA (Instituto Nacional do Câncer), o número de casos novos de câncer aumentará 22 milhões nas duas décadas seguintes. No Brasil é o tipo de câncer mais comum entre as mulheres, com estimativas de 66.280 novos casos para o ano 2023. O câncer de mama também acontece em homens, porém é raro, representando apenas 1% do total de casos da doença (1).

Os carcinomas mamários podem, ainda, ser chamados de adenocarcinoma quando, além de apresentarem alterações nas células epiteliais ductal, também apresentam alterações no padrão de crescimento glandular. A maioria dos tumores de mama é classificada em adenocarcinoma (2).

A classificação pode ser de quatro tipos de câncer: receptor do fator de crescimento epidérmico tipo 2 (HER2), tipo basal enriquecido (sem expressão do receptor de estrogênio [ER]), luminal A e luminal B (que expressa o ER). As células de câncer de mama podem ter um, ambos ou nenhum desses receptores e são sub-classificados da seguinte forma: i) câncer de mama triplo negativo (TNBC) são tumores que não expressam ER, HER2 ou receptor de progesterona (PR) e ii) positivo os receptores hormonais (ER-positivos) são tumores que expressam ER e/ou PR (3). No entanto, aproximadamente 70% dos canceres de mama são classificados como ER-positivos, enquanto os TNBC representam 15% (4).

As células MCF-7, SKBR-3, MDA e BT549 são linhagens de células de câncer de mama amplamente estudadas em pesquisas científicas. Elas possuem diferenças significativas em termos de expressão de receptores hormonais, amplificação do gene HER2/neu e características comportamentais (5). As células MCF-7 são receptoras de estrogênio (ER+), e tendem a crescer em agregados. As células SKBR-3 são caracterizadas pela amplificação do gene HER2/neu e superexpressão do receptor HER2. Elas são negativas para receptores hormonais (ER-) e apresentam alta capacidade de proliferação. As células MDA são triplo-negativas ademais altamente invasivas e metastáticas, o que as torna mais agressivas e resistentes ao tratamento hormonal. As células BT549 também são consideradas triplo-negativas e exibem características mesenquimais (6). Cada uma dessas linhagens celulares

oferece um modelo valioso para o estudo de diferentes aspectos do câncer de mama, como resposta hormonal, amplificação do HER2 e comportamento invasivo.

A OMS realiza e promove o controle do câncer de mama, o qual exige ações múltiplas. Essas ações são acompanhadas de prevenção, diagnóstico precoce e tratamento. Existem quatro procedimentos principais para o tratamento do câncer, incluindo cirurgia, radiação, terapia hormonal e quimioterapia. No entanto, a resistência multidrogas (MDR) é uma condição em que as células cancerosas se tornam resistentes aos efeitos citotóxicos de vários agentes quimioterapêuticos estruturais e não relacionados mecanicamente. Este é um grande problema no tratamento clínico do câncer (7). Durante tratamento prolongado, muitos pacientes sofrem de MDR, o que pode reduzir a eficiência terapêutica e levar a uma falha no tratamento e a uma chance de sobrevivência.

Por outro lado, a maioria dos quimioterápicos age tanto em células tumorais como em células normais e isto causa toxicidade sistêmica e efeitos indesejáveis ao organismo. Isto ocorre porque os quimioterápicos agem mais intensamente em células saudáveis do que em células cancerígenas (8). Além disso, a rápida eliminação e ampla distribuição de quimioterápicos em tecidos não alvos requerem sua administração em grande quantidade, o que é impraticável devido à toxicidade inespecífica inerente dos agentes quimioterápicos (9).

A ineficiência e efeitos indesejáveis da quimioterapia atuais são causados, principalmente, pela formulação e farmacocinética dos quimioterápicos. Estes quimioterápicos por exemplo são: os taxanos (docetaxel e paclitaxel), antraciclinas (doxorrubicina, doxorrubicina lipossômica peguilada e epirrubicina), agentes da platina (cisplatina, carboplatina), entre outros. Por outro lado, seu sucesso depende da liberação controlada destes fármacos dirigida especificamente às células cancerígenas, com uma dose suficiente segura para os organismos por um longo período de tempo, podendo causar muitos efeitos colaterais, dependendo dos medicamentos administrados e do tempo tratamento (10).

Sendo assim, a busca de novos agentes quimioterapêuticos, dentre eles os provenientes de plantas, vem aumentando significativamente nos últimos anos. Várias plantas medicinais têm servido como fonte de estudos de anticancerígenos e mais de 60% dos atuais fármacos contra o câncer, como vimblastina, topotecano, etoteca e paclitaxel, são compostos derivados de plantas (11, 12).

1.2 Piperina

A piperina (PIP), também conhecida como (E, E) -1-piperoilpiperidina e (E, E) -1- [5- (1, 3-benzodioxol-5-il) -1-oxo-2, 4-pentidenil] piperidina (**Figura 1**), é um alcaloide extraído de sementes de plantas da família Piperácea, como são, por exemplo, a pimenta preta (3-9%) e a pimenta longa (3-5%) (13). Este composto tem sido utilizado como antimicrobiano, antiparasitário (14), antidepressivo (15), e modulador do carcinógeno de estresse oxidativo induzido (16). Sua estrutura química é dividida em três partes: um anel heterocíclico aromático, um anel piperidina e uma cadeia hidrocarbonada alifática (17). O anel piperidina é uma farmacóforo heterocíclico com alta atividade anticancerígena que pode inibir a telomerase, metaloproteases, topoisomerases e proteassomas, além de atuar em vários receptores nas células cancerígenas (18). Possui características químicas que a tornam insolúvel em água. Sua estrutura molecular hidrofóbica, a ausência de grupos hidrofílicos e sua polaridade apolar dificultam a interação com a água, tornando-a insolúvel. No entanto, a piperina é solúvel em solventes orgânicos apolares, como álcool e éter. Esses solventes possuem características semelhantes à PIP, o que permite sua dissolução (19).

Figura 1. Estrutura química da piperina (PIP)

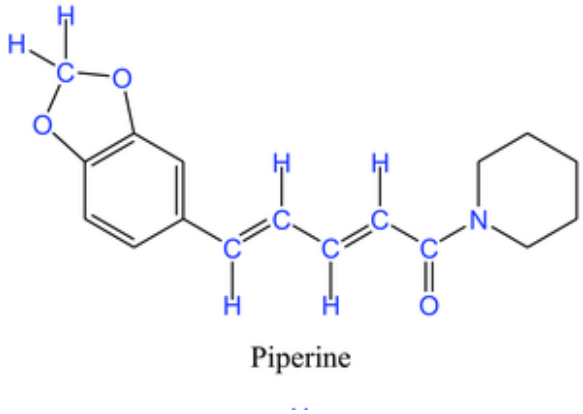

Fonte: (20)

A PIP pode inibir a proliferação de células do câncer de mama, por meio dos seguintes mecanismos: a) redução dos fatores de transcrição; b) indução de parada do ciclo celular e apoptose; c) inibição do crescimento do tumor; e d) alteração da expressão da proteína de sinalização (**Figura 2**), conforme evidenciado em estudos *in vitro* e *in vivo* com linhagens celulares de câncer de mama MCF-7 e MDA-MB-231 (21, 22).

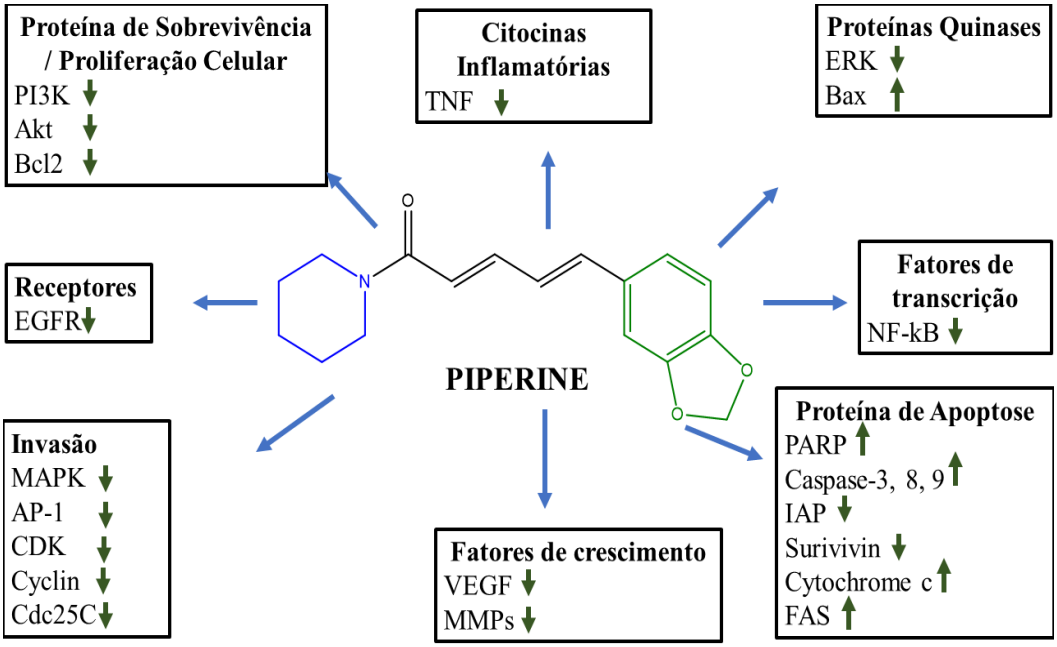

Figura 2. Alvos moleculares da piperina no câncer de mama. (23)
Nota: Fosfoinositídeo 3-quinases (PI3Ks); Proteína quinase B (Akt); linfoma de células B-2 (Bcl-2); Receptor do fator de crescimento epidérmico (EGFR); Proteína quinase ativada por mitógeno (MAPK); proteína ativadora 1 (AP-1); inibidor de quinase dependente de ciclina (CDK); fator de crescimento endotelial vascular (VEGF); Metaloproteinases de matriz (MMP); fator de necrose tumoral (TNF); quinases reguladas por sinal extracelular (ERKs); Intensificador de cadeia leve de fator nuclear de células B ativadas (NF-κB); Poli(ADP-ribose) polimerase (PARP); proteínas de apoptose (IAP); sintase de ácido gordo (FAS); ↓ Down-regulated targets; ↑ Up-regulated targets.

No entanto, o uso da piperina enfrenta algumas dificuldades em virtude de seu elevado requisito de concentração, devido à sua natureza hidrofóbica, causando problemas relacionados à biodisponibilidade, imunotoxicidade e toxicidade (24, 25). Desta forma, a sua incorporação em um sistema de liberação nanoestruturado pode ser uma alternativa viável para viabilizar o seu emprego.

Estes nanossistemas carregados com PIP devem ter diversas características como: uma alta capacidade de carga, liberação controlada de drogas e atividade anticancerígena melhorada, em comparação com a PIP livre. Atualmente as nanoestruturas carregadas de PIP contra câncer de mama já foram relatados como nanopartículas poliméricas, nanotubos de carbono e lipossomas (**Tabela 1**).

Tabela 1.- Diferentes nanosistemas carregados de piperina contra o câncer de mama.

Nanossistemas	Eficiência de encapsulação da PIP (%)	Tempo de liberação	Linha celular de câncer de mama	Concentração inibitória meia máxima (IC_{50})	Referência bibliográfica
PIP-PLGA	36.23 ± 5.6	Sem informação	MCF-7	128.2 ± 11.3 µM	(28)
PIP-PEG-PLGA	37.82 ± 6.8	16 dias	MCF-7	129.6 ± 9.2 µM	
APT-PIP-PEG-PLGA	33.4 ± 3.4	Sem informação	MCF-7	125.8 ± 8.7 µM	
PIP Lipossomas	56 ± 2.64	3 dias	MDA-MB-231	55.39 ± 1.1 µg/mL	(29)
Piperine-MWCNTs	Sem informação	Sem informação	MDA-MB-231	6 µg/mL	(30)

Nota: PIP: Piperina; PEG–PLGA: Polietileno glicol–ácido poliláctico–ácido co-glicólico; APT: Aptámero; MWCNTs: nanotubos de carbono de paredes múltiplas (23).

Lipossomas são vesículas esféricas compostas por uma dupla camada de fosfolipídios e colesterol, utilizadas como sistemas de transporte de fármacos. Eles são biodegradáveis, biocompatíveis e estáveis, protegendo os fármacos da degradação e reduzindo a toxicidade não específica. Lipossomas são amplamente aplicados no transporte de antibióticos, fungicidas, vacinas e anti-inflamatórios.

Nanolipossomas, formados a partir de fosfolipídios TPGS, têm se mostrado eficazes no tratamento de várias doenças, como o câncer de mama. Eles são utilizados como veículos para quimioterápicos lipossomais, como o Doxil, usado no tratamento do câncer de mama recorrente. O cetuximabe, um anticorpo monoclonal que bloqueia o antígeno EGFR, é frequentemente combinado com nanolipossomas para tratamento do câncer de mama triplo-negativo (TNBC), que é mais difícil de tratar devido à ausência de expressão dos genes ER, PR e HER2. Além dos lipossomas, as nanopartículas poliméricas também são amplamente utilizadas na entrega de fármacos. O ácido polilático-co-glicólico (PLGA) é um copolímero biodegradável e biocompatível com capacidade de liberação controlada de fármacos (27). Estudos demonstraram que o PLGA pode ser usado para encapsular a rapamicina (RA), um composto que inibe a proliferação celular e o crescimento tumoral. A presença do fosfatidilinositol-3-fosfato (PIP) em nanopartículas de PLGA aumentou a absorção oral da RA, melhorando sua eficácia no tratamento do câncer (26).

1.3 Nanossistemas

Os nanossistemas são categorizados como nanomateriais inorgânicos (por exemplo, nanopartículas de óxido de ferro, nanopartículas de ouro e zeólitos), nanomateriais orgânicos (por exemplo, nanopartículas poliméricas, micelas, dendrímeros e lipossomas) e finalmente uma terceira categoria, que são chamados de redes metalorgânicas ou polímeros de coordenação porosos (MOFs) (29).

1.3.1 Redes Metalorgânicas

Os MOFs são materiais porosos construídos a partir da cristalização controlada de íons metálicos ou aglomerados de metais de maior nuclearidade (clusters) com ligantes orgânicos multitópicos (30), os quais são capazes de superar as limitações dos sistemas nanoestruturados, como a baixa capacidade de carga e liberação de fármaco (31).

Os diversos métodos que são utilizados para a síntese de MOFs proporcionam a oportunidade de projetar e controlar as propriedades químicas e físicas desses materiais (32). Os MOFs são construídos a partir da montagem, exclusivamente por fortes ligações covalentes, subunidades inorgânicas e ligantes orgânicos, que podem ser quimicamente ajustáveis (por exemplo, carboxilatos, fosfonatos e imidazolatos), levando a estruturas cristalinas com porosidades, por vezes, muito altas e regulares (33). Além disso, a alta flexibilidade estrutural de alguns MOFs porosos permite a adaptação da sua porosidade à forma da molécula hospedada (34).

1.3.1.1 MIL-100(Fe)

Um exemplo destes MOFs é o MIL-100 (Fe) (MIL: *Materials of Institute Lavoisier*), que tem uma forma de um pó policristalino, sendo formado a partir de íons ferro(III) e o ácido 1,3,5-benzenotricarboxílico (35). As características do MIL-100 (Fe), como a presença de porosidade característica de materiais mesoporosos (25 e 29 Å), alta área superficial (S_{BET} ~ 2.000 $m^2.g^{-1}$, Vp ~ 1,2 $cm^3.g^{-1}$), estrutura regular e a combinação com seu microambiente anfifílico interno (metal polar anfifílico e ligante não polar), permitem o carreamento de grandes quantidades de fármacos (hidrofílico, hidrofóbico e anfifílico) e também possibilita a cinética de liberação controlada (29, 36-39). O encapsulamento dos fármacos nestes MOFs tem duas vantagens importantes: (i) eliminar qualquer possibilidade de complexação, protegendo-os de íons e protegendo os sítios de coordenação disponíveis e (ii) aumentar a solubilidade do fármaco (40).

1.3.1.2 Citotoxicidade de MIL-100(Fe)

O MIL-100(Fe) não apresenta citotoxicidade em alguns tipos de células, como câncer de pulmão humano (Calu-3), adenocarcinomas epiteliais alveolares basais humanos (A549), carcinoma de fígado humano (HepG2) (concentração < 0,064 mg mL^{-1}) (41), adenocarcinomas colorretais epiteliais humanos heterogêneos (CACO-2) e câncer de mama (MCF-7) (concentração < 1,2 mg mL^{-1}) (29). Esta baixa citotoxicidade pode estar relacionada com a redução do íon ferro na estrutura do MIL-100 (Fe) (na superfície interna e externa), gerando radicais hidroxila ou outras espécies reativas (*Haber-Weiss* e reação de Fenton) dentro da célula (41).

1.3.1.3 Métodos de sínteses do MIL-100(Fe)

O MIL-100(Fe) pode ser sintetizado por vários métodos, incluindo as técnicas hidrotermal assistida por micro-ondas, eletroquímica, mecanoquímica, sonoquímica, entre outras (42). No entanto, a síntese assistida por micro-ondas apresenta vantagens sobre as demais, como tempos de reação mais curtos, aquecimento homogêneo e menor polidispersidade, além de rápida formação, crescimento e tamanho de cristais em nanoescala. Além disso, estruturas em nanoescala têm sido amplamente utilizadas devido à sua capacidade de superar drogas e barreiras biológicas de forma eficiente ao microambiente tumoral (36, 43-46).

1.3.1.4 Estratégias de encapsulação

Diversas estratégias de encapsulamento de fármacos têm sido relatadas para MIL-100 (Fe), como os métodos de impregnação, de alta pressão ou mecanoquímico (47). Um estudo realizado por Singco, Liu (48) utilizou uma nova estratégia de encapsulamento *in situ* durante a formação do MIL-100 (Fe) para a incorporação de ácido acetilsalicílico. Esta estratégia implica que algumas moléculas ou pró-drogas estejam diretamente ligadas através da coordenação disponível (49). Desta forma, o carreamento de fármacos com estruturas menores poderia ser realizado, evitando o vazamento do fármaco antes da degradação do carreador. No entanto, uma forte interação entre os fármacos e MOFs é essencial para alcançar um comportamento de carga e liberação de fármaco satisfatório, como a utilização de grupos funcionais especiais (COOH, SO_3H, C=O, etc.) ou carga oposta que ajuda com sucesso no encapsulamento *in situ* com o MOF (50).

1.3.1.5 Modificações de superfície de MOFs

Estratégias de modificação de superfície de nanopartículas de MOFs tem sido desenvolvida recentemente, cujo objetivo é melhorar a estabilidade química e coloidal dos materiais. Além disso, está funcionalização poderia ser adequada para administração intravenosa, o que permitiria um aumento das interações do MIL-100(Fe) com receptores específicos (*targeting*) e/ou escape do sistema imunitário associado com tempos de circulação mais prolongados.

Dentro desse contexto, o biopolímero quitosana (QUI) poderia proteger a matriz e permanecer maior tempo em circulação e ser lentamente eliminado pelo organismo. Outras propriedades biológicas como a biocompatibilidade, baixa toxicidade e imunoestimulante, fazem atrativo o revestimento do MIL-100(Fe) por esse biopolímero.

Outra estratégia que vem sendo investigada na engenharia de materiais é a combinação dos sistemas de liberação de fármacos com materiais naturais. Dentro dessa perspectiva, as membranas de revestimento celular são um novo tipo de nanoestruturas biomiméticas que combinam as funções da membrana celular e a engenharia de nanomateriais sintéticos, objetivando melhor entrega de agentes quimioterapêuticos (51). Uma delas consiste na utilização de membranas de macrófagos. Estas células são um tipo de glóbulos brancos que encontram e fagocitam detritos celulares, células cancerosas e quaisquer substâncias estranhas que não possuem os biomarcadores específicos das células do corpo saudáveis em sua superfície.

Desta forma, a vantagem de recobrir nanoestruturas com membranas de macrófagos ou quitosana é a potencialidade de camuflagem, de forma a se evitar a depuração dos sistemas de fagócitos mononucleares e ter maior circulação sanguínea prolongada (52). Se as nanoestruturas podem ser camufladas com membranas de macrófagos ou quitosana, torna-se possível utilizar esta adesão célula-célula no combate ao câncer (52-54).

Inspirados por esses avanços científicos e tecnológicos, no presente trabalho, foram obtidas vesículas de membrana de macrófagos naturais juntamente com suas proteínas de membrana; além disso, o biopolímero quitosana também foi utilizado para revestir o MIL-100 (Fe). Previamente estes MOFs foram encapsulados com a PIP *in situ* mediante síntese em micro-ondas (PIP@MIL-100 (Fe)). Foram também realizados nesse trabalho estudos de eficácia destes sistemas nanoestruturados *in-vitro* contra células do câncer de mama. Pretende-se obter um sistema que seja estável em fase aquosa, que aumente a biodisponibilidade da piperina e reduza a toxicidade não específica deste fármaco.

1.4 OBJETIVO

Avaliar o potencial da piperina encapsulada em *metal-organic frameworks* revestidos com modificações de superfície no tratamento do câncer de mama.

1.5 OBJETIVOS ESPECÍFICOS

- Encapsular a piperina (PIP) no MOF de ferro, MIL-100(Fe), mediante síntese *in situ* por micro-ondas, obtendo o material PIP@MIL-100(Fe);
- Avaliar a eficiência de encapsulação da PIP na matriz PIP@MIL-100(Fe) por cromatografia CLAE;
- Produzir as vesículas derivadas da membrana dos macrófagos RAW 264.7 (vesículas MM) mediante o método citólise hipotônica;
- Revestir as membranas de células de macrófagos RAW 264.7 (MM), via impregnação, no material PIP@MIL-100(Fe), obtendo o nanosistema MM@PIP@MIL-100(Fe);
- Determinar e comparar as proteínas das vesículas MM das células de macrófago RAW 264.7 com aquelas nas nanoestruturas MM@PIP@MIL-100(Fe) empregando ensaios de SDS-PAGE e dispersão de luz dinâmica (DLS);
- Revestir a matriz PIP@MIL-100(Fe) com quitosana (QUI) por impregnação, com a preparação do biocompósito QUI@PIP@MIL-100(Fe);
- Caracterizar as diferentes MOFs por meio de microscopia eletrônica de varredura, microscopia eletrônica de transmissão, medidas de dispersão de luz dinâmica (DLS), difração de raios X (XRD), análise térmica (TGA), porosidade por isotermas de adsorção de nitrogênio, espectroscopia no infravermelho (IR) e analises elementar;
- Determinar a estabilidade da matriz PIP@MIL-100(Fe) em presença de PBS a 37 °C por meio de difração de raios X e microscopia eletrônica de transmissão;
- Analisar a estabilidade da nanosistema MM@PIP@ MIL-100(Fe) por meio de DLS;
- Avaliar o perfil de liberação da piperina a partir das diferentes nanoestruturas por CLAE;
- Avaliar a citoxicidade dos diferentes tratamentos por método de ensaio colorimétrico em diferentes linhagens celulares de câncer de mama.

1.6 REFERÊNCIAS

1. INCA. Ministério da Saúde. Instituto Nacional de Câncer 2021 [Available from: http://www2.inca.gov.br/wps/wcm/connect/acessoainformacao/site/home/.

2. Robbins SL, Cotran RS, Kumar V, Abbas AK, Fausto N. Patologia: bases patológicas das doenças: Elsevier; 2005.

3. Sørlie T, Perou CM, Tibshirani R, Aas T, Geisler S, Johnsen H, et al. Gene expression patterns of breast carcinomas distinguish tumor subclasses with clinical implications. 2001;98(19):10869-74.

4. Yao H, He G, Yan S, Chen C, Song L, Rosol TJ, et al. Triple-negative breast cancer: is there a treatment on the horizon? 2017;8(1):1913.

5. Ninio-Many L, Hikri E, Burg-Golani T, Stemmer SM, Shalgi R, Ben-Aharon IJFio. miR-125a induces HER2 expression and sensitivity to trastuzumab in triple-negative breast cancer lines. 2020;10:191.

6. Chen J-Q, Russo JJBeBA-RoC. ERα-negative and triple negative breast cancer: molecular features and potential therapeutic approaches. 2009;1796(2):162-75.

7. Ho EA, Soo PL, Allen C, Piquette-Miller M. Impact of intraperitoneal, sustained delivery of paclitaxel on the expression of P-glycoprotein in ovarian tumors. Journal of controlled release : official journal of the Controlled Release Society. 2007;117(1):20-7.

8. Brannon-Peppas L, Blanchette JO. Nanoparticle and targeted systems for cancer therapy. Advanced drug delivery reviews. 2004;56(11):1649-59.

9. Gu FX, Karnik R, Wang AZ, Alexis F, Levy-Nissenbaum E, Hong S, et al. Targeted nanoparticles for cancer therapy. Nano today. 2007;2(3):14-21.

10. Barrios C, Freitas-Junior R, Martins S, Bines J, Estevez-Diz MDP, Caleffi MJJGO. Challenge of Incorporating New Drugs for Breast Cancer in Brazil: A Proposed Framework for Improving Access to Innovative Therapies. 2021;7:474-85.

11. Newman DJ, Cragg GM, Snader KM. Natural products as sources of new drugs over the period 1981-2002. Journal of natural products. 2003;66(7):1022-37.

12. Cragg GM, Newman DJ. Plants as a source of anti-cancer agents. Journal of ethnopharmacology. 2005;100(1-2):72-9.

13. Srinivasan K. Black pepper and its pungent principle-piperine: a review of diverse physiological effects. Critical reviews in food science and nutrition. 2007;47(8):735-48.

14. Mitra M, Mandal AK, Chatterjee TK, Das N. Targeting of mannosylated liposome incorporated benzyl derivative of Penicillium nigricans derived compound MT81 to

reticuloendothelial systems for the treatment of visceral leishmaniasis. Journal of drug targeting. 2005;13(5):285-93.

15. Li S, Wang C, Wang M, Li W, Matsumoto K, Tang Y. Antidepressant like effects of piperine in chronic mild stress treated mice and its possible mechanisms. Life sciences. 2007;80(15):1373-81.

16. Khajuria A, Thusu N, Zutshi U, Bedi KL. Piperine modulation of carcinogen induced oxidative stress in intestinal mucosa. Molecular and cellular biochemistry. 1998;189(1-2):113-8.

17. Zadorozhna M, Tataranni T, Mangieri DJMbr. Piperine: role in prevention and progression of cancer. 2019;46(5):5617-29.

18. Goel P, Alam O, Naim MJ, Nawaz F, Iqbal M, Alam MIJEJoMC. Recent advancement of piperidine moiety in treatment of cancer-A review. 2018;157:480-502.

19. Yan X, Li M, Xu X, Liu X, Liu FJFiN. Zein-based nano-delivery systems for encapsulation and protection of hydrophobic bioactives: A review. 2022;9:999373.

20. Gorgani L, Mohammadi M, Najafpour GD, Nikzad M. Piperine—the bioactive compound of black pepper: from isolation to medicinal formulations. Comprehensive Reviews in Food Science and Food Safety. 2017;16(1):124-40.

21. Lai LH, Fu QH, Liu Y, Jiang K, Guo QM, Chen QY, et al. Piperine suppresses tumor growth and metastasis in vitro and in vivo in a 4T1 murine breast cancer model. Acta pharmacologica Sinica. 2012;33(4):523-30.

22. Bezerra DP, Castro FO, Alves AP, Pessoa C, Moraes MO, Silveira ER, et al. In vivo growth-inhibition of Sarcoma 180 by piplartine and piperine, two alkaloid amides from Piper. Brazilian journal of medical and biological research = Revista brasileira de pesquisas medicas e biologicas. 2006;39(6):801-7.

23. Quijia CR, Chorilli MJPR. Piperine for treating breast cancer: A review of molecular mechanisms, combination with anticancer drugs, and nanosystems. 2022;36(1):147-63.

24. Chuchawankul S, Khorana N, Poovorawan Y. Piperine inhibits cytokine production by human peripheral blood mononuclear cells. Genetics and molecular research : GMR. 2012;11(1):617-27.

25. Daware MB, Mujumdar AM, Ghaskadbi S. Reproductive toxicity of piperine in Swiss albino mice. Planta medica. 2000;66(3):231-6.

26. Pachauri M, Gupta ED, Ghosh PCJJodds, technology. Piperine loaded PEG-PLGA nanoparticles: Preparation, characterization and targeted delivery for adjuvant breast cancer chemotherapy. 2015;29:269-82.

27. Imam SS, Alshehri S, Altamimi MA, Hussain A, Qamar W, Gilani SJ, et al. Formulation of piperine–chitosan-coated liposomes: characterization and In Vitro Cytotoxic Evaluation. 2021;26(11):3281.

28. Raza K, Kumar D, Kiran C, Kumar M, Guru SK, Kumar P, et al. Conjugation of docetaxel with multiwalled carbon nanotubes and codelivery with piperine: implications on pharmacokinetic profile and anticancer activity. 2016;13(7):2423-32.

29. Rezaei M, Abbasi A, Varshochian R, Dinarvand R, Jeddi-Tehrani M. NanoMIL-100(Fe) containing docetaxel for breast cancer therapy. Artificial Cells Nanomedicine and Biotechnology. 2018;46(7):1390-401.

30. Carne A, Carbonell C, Imaz I, Maspoch D. Nanoscale metal-organic materials. Chemical Society reviews. 2011;40(1):291-305.

31. Wu MX, Yang YW. Metal-Organic Framework (MOF)-Based Drug/Cargo Delivery and Cancer Therapy. Adv Mater. 2017;29(23).

32. Giménez-Marqués M, Hidalgo T, Serre C, Horcajada P. Nanostructured metal–organic frameworks and their bio-related applications. Coordination Chemistry Reviews. 2016;307:342-60.

33. Férey G. Hybrid porous solids: past, present, future. Chemical Society reviews. 2008;37(1):191-214.

34. Férey G, Serre C. Large breathing effects in three-dimensional porous hybrid matter: facts, analyses, rules and consequences. Chemical Society reviews. 2009;38(5):1380-99.

35. Horcajada P, Surble S, Serre C, Hong DY, Seo YK, Chang JS, et al. Synthesis and catalytic properties of MIL-100(Fe), an iron(III) carboxylate with large pores. Chem Commun (Camb). 2007(27):2820-2.

36. Bellido E, Hidalgo T, Lozano MV, Guillevic M, Simon-Vazquez R, Santander-Ortega MJ, et al. Heparin-Engineered Mesoporous Iron Metal-Organic Framework Nanoparticles: Toward Stealth Drug Nanocarriers. Advanced Healthcare Materials. 2015;4(8):1246-57.

37. Marcos-Almaraz MT, Gref R, Agostoni V, Kreuz C, Clayette P, Serre C, et al. Towards improved HIV-microbicide activity through the co-encapsulation of NRTI drugs in biocompatible metal organic framework nanocarriers. Journal of Materials Chemistry B. 2017;5(43):8563-9.

38. Horcajada P, Chalati T, Serre C, Gillet B, Sebrie C, Baati T, et al. Porous metal–organic-framework nanoscale carriers as a potential platform for drug delivery and imaging. Nature materials. 2010;9(2):172.

39. Li X, Semiramoth N, Hall S, Tafani V, Josse J, Laurent F, et al. Compartmentalized Encapsulation of Two Antibiotics in Porous Nanoparticles: an Efficient Strategy to Treat Intracellular Infections. Particle & Particle Systems Characterization. 2019;36(3).

40. Taherzade SD, Soleimannejad J, Tarlani A. Application of Metal-Organic Framework Nano-MIL-100(Fe) for Sustainable Release of Doxycycline and Tetracycline. Nanomaterials (Basel). 2017;7(8).

41. Grall R, Hidalgo T, Delic J, Garcia-Marquez A, Chevillard S, Horcajada P. In vitro biocompatibility of mesoporous metal (III; Fe, Al, Cr) trimesate MOF nanocarriers. Journal of Materials Chemistry B. 2015;3(42):8279-92.

42. Han Y, Yang H, Guo XJSM, Crystallization. Synthesis methods and crystallization of MOFs. 2020:1-23.

43. Agostoni V, Anand R, Monti S, Hall S, Maurin G, Horcajada P, et al. Impact of phosphorylation on the encapsulation of nucleoside analogues within porous iron(III) metal-organic framework MIL-100(Fe) nanoparticles. Journal of Materials Chemistry B. 2013;1(34):4231-42.

44. Bellido E, Guillevic M, Hidalgo T, Santander-Ortega MJ, Serre C, Horcajada PJL. Understanding the colloidal stability of the mesoporous MIL-100 (Fe) nanoparticles in physiological media. Langmuir. 2014;30(20):5911-20.

45. Hidalgo T, Alonso-Nocelo M, Bouzo B, Reimondez-Troitiño S, Abuin-Redondo C, de la Fuente M, et al. Biocompatible iron (iii) carboxylate metal–organic frameworks as promising RNA nanocarriers. 2020;12(8):4839-45.

46. Rodriguez-Ruiz V, Maksimenko A, Anand R, Monti S, Agostoni V, Couvreur P, et al. Efficient "green" encapsulation of a highly hydrophilic anticancer drug in metal-organic framework nanoparticles. Journal of Drug Targeting. 2015;23(7-8):759-67.

47. Quijia CR, Lima C, Silva C, Alves RC, Frem R, Chorilli MJJoDDS, et al. Application of MIL-100 (Fe) in drug delivery and biomedicine. 2020:102217.

48. Singco B, Liu LH, Chen YT, Shih YH, Huang HY, Lin CH. Approaches to drug delivery: Confinement of aspirin in MIL-100(Fe) and aspirin in the de novo synthesis of metal-organic frameworks. Microporous and Mesoporous Materials. 2016;223:254-60.

49. Valekar AH, Batule BS, Kim MI, Cho KH, Hong DY, Lee UH, et al. Novel amine-functionalized iron trimesates with enhanced peroxidase-like activity and their applications for the fluorescent assay of choline and acetylcholine. Biosensors & Bioelectronics. 2018;100:161-8.

50. Zhang H, Li Q, Liu R, Zhang X, Li Z, Luan YJAFM. A Versatile prodrug strategy to in situ encapsulate drugs in MOF nanocarriers: a case of cytarabine-IR820 prodrug encapsulated ZIF-8 toward chemo-photothermal therapy. 2018;28(35):1802830.

51. Meyer RA, Sunshine JC, Green JJ. Biomimetic particles as therapeutics. Trends in biotechnology. 2015;33(9):514-24.

52. Xuan M, Shao J, Dai L, He Q, Li J. Macrophage cell membrane camouflaged mesoporous silica nanocapsules for in vivo cancer therapy. Advanced healthcare materials. 2015;4(11):1645-52.

53. Rao L, He ZB, Meng QF, Zhou ZY, Bu LL, Guo SS, et al. Effective cancer targeting and imaging using macrophage membrane-camouflaged upconversion nanoparticles. Journal of Biomedical Materials Research Part A. 2017;105(2):521-30.

54. Xuan MJ, Shao JX, Dai LR, Li JB, He Q. Macrophage Cell Membrane Camouflaged Au Nanoshells for in Vivo Prolonged Circulation Life and Enhanced Cancer Photothermal Therapy. Acs Applied Materials & Interfaces. 2016;8(15):9610-8.

55. Brasil AJDOdRFd. Agência Nacional de Vigilância Sanitária, Resolução RDC N° 166, de 24 de Julho de 2017. 2017.

56. Reyes Solís LM, Sánchez RA, Restrepo JJRdC. Encapsulation of the Piperine Present in Piper tuberculatum Species Using Multilamellar Vesicles and Determination of its Antioxidant Power. 2017;21(2):11-28.

57. Taherzade SD, Soleimannejad J, Tarlani A. Application of Metal-Organic Framework Nano-MIL-100(Fe) for Sustainable Release of Doxycycline and Tetracycline. Nanomaterials. 2017;7(8).

58. Guo AL, Durymanov M, Permyakova A, Sene S, Serre C, Reineke J. Metal Organic Framework (MOF) Particles as Potential Bacteria-Mimicking Delivery Systems for Infectious Diseases: Characterization and Cellular Internalization in Alveolar Macrophages. Pharmaceutical Research. 2019;36(4).

59. Simon MA, Anggraeni E, Soetaredjo FE, Santoso SP, Irawaty W, Thanh TC, et al. Hydrothermal Synthesize of HF-Free MIL-100 (Fe) for Isoniazid-Drug Delivery. Scientific reports. 2019;9(1):1-11.

60. Guideline IHTJQ. Validation of analytical procedures: text and methodology. 2005;1:1-15.

61. Brasil BJDORFd. Dispõe sobre a validação de métodos analíticose dá outras providências (Resolução RDC nº 166, de 24 de julho de 2017). 2017.

62. Mendonça RJRMAI. Instituto Nacional de Metrologia, Normalização e Qualidade Industrial. 2006;15(1):1-10.

2 CAPÍTULO 2: In Situ Synthesis Of Piperine-Loaded MIL-100 (Fe) In Microwave For Breast Cancer Treatment

Artigo publicado em setembro 2022 no periódico Journal of Drug Delivery Science and Technology

DOI: 10.1016/j.jddst.2022.103718

IN SITU SYNTHESIS OF PIPERINE-LOADED MIL-100 (Fe) IN MICROWAVE FOR BREAST CANCER TREATMENT

Christian Rafael Quijia [a], Marcela Tavares Luiz [b], Richard Perosa Fernandes [c], Rafael Miguel Sábio [a], Regina Frem [c] and Marlus Chorilli [a]

[a]School of Pharmaceutical Sciences, São Paulo State University (UNESP), Araraquara, São Paulo, Brazil

[b]School of Pharmaceutical Science of Ribeirão Preto, University of São Paulo (USP), Ribeirão Preto, SP, Brazil

[c]Institute of Chemistry, São Paulo State University (UNESP), Araraquara, São Paulo, Brazil

ABSTRACT:

Piperine (PIP) is a natural alkaloid that has strong activity against breast cancer. However, due to its low solubility and bioavailability, it is unfeasible for clinical applications. Herein, we proposed an *in-situ* method for PIP encapsulation into the Materials of the Institut Lavoisier (MIL-100 (Fe)) using microwaves technique for fabricating novel drug delivery nanocarriers. The PIP-loaded MIL-100 (Fe) (labeled PIP@MIL-100 (Fe)) exhibited a hydrodynamic diameter of 98 ± 27.83 nm, zeta potential of +7 ± 0.6 mV, and polydispersity index of 0.03 ± 0.006. Morphological analysis of the nanosystems revealed a rhombohedral shape and particle size up to 120 nm. PIP encapsulation efficiency (EE) was found to be 95 ± 3% and PIP loading capacity was 11.02 % by weight (0.12 g g^{-1}), according to high-performance liquid chromatography (HPLC) and thermogravimetric analysis (TGA) data, respectively. Cytotoxicity studies on breast cancer cell lines (MCF-7 and 4T1) displayed cytotoxicity (IC_{50}) approximately three times higher than that of the free PIP within 48 h. The PIP@MIL-100(Fe) fabrication comprises a simple and cheap method for designing novel drug delivery nanosystems for further clinical assays and breast cancer treatment.

Keywords: Metal-organic framework-based, nanoparticles, MCF-7 cells, 4T1 cells, breast cancer treatment.

1. INTRODUCTION

Metal-organic frameworks (MOFs) are built exclusively by inorganic subunits, strong bonds of covalent ions, and easily adjustable organic ligands (e.g. phosphonates, carboxylates, imidazolates, etc.), leading to crystal structures with sometimes very high and regular porosities [1]. In recent years, these MOFs have attracted considerable attention in the field of biomedical applications [2]. This interest in MOFs is due to their structure, pore-volume, high porosity, and large surface area for drug encapsulation, chemical-thermal stability, and easy

chemical functionalization. These attributes enhance MOFs ability to transport various types of drugs and facilitate controlled release [3].

Ferey et al. synthesized for the first-time chromium (III) carboxylate, called MIL (MIL: Materials of the Institut Lavoisier) [4]. Currently, the most widely studied MIL has been mesoporous iron (III) carboxylate, or MIL-100 (Fe), with molecular formula $Fe_3O(H_2O)_2OH(BTC)_2$. These MOFs have received much attention in the last years as drug carriers due to their high specific surface area (S~2000 $m^2\ g^{-1}$, V~1.2 $cm^3\ g^{-1}$), high porosity (smaller cages [25 Å] accessible through larger cages [29 Å] and windows pentagonal microporous [5.6 Å] also delimited by hexagonal openings [8.6 Å]) and stability in a biological environment [5].

These MOFs have an internal amphiphilic microenvironment (non-polar linker and amphiphilic polar metal) that allows the loading of large drugs amount (hydrophilic, hydrophobic, or amphiphilic) and controlled release kinetics. This behavior is assigned to the numerous coordinatively unsaturated (open) metal sites (CUS) available, which can act as a strong bond between coordination sites and therapeutic drug molecules [6].

MIL-100(Fe) does not show cytotoxicity in some cell types such as human lung cancer (Calu-3), human alveolar basal epithelial adenocarcinomas (A549), human liver carcinoma (HepG2) (concentration < 0.064 mg mL^{-1}) [7], heterogeneous human epithelial colorectal adenocarcinomas (Caco-2), and breast cancer (MCF-7) (concentration < 1.2 mg mL^{-1}) [8]. This low cytotoxicity could be related to the reduction of the iron in the framework of the MIL-100 (Fe) (on the internal and external surface), generating hydroxyl radicals or other reactive species (Haber-Weiss and the Fenton reaction) within the cell[7].

In vivo studies conducted by Simon-Yarza et al. employed Wistar rats (235 ± 15 g kg^{-1}) and administered MIL-100(Fe) intravenously. This study reported the progressive degradation in the constitutive components, iron and organic linker (BTC), of the MIL-100 (Fe) in contact with the blood. The degradation allowed the direct removal of the precursors by the urine and feces without any biotransformation [9].

These MOFs have been synthesized using several methods, including the microwave-assisted hydrothermal technique, electrochemistry, mechanochemistry, sonochemistry, among others [10]. However, microwave-assisted synthesis has advantages over the others, such as shorter reaction times, homogeneous heating, and lower polydispersity, as well as rapid crystal formation, growth, and size at the nanoscale. Furthermore, nanoscale structures has

been widely used due to their ability to overcome deliver drugs and biological barriers efficiently to the tumor microenvironment [11-16].

Various drug encapsulation strategies have been reported in MIL-100 (Fe) such as impregnation method, high pressure, and encapsulation assisted by mechanochemistry [1]. The impregnation method is the most widely used, but it often turns out to have a low drug loading capacity, due to its slow diffusion process. According to studies realized by Horcajada et al., encapsulation/entrapment efficiency can increase with the contact time, the nature of the solvent, and the ratio of drug to MOF [17]. In addition, this method is employed for drugs with a size smaller than the pores in MOFs. The latest studies have shown low encapsulation efficiency of hydrophobic drugs such as ibuprofen, doxorubicin [18], and docetaxel [8] (11, 11.2, and 10%, respectively).

In anti-cancer drugs loaded in MIL-100(Fe), efficacy has been observed against some cell lines such as those in cervical cancer (Hela) [19], adenocarcinoma human alveolar basal epithelial cells (A549), human epithelial colorectal adenocarcinoma cells (Caco-2), lung cancer (Calu-3) cells[7], human colorectal cancer cells (SW480) [16], and brain glioma cells (C6) [20].

Singco et al. used the in situ encapsulation strategy during the formation of MIL-100 (Fe) for the release of aspirin [21]. This strategy implies that some molecules or prodrugs are directly linked through available coordination sites [22]. In this way, the loading of drugs with smaller structures could be carried out, avoiding the leakage of the drug before carrier degradation. However, a strong interaction between drugs and MOFs is essential to achieve satisfactory drug loading and controlled release behavior. This interaction can be performed by functional groups (COOH, SOH, CO, etc.) or opposite charges that successfully help the in situ drug encapsulation with the MOF [23].

Breast cancer is the second most common type of cancer and the leading cause of death among women with cancer worldwide. According to data from the World Health Organization (WHO), it is predicted that by 2030 there will be 30 million new cases and 13 million deaths related to this cancer, due to its high metastatic capacity [24]. The inefficiency and undesirable effects of current chemotherapy are mainly caused by the formulation and pharmacokinetics of chemotherapy. These chemotherapeutics for example are taxanes (docetaxel and paclitaxel), anthracyclines (doxorubicin, pegylated liposomal doxorubicin, and epirubicin), platinum agents (cisplatin, carboplatin), etc.

On the other hand, its success depends on the controlled release of these drugs specifically aimed at cancer cells, with a sufficient dose safe for organisms for a long period, which can cause many side effects, depending on the drugs administered and the time of treatment [25]. Therefore, the search for new chemotherapeutic agents, including those from plants, has increased significantly in recent years. Several medicinal plants have served as a source of anticancer studies and over 60% of current cancer drugs such as vinblastine, topotecan, etoteca, and paclitaxel are plant-derived compounds. [26, 27].

Piperine (PIP) is the alkaloid responsible for the pungency of long pepper (*Piper longum*) and black pepper (*Piper nigrum*). This hydrophobic drug has shown several therapeutic biological properties such as anticancer, antidiabetic, antidiarrhea, antibacterial activity, and among others [28]. Recent studies have shown that PIP can inhibit the proliferation of breast cancer cells, through the following mechanisms: a)reduction of transcription factors; b) apoptosis and induction of cell cycle arrest; c) inhibition of tumor growth; and d) alteration of the expression of the signaling protein [29].

However, PIP poor water solubility and bioavailability make its application challenging. Therefore, strategies, such as nanotechnology, have been used to overcome this problem. The use of nanotechnology in breast cancer therapies aims to increase the solubility of drugs and the bioavailability within the body [30]. PIP-loaded nanosystems must have a high loading capacity, controlled drug release, and improved anticancer activity, in comparison with free PIP, while being non-toxic to normal cells. PIP-loaded nanosystems against breast cancer have been reported to include polymer nanoparticles, carbon nanotubes, and liposomes and to have biological efficacy in breast cancer. [31-34]

Relying upon these premises, this study aimed to apply an *in-situ* microwave method for the manufacture of PIP-encapsulated MIL-100 (Fe), designated PIP@MIL-100 (Fe). We also investigated the encapsulation efficiency, release behavior in a physiological medium, and cytotoxic activity on breast cancer cells (MCF-7).

2. EXPERIMENTAL SECTION

2.1. Materials

Piperine (Sigma Aldrich, St. Louis, MO, USA), Trimesic acid (BTC) (Sigma Aldrich, St. Louis, MO, USA), Iron (III) chloride hexahydrate (Sigma Aldrich, St. Louis, MO, USA), Ethanol 99% (Neon, Brazil), Methanol HPLC grade (Sigma Aldrich, St. Louis, MO, USA), Resazurin (Sigma Aldrich, St. Louis, MO, USA), RPMI-1640 supplemented with 10% fetal

bovine serum (FBS) and 1% antibiotic (10,000 UI of penicillin and 10 mg of streptomycin per mL solution) (Sigma Aldrich, St. Louis, MO, USA) were used as received.

2.2. Synthesis of MIL-100(Fe)

The synthesis of MIL-100(Fe) was based on a previous procedure with some modifications [35]. This procedure consisted in dissolving iron (III) chloride hexahydrate (0.081 mg; 0.29 mmol) and BTC (0.028 mg; 0.13 mmol) in distilled water (1 mL). The reaction was heated to 130 ºC for 30 s and kept at this temperature for 7 min (300 W) (Mars-5, CEM, US: power maximum output 300 W, the frequency at full power 60 Hz). The MIL-100 (Fe) obtained was recovered by centrifugation at 5600 g for 8 min. Then, the activation of the solid consisted in redispersing in absolute ethanol (1 mL) and centrifuging at 5600 g for 8 min, and 4 cycles were carried out under the same conditions. An orange solid was thus recovered (40 mg, 98%). Finally, the nanostructure was stored in absolute ethanol at 4 ºC.

2.3. In situ of PIP@MIL-100(Fe)

In-situ microwave synthesis of PIP@MIL-100(Fe) was performed as described above, except that different concentrations of PIP were introduced into the initial synthesis solution (1; 4; 18; 38 mg). Then the PIP@MIL-100(Fe) obtained was recovered by centrifugation at 5600 g for 8 min, and the best chemical performance was chosen for subsequent studies. PIP@MIL-100(Fe) was then redispersed in absolute ethanol (1 mL) and centrifuged at 5600 g for 8 min, and 4 cycles were performed under the same conditions. An orange solid was thus recovered (40 mg, 96%). Finally, to maintain the nanostructure until its use, it was placed in absolute ethanol at 4 °C (**Fig. 1.**).

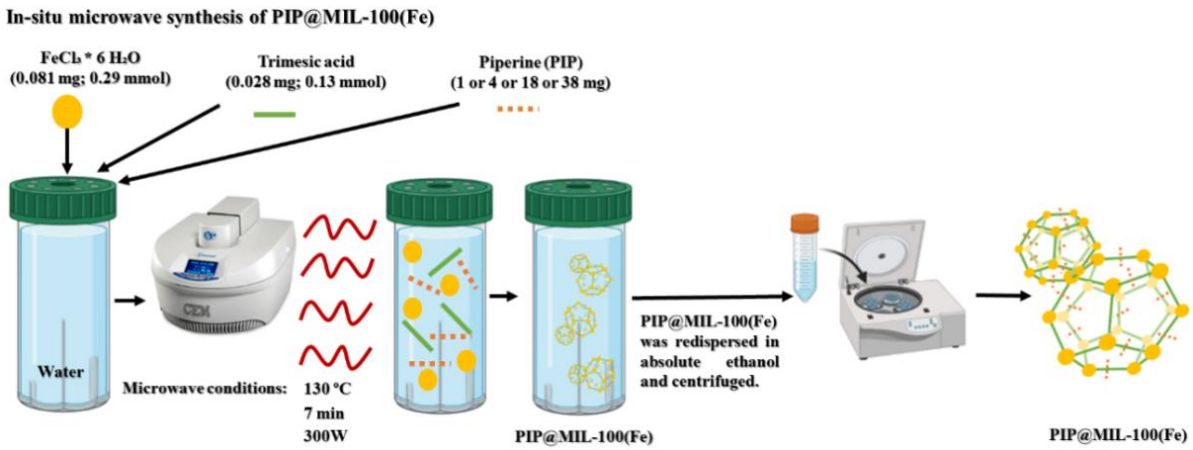

Figure 1. *In-situ* microwave synthesis of PIP@MIL-100(Fe) consisted in dissolving iron (III) chloride hexahydrate (0.081 mg; 0.29 mmol), BTC (0.028 mg; 0.13 mmol) and different concentrations of PIP (1; 4; 18; 38 mg) in distilled water (1 mL). The reaction was heated to 130 ºC for 30 s and kept at this temperature for 7 min (300 W). PIP@MIL-100(Fe) was then redispersed in absolute ethanol (1 mL) and centrifuged at 5600 g for 8 min, and 4 cycles were performed under the same conditions. An orange solid was thus recovered (40 mg, 96%).

To determine the entrapment efficiency of the drug (EE), the previously extracted supernatant was quantified in triplicate by high-performance liquid chromatography (HPLC) analysis. The EE was calculated from the mass balances using **equation 1** [36], as follows:

$$Entrapment\ efficiency\ (\%) = \frac{m_0 - m_f}{m_0}\ x\ 100$$

Equation 1.

where m_f is final mass (mg) of PIP present in the final supernatant and m_0 is the initial mass (mg) of PIP in the solution.

2.4. In vitro PIP release kinetics

PIP release experiments were carried out at 37 °C under two-dimensional agitation (stirring frequency = 150 rpm), using phosphate-buffered saline (PBS, pH=5 or pH=7.4) with Tween 20 (5% v/v) and ethanol (5% v/v) [37]. Initially, 10 mg of PIP@MIL-100(Fe) was dissolved in 5 mL of the receptor medium. After selected time intervals (1 – 180 h), the samples were centrifuged and 1 mL aliquot of the supernatants was removed to determine the PIP concentration. Subsequently, 1 mL of receptor medium was added to the replacement medium.

The extracted aliquots were subjected to HPLC analysis to determine the amount of PIP released. An add-in program (DDSolver) in Microsoft Excel was used to evaluate the drug release kinetics of the acquired dissolution curves by fitting the data to various equations [38].

2.5. HPLC assay for PIP

The experiments were carried out in high-efficiency liquid chromatography (HPLC) (Perkin Elmer, Brazil), equipped with a diode array detector (DAD), detection at 340 nm, with an LC-20A pump. Separation was performed on a C18 column (Zorbax Extend 150 x 4.6 mm; 5 µm). The mobile phase consisted of methanol and deionized water (75:25 v/v), with a mobile phase flow of 0.8 mL min^{-1} and an injection volume of 10 µL, and the run time was 5 min for each sample [39].

2.6. Powder X-ray diffraction (XRD)

The diffractograms were obtained using a Rigaku Rint 2000 diffractometer, at room temperature, under Cu-Kα radiation (λ = 1.5406 Å), with a power of 40 kV and an electrical current of 50 mA. The spectra of the samples were obtained with 2θ open-angle X-ray scanning between 2º and 30º and using 2.5 s per step in continuous mode and step size of 0.02º [40]. The patterns were then normalized with respect to the most intense peak (plane (022)) in the pattern [0-1].

2.7. Thermogravimetric analysis (TGA)

TGA was performed using TGA-Q500 (TA instruments). Approximately 5 mg of each sample was placed on a platinum pan (maximum volume 50 µL) and heated from 30 to 600 °C at a heating rate of 10 °C min^{-1}. The measurements for PIP@MIL-100(Fe) were performed under a dry nitrogen flow of 40 mL min^{-1} to guarantee complete decomposition of the PIP and accurate PIP loading determination.

The PIP loading was calculated from the TGA plot analysis according to the **equation 2** [41]:

$$wt\% = \frac{m_{loss(PIP@MIL-100(Fe))} - m_{loss(MIL-100(Fe))}}{m_{loss(PIP@MIL-100(Fe))}} * 100$$

$$\frac{g}{g} = \frac{m_{loss(PIP@MIL-100(Fe))} - m_{loss(MIL-100(Fe))}}{m_{loss(MIL-100(Fe))}}$$

Equation 2.

2.8. Dynamic Light Scattering, Particle Size, and Zeta Potential

The polydispersity index (PdI) and particle size (hydrodynamic diameter) were measured using dynamic light scattering technique, zeta potential was carried out through electrophoretic mobility method using Zetasizer software (Malvern Instruments 7.1). Samples were prepared by dispersing at 50 µg mL^{-1} by the use of an ultrasound tip (30% amplitude for 2 min; Digital Sonifer 450, Branson). All analyses were performed three times at room temperature and a detection angle of 173º was used during particle size and PdI analysis.

2.9. Field emission gun-scanning electron microscopy (FEG-SEM)

FEG-SEM micrographs were obtained from a JEOL JSM-7000F microscope with acceleration voltage of 2 kV. The samples 3 µL were added to the stubs containing a carbon thin film and then covered with sputtered gold layer.

2.10. High resolution-transmission electron microscopy (HR-TEM)

The nanosystems were diluted and then 3 µL were added to the copper grids. The sample excess was drained with a paper and then stained with aqueous uranyl acetate (2% w/v). The grids were kept with aqueous uranyl acetate for 3 min. After that, uranyl acetate excess was drained with paper and dried at room temperature. The grids were subjected to analysis on a JEOL JEM-2100 (LaB_6 emission gun) with acceleration voltage of 100 kV, available at LME IQSC-USP, São Carlos (Brazil).

2.11. Nitrogen Adsorption Porosimetry

The activated nanoparticles (≈ 40 mg) were then recovered by centrifugation at 2500 g for 10 min and dried at room temperature. N_2 adsorption measurements were obtained at 77 ºk using nitrogen sorption–desorption experiments and nano MOFs were outgassed at 100 °C for 6 hours (ASAP 2020- Micrometrics) [42]. Pore volume and pore size were calculated by a non-local density functional theory (NLDFT).

2.12. Cell Viability Assay

Cells were seeded in $4x10^3$ cells/well in 96-well plates with overnight incubation in DMEM supplemented medium. Then, the treatments were prepared at a 3-fold higher concentration (due to a direct 1/3 direct dilution in the well, as 50 µL of MOFs solutions were added to a final volume of 200 µL per well), and exposed to certain concentrations of MIL-100 (Fe) (3000-300 µg mL^{-1}), PIP, and PIP@MIL-100 (Fe) (250- 25 µM) for 48 h of incubation. Then, the nanosystems were removed and the plates were washed with PBS. Finally, 20 µL of resazurin (0,1 mg mL^{-1}) was added to each well, followed by incubation for 4 h. Fluorescence was read on a SpectraMax microplate reader (570 nmex/595 nmem). The concentration needed to kill 50% of MCF-7 and 4T1 cells (IC_{50}) was calculated by nonlinear regression in GraphPad Prism version 7.0 (GraphPad Software, San Diego, CA, USA).

2.13. Statistical analyzes

All experiments were performed in triplicate (n=3). Results were expressed as mean ± standard deviation. For data comparison, ANOVA with post-test was used, or t-student in all cases, significance will be considered when $p<0.05$. In addition, all these analyzes were performed using the GraphPad Prism® statistical software version 7.0.

For other analyses, their respective statistical tests will be carried out, such as:

- To determine the modal diameter of the nanostructures, the distribution of their diameters was obtained using the best fit for polydispersity according to a log-normal.
- The inhibitory concentration (IC_{50}) values and their 95% confidence intervals were derived from a linear regression model, based on a dose-response curve.

3. RESULTS AND DISCUSSION

3.1. Characterization of MOFs

The MIL-100 (Fe) and PIP@MIL-100 (Fe) powder samples were analyzed by X-ray diffraction (XRD) patterns as shown in **Fig. 2.** The results confirm the successful synthesis of crystalline MOFs through *in situ* microwave synthesis (**Fig. 2.**). The diffraction peaks of the synthesized and simulated MIL-100 (Fe) (obtained from the CIF file No. 640536), indicated a consistent pattern of diffraction intensity at $2\theta = 3.34^{o}$; 3.94^{o}; 4.72^{o}; 6.2^{o}; 10.26^{o}; and 10.9^{o} [42-45]. However, the peak intensities of the PIP@MIL-100(Fe) (**Fig. 2**, green line) decreased suggesting the partial loss of crystallinity resulting from the filling of the pores with PIP.

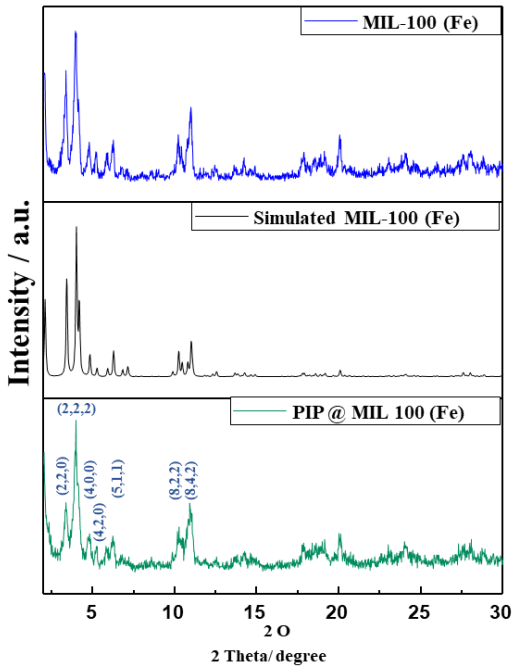

Figure 2. XRD of the simulated (Black line) and synthesized pattern of MIL-100(Fe) (Blue line) and PIP@MIL-100(FE) (Green line), angle (2 θ) 2-30º.

The crystalline structure of MIL-100 (Fe) is cubic and the size of the crystallite can be calculated from the Debye-Scherrer according to the **equation 4** [46]:

$$D = \frac{0.94\,\lambda}{\beta\,cos\theta}$$

Equation 4. Debye-Scherrer

where θ is the angle between the incident ray and the dispersion, λ is the incident X-ray irradiation wavelength, D is the size of the crystallite (nm), and β is the total width at half the maximum. The average crystallite size of MIL-100 (Fe) and PIP@MIL-100(Fe) was calculated to be between 18.3 and 76.2 nm, respectively.

Fig. 3 exhibited zeta potential and particle size of MIL-100 (Fe) and PIP@MIL-100 (Fe). With respect to MIL-100(Fe), the positive zeta potential is similar to what was previously reported. [13, 47] MIL-100 (Fe) and PIP@MIL-100 (Fe) did not show significant changes in their shape and size with hydrodynamic diameter of 128 ± 44.6 nm (PdI = 0.10 ± 0.11) and 98 ± 27.83 nm (PdI = 0.03 ± 0.006) for MIL-100 (Fe) and PIP@MIL-100 (Fe), respectively. The outer surface of MIL-100 (Fe) may contain organic ligands composed of free pendant protonated carboxylate groups showing a positive zeta potential of + 30.7 ± 0.5 mV. However, when the MOF was impregnated with PIP (sample PIP@MIL-100 (Fe)), the material showed a decrease in ζ potential to + 7.69 ± 0.6 mV, probably due to a fraction of

PIP being located close to the MOF outer surface, affecting and reducing its positive surface charge value.

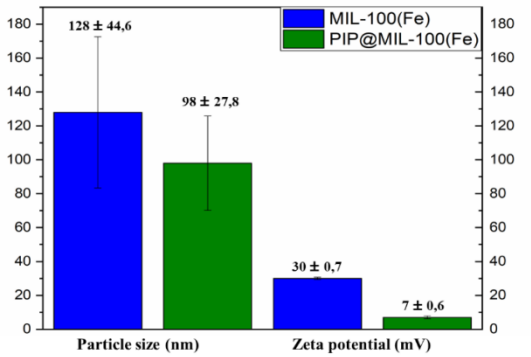

Figure 3. DLS size and Zeta potential of aqueous suspension of MIL-100 (Fe) and PIP@MIL-100 (Fe) (blue and green columns, respectively).

The morphology and particle size of the MIL-100(Fe) and PIP@MIL-100 (Fe) were examined using FEG-SEM and HR-TEM analysis. **Fig. 4** revealed the predominance of crystalline particles with irregular octahedral morphology of the MOF at nanoscale, with an average size of 29.67 ± 22.88 nm and 46.27 ± 32.80 nm for MIL-100 (Fe) and PIP@MIL-100 (Fe), respectively. These results are in agreement with previous study reported by Tamames-Tabar et al. (2014) [19]. The histograms of particle size distribution values (n = 100 particles) obtained from FEG-SEM images of

images.

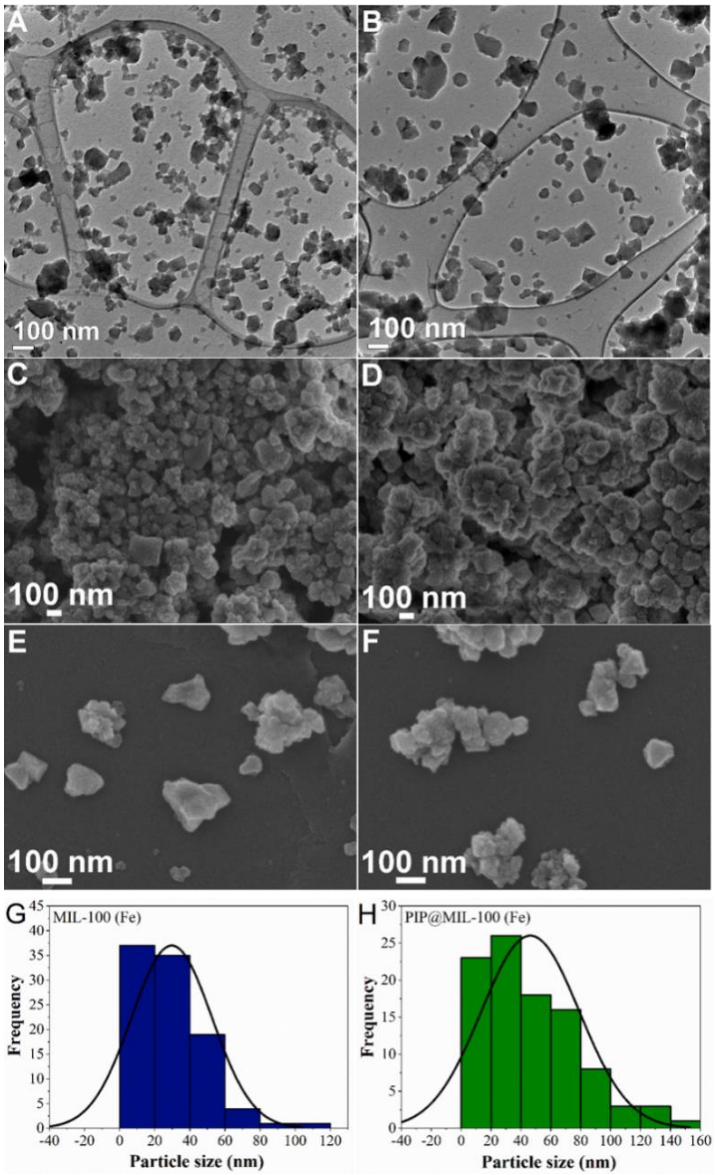

Figure 4. HR-TEM of (A) MIL-100 (Fe) and (B) PIP@MIL-100 (Fe); FE-SEM of (C and E) MIL-100 (Fe) and (D and F) PIP@MIL-100 (Fe) and the histograms of particle size distribution (n = 100 particles) of (G) MIL-100 (Fe) and (H) PIP@MIL-100 (Fe) obtained from FEG-SEM images (C and D, respectively).

3.2. PIP-loaded MIL-100(Fe)

Two drug-loading strategies were presented here. First, the *ex-situ* method was carried out by impregnation in a saturated ethanolic solution of PIP for 24, 48, and 72 h (**Table S1**). This method exhibited an encapsulation efficiency of up to 15%, probably because MOFs need a high pore volume to achieve large amounts of trapped PIP [17]. For this reason, we focused on the *in situ* encapsulation of PIP in MIL-100 (Fe) synthesis.

The *in situ* PIP encapsulation in MIL-100(Fe) was evaluated using distinct values of PIP concentration (**Table S2**). The yield of PIP-loaded MIL-100 (Fe) was analyzed using HPLC method. A high nanosystem yield of 96% was achieved at the PIP concentration of 1 mg. The higher PIP concentration, lower the nanosystems yield, which suggests that by increasing PIP concentration the ability of trimesic acid to coordinate with the metal may be reduced [21], in agreement with results in **Table S2**.

Furthermore, **Fig. 5a** displayed differences in the N_2 adsorption isotherms profiles of PIP@MIL-100 (Fe) in comparison with the MIL-100 (Fe). *In situ* PIP-loaded MIL-100 (Fe) exhibited a higher surface area than MIL-100 (Fe) (**Fig. 5**). It is suggested that for the formation of the composite PIP@MIL-100(Fe), there is a non-covalent interaction of the π-π stacking type, between the hydrophobic parts of ligands (aromatic rings of 1,3,5-benzene tricarboxylic) and the π electronic clouds of PIP. Besides, the pore size distribution was also different for both MIL-100 (Fe) and PIP @ MIL-100 (Fe). (**Fig. 5b**). This feature is similar to that reported by Singco, Liu et al. (2016) during the *in situ* encapsulation of this same MOF with acetylsalicylic acid, whose results also pointed to a higher surface area (2358 $m^2 g^{-1}$) for the material encapsulated with the drug than that obtained for MIL-100(Fe) (1774 $m^2 g^{-1}$). Also, it revealed that the incorporation of PIP did not affect the porosity of the MOF matrix [48].

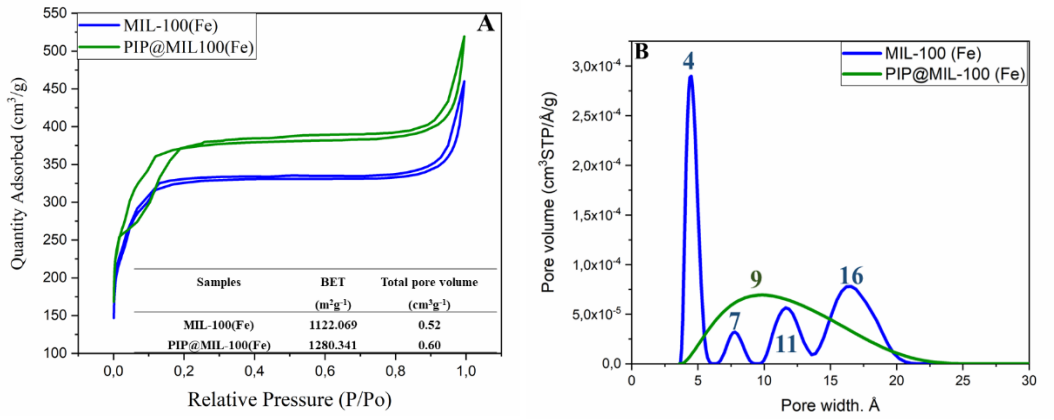

Figure 5. (a) Adsorption-desorption N_2 curves and (b) pore size distribution by non-local density functional theory (NLDFT) of MIL-100(Fe) and PIP@MIL-100(Fe) (blue and green lines, respectively).

The PIP EE (%) determined by HPLC analysis was 95 ± 3%, which suggests a strong interaction between PIP and trimesic acid during the encapsulation process. The main advantage of this method does not rely on the pore size of the nanosystem besides better drug loading than the impregnation method [49]. This result showed an efficiency of drug

encapsulation in MIL-100 (Fe) greater than 75% compared to other studies, for example: urea, benzophenone 4, Cidofovir, ibuprofen, benzophenone 3[18], docetaxel[8], and doxorubicin (DOX) [18], resulted in 2.1%, 22.8%, 46.2%, 11%, 74%, 10%, and 88.2 % respectively. In addition, studies carried out with other nanosystems showed less than 70% encapsulation efficiency, such as polymerics[33], multiwalled carbon nanotubes[50], and nanoparticles [51], which resulted in 36.23 %, 62.8 %, and 70 %.

Table S3 and **Fig. 6** showed TGA results of PIP, MIL-100(Fe), and PIP@MIL-100(Fe) (dashed, blue and green lines, respectively). An increase in the percentage of weight loss was observed for the PIP@MIL-100(Fe) (m_{loss} = 22.58 %) in comparison with MIL-100(Fe) (m_{loss} = 20.09 %). This difference corresponds to the encapsulated PIP into the nanosystem. In addition, the PIP loading capacity was determined to be 11% by weight (0.12 g g^{-1} MOF), according to TGA data.

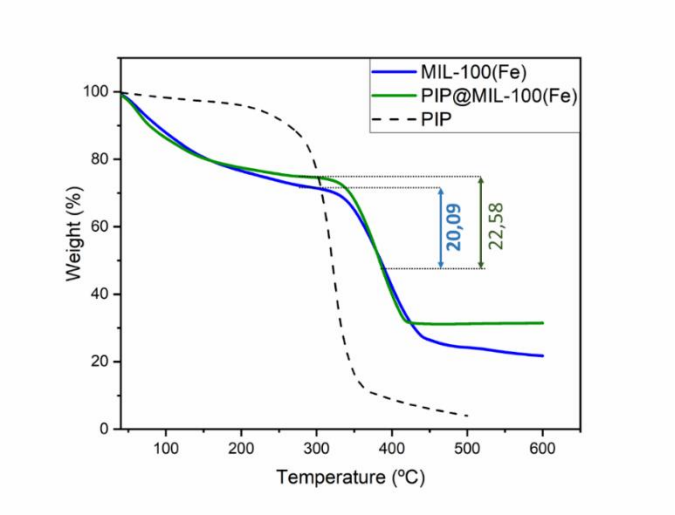

Figure 6. Thermogravimetric curves of MIL-100(Fe) (blue line); PIP@MIL-100(Fe) (green line) and PIP (blue, green and black dashed lines, respectively).

3.3. Release study

The PIP release profile was studied in PBS, at pH 5.0 and pH 7.4 to simulate physiological conditions, such as blood circulation or acidic microenvironments in tumor sites, respectively. The pH 5.0 was chosen because most of the nanostructures are internalized through endocytosis in cancer cells and are trapped within the endosomal and lysosomal compartments, these are usually in the range of 4.5 to 5.5. [52]. Therefore, pH-sensitive delivery systems are valuable for controlling drug delivery in breast cancer. Tween 20 (5% v/v) and ethanol (5%v/v), at 37 ºC [42], were also used. [53].

The PIP release from PIP@MIL-100(Fe) was more controlled in the PBS solution at both pH values. Approximately 51% of PIP was released within 300 min (**Fig. 7**), indicating that a certain amount of PIP was easily released due to the simple diffusion method of loosely bound PIP and the dissolution of the PIP molecules in an aqueous solution.

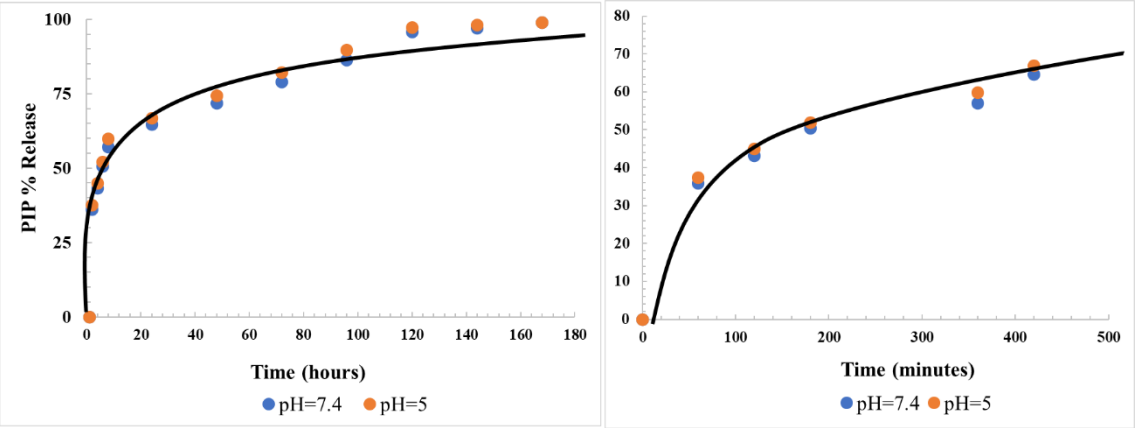

Figure 7. PIP release profiles of PIP@MIL-100(Fe) at pH = 5 (orange trace fit) and at pH = 7.4 (blue trace fit), revealing the cumulative release within 180 h.

On the other hand, the rest of the PIP (99%) was released after 7 days, which demonstrates that part of the PIP molecules performs a remarkable interaction with the MOFs structure (Fe^{+3} and BTC) [54]. Furthermore, previous studies have shown that MIL-100(Fe) is degraded in the presence of PBS, losing their constituent trimesate linkers, transforming into inorganic buildings, and becoming amorphous. PIP release data were fitted using the Korsmeyer-Peppas Model, zero-order model, and first-order model, which are summarized in **Table 1**. The values of the correlation coefficient R^2 for the Korsmeyer-Peppas model were higher than those for the zero-order model and the first-order. Therefore, it is evident that PIP was released from MIL-100 (Fe) by a non-swelling porous matrix drug delivery system. The kinetic constants determined from the Korsmeyer-Peppas model were 32.85 and 34.56 for pH 7.4 and 5, respectively.

Table 1. Fitting results of equation

	Model	Equation	R^2
pH 5	Zero-order equation	M=0.4658t + 46.472	0.649
	First-order equation	M=-0.0132t + 1.7816	0.969
	Korsmeyer-Peppas Model	$M= 34.56*t^{0.2}$	**0.981**
pH 7.4	Zero-order equation	M=0.4742t + 44.436	0.680
	First-order equation	M=-0.0129t + 1.8107	0.954
	Korsmeyer-Peppas Model	$M= 32.85*t^{0.2}$	**0.981**

M, t represents the % cumulative release and release time (h), respectively

3.4. Cell Viability Assay

The cellular toxicities of PIP, MIL-100 (Fe), and PIP@MIL-100 (Fe) were investigated on the MCF-7 and 4T1 cell lines at concentrations from 50 to 250 µM. Untreated cells served as a control. As shown in **Fig. 8**, MIL-100 (Fe) did not cause any cytotoxic effect on cells; however, at 250 µM, it revealed cell viability of 89% for both cells, which proved to be an appropriate nanocarrier at the concentrations examined to administer anti-drugs for breast cancer, as previously reported [8, 55]. The IC_{50} of PIP@MIL-100 (Fe) and PIP was measured by GraphPad software at 48 h. The PIP showed IC_{50} = 183.1 ± 19.2 µM, and PIP@MIL-100 (Fe) exhibited IC_{50} = 69.49 ± 14.63 µM to MCF-7 and The PIP showed IC_{50} = 130.1 ± 11.2 µM, and PIP@MIL-100 (Fe) exhibited IC_{50} = 96.43 ± 12.63 µM to 4T1. Statistical analysis Student's t-test compared to IC_{50} confirmed that PIP@MIL-100 (Fe) had more significant toxic impact ($p < 0.05$) on both tumor cells than PIP. In addition, the release of PIP from MOFs exhibits a Fickian diffusion in the first 48 hours at both pH 5 and 7.4, this controlled release probably contributes to toxicity against cancer cells. [56] In addition, This cytotoxic effect can be caused by the acidic pH of lysosomal enzymes, which affects the cytoplasm by releasing PIP into the cytoplasm, ultimately resulting in cell death. [57] Compared to other nanosystems against MCF-7 cancer cells, the polymeric nanoparticle showed an IC_{50} greater than 100 uM, [33] concluding that MOFs are much more cytotoxic and promising for applications with other types of breast cancer.

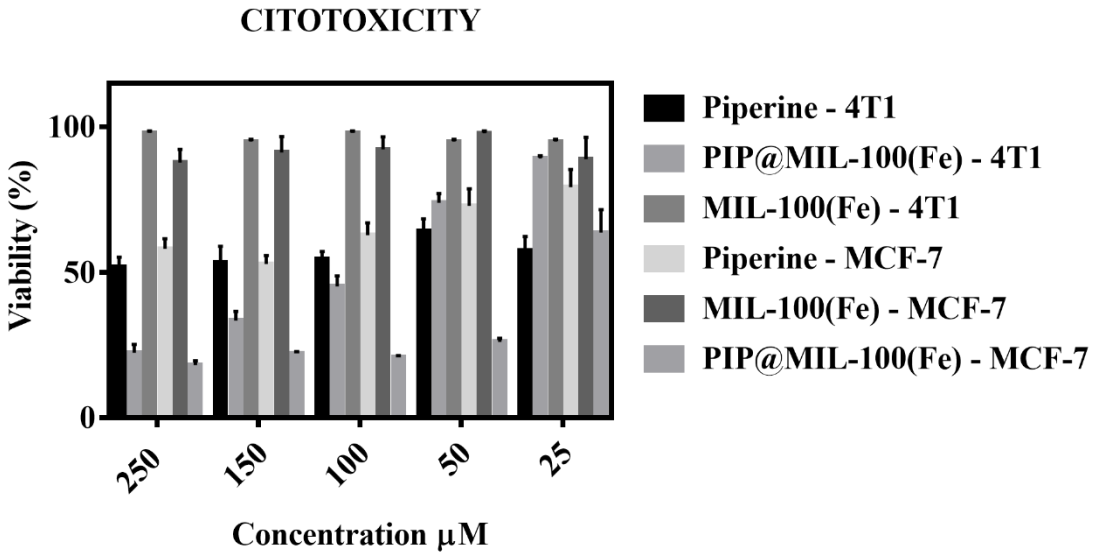

Figure 8. Cell viability of MCF-7 and 4T1 for 48 h. Piperine (250−25 µM); MIL-100 (Fe) concentration was 3000−300 µg/mL; and PIP@MIL-100(Fe) loading was 2.5 wt% (3000−300 µg/mL).

4. CONCLUSION

PIP drawbacks such as low stability and bioavailability in biological media can be overcome using *in situ* PIP-loaded MIL-100 (Fe) synthesis via microwave method, The nanosystem was successfully prepared and characterized by physicochemical techniques. High values of PIP encapsulation efficiency and loading capacity of 95 and 11% were achieved, respectively. In comparison with the traditional method of encapsulation *ex-situ* in the MOF that showed an EE of less than 15%. The slow diffusion of PIP from MIL-100 (Fe) would improve the therapeutic activity in the transport of large amounts of drugs in the blood. Furthermore, our results demonstrated high cytotoxicity of PIP@MIL-100 (Fe) against MCF-7 cancer cells compared with PIP, which suggests that this nanosystem improved the PIP anticancer activity *in vitro*. Relying upon these premises, *in situ* PIP-loaded MIL-100 (Fe) is an effective strategy to avoid low drug loading by using the impregnation method besides establishing a novel method for designing efficient drug delivery nanosystems for *in vivo* evaluation and further clinical assays.

5. CONFLICTS OF INTEREST

There are no conflicts to declare.

6. ACKNOWLEDGMENTS

The authors acknowledge FAPESP (process 2018/21119-0) for the financial support given for the development of this work.

7. REFERENCE BIBLIOGRAPHIC

1. Quijia, C. R.; Lima, C.; Silva, C.; Alves, R. C.; Frem, R.; Chorilli, M. J. J. o. D. D. S.; Technology, Application of MIL-100 (Fe) in drug delivery and biomedicine. **2020**, 102217.
2. Sun, Y.; Zheng, L.; Yang, Y.; Qian, X.; Fu, T.; Li, X.; Yang, Z.; Yan, H.; Cui, C.; Tan, W. J. N.-M. L., Metal–organic framework nanocarriers for drug delivery in biomedical applications. **2020,** 12, (1), 1-29.
3. Stock, N.; Biswas, S. J. C. r., Synthesis of metal-organic frameworks (MOFs): routes to various MOF topologies, morphologies, and composites. **2012,** 112, (2), 933-969.
4. Férey, G.; Mellot-Draznieks, C.; Serre, C.; Millange, F.; Dutour, J.; Surblé, S.; Margiolaki, I. J. S., A chromium terephthalate-based solid with unusually large pore volumes and surface area. **2005,** 309, (5743), 2040-2042.
5. Horcajada, P.; Surblé, S.; Serre, C.; Hong, D.-Y.; Seo, Y.-K.; Chang, J.-S.; Grenèche, J.-M.; Margiolaki, I.; Férey, G. J. C. C., Synthesis and catalytic properties of MIL-100 (Fe), an iron (III) carboxylate with large pores. *Chemical Communications* **2007**, (27), 2820-2822.
6. Matsuyama, K.; Hayashi, N.; Yokomizo, M.; Kato, T.; Ohara, K.; Okuyama, T., Supercritical carbon dioxide-assisted drug loading and release from biocompatible porous metal-organic frameworks. *Journal of Materials Chemistry B* **2014,** 2, (43), 7551-7558.
7. Grall, R.; Hidalgo, T.; Delic, J.; Garcia-Marquez, A.; Chevillard, S.; Horcajada, P., In vitro biocompatibility of mesoporous metal (III; Fe, Al, Cr) trimesate MOF nanocarriers. *Journal of Materials Chemistry B* **2015,** 3, (42), 8279-8292.
8. Rezaei, M.; Abbasi, A.; Varshochian, R.; Dinarvand, R.; Jeddi-Tehrani, M., NanoMIL-100(Fe) containing docetaxel for breast cancer therapy. *Artificial Cells Nanomedicine and Biotechnology* **2018,** 46, (7), 1390-1401.
9. Simon-Yarza, T.; Baati, T.; Neffati, F.; Njim, L.; Couvreur, P.; Serre, C.; Gref, R.; Najjar, M. F.; Zakhama, A.; Horcajada, P. J. I. j. o. p., In vivo behavior of MIL-100 nanoparticles at early times after intravenous administration. *International journal of pharmaceutics* **2016,** 511, (2), 1042-1047.
10. Han, Y.; Yang, H.; Guo, X., Synthesis Methods and Crystallization of MOFs. In *Synthesis methods and Crystallization*, IntechOpen: 2020.
11. Agostoni, V.; Anand, R.; Monti, S.; Hall, S.; Maurin, G.; Horcajada, P.; Serre, C.; Bouchemal, K.; Gref, R., Impact of phosphorylation on the encapsulation of nucleoside analogues within porous iron(III) metal-organic framework MIL-100(Fe) nanoparticles. *Journal of Materials Chemistry B* **2013,** 1, (34), 4231-4242.
12. di Nunzio, M. R.; Agostoni, V.; Cohen, B.; Gref, R.; Douhal, A., A "Ship in a Bottle" Strategy To Load a Hydrophilic Anticancer Drug in Porous Metal Organic Framework Nanoparticles: Efficient Encapsulation, Matrix Stabilization, and Photodelivery. *Journal of Medicinal Chemistry* **2014,** 57, (2), 411-420.
13. Bellido, E.; Guillevic, M.; Hidalgo, T.; Santander-Ortega, M. J.; Serre, C.; Horcajada, P. J. L., Understanding the colloidal stability of the mesoporous MIL-100 (Fe) nanoparticles in physiological media. *Langmuir* **2014,** 30, (20), 5911-5920.

14. Bellido, E.; Hidalgo, T.; Lozano, M. V.; Guillevic, M.; Simon-Vazquez, R.; Santander-Ortega, M. J.; Gonzalez-Fernandez, A.; Serre, C.; Alonso, M. J.; Horcajada, P., Heparin-Engineered Mesoporous Iron Metal-Organic Framework Nanoparticles: Toward Stealth Drug Nanocarriers. *Advanced Healthcare Materials* **2015,** 4, (8), 1246-1257.
15. Rodriguez-Ruiz, V.; Maksimenko, A.; Anand, R.; Monti, S.; Agostoni, V.; Couvreur, P.; Lampropoulou, M.; Yannakopoulou, K.; Gref, R., Efficient "green" encapsulation of a highly hydrophilic anticancer drug in metal-organic framework nanoparticles. *Journal of Drug Targeting* **2015,** 23, (7-8), 759-767.
16. Hidalgo, T.; Alonso-Nocelo, M.; Bouzo, B.; Reimondez-Troitiño, S.; Abuin-Redondo, C.; De La Fuente, M.; Horcajada, P. J. N., Biocompatible iron (iii) carboxylate metal–organic frameworks as promising RNA nanocarriers. *Nanoscale* **2020,** 12, (8), 4839-4845.
17. Horcajada, P.; Serre, C.; Maurin, G.; Ramsahye, N. A.; Balas, F.; Vallet-Regi, M.; Sebban, M.; Taulelle, F.; Férey, G. J. J. o. t. A. C. S., Flexible porous metal-organic frameworks for a controlled drug delivery. **2008,** 130, (21), 6774-6780.
18. Horcajada, P.; Chalati, T.; Serre, C.; Gillet, B.; Sebrie, C.; Baati, T.; Eubank, J. F.; Heurtaux, D.; Clayette, P.; Kreuz, C. J. N. m., Porous metal–organic-framework nanoscale carriers as a potential platform for drug delivery and imaging. *Nature materials* **2010,** 9, (2), 172.
19. Tamames-Tabar, C.; Cunha, D.; Imbuluzqueta, E.; Ragon, F.; Serre, C.; Blanco-Prieto, M. J.; Horcajada, P. J. J. o. M. C. B., Cytotoxicity of nanoscaled metal–organic frameworks. *Journal of Materials Chemistry B* **2014,** 2, (3), 262-271.
20. Ke, X.; Qin, N.; Zhang, T.; Ke, F.; Yan, X. J. J. o. I.; Polymers, O.; Materials, Highly Augmented Antioxidant and Anticancer Effect of Biocompatible MIL-100 (Fe)@ SiO 2-Immobilized Green Tea Catechin. *Journal of Inorganic and Organometallic Polymers and Materials* **2020,** 30, (3), 935-942.
21. Singco, B.; Liu, L. H.; Chen, Y. T.; Shih, Y. H.; Huang, H. Y.; Lin, C. H., Approaches to drug delivery: Confinement of aspirin in MIL-100(Fe) and aspirin in the de novo synthesis of metal-organic frameworks. *Microporous and Mesoporous Materials* **2016,** 223, 254-260.
22. Valekar, A. H.; Batule, B. S.; Kim, M. I.; Cho, K. H.; Hong, D. Y.; Lee, U. H.; Chang, J. S.; Park, H. G.; Hwang, Y. K., Novel amine-functionalized iron trimesates with enhanced peroxidase-like activity and their applications for the fluorescent assay of choline and acetylcholine. *Biosensors & Bioelectronics* **2018,** 100, 161-168.
23. Zhang, H.; Li, Q.; Liu, R.; Zhang, X.; Li, Z.; Luan, Y. J. A. F. M., A Versatile prodrug strategy to in situ encapsulate drugs in MOF nanocarriers: a case of cytarabine-IR820 prodrug encapsulated ZIF-8 toward chemo-photothermal therapy. **2018,** 28, (35), 1802830.
24. INCA Ministério da Saúde. Instituto Nacional de Câncer. http://www2.inca.gov.br/wps/wcm/connect/acessoainformacao/site/home/
25. Barrios, C.; Freitas-Junior, R.; Martins, S.; Bines, J.; Estevez-Diz, M. D. P.; Caleffi, M. J. J. G. O., Challenge of Incorporating New Drugs for Breast Cancer in Brazil: A Proposed Framework for Improving Access to Innovative Therapies. **2021,** 7, 474-485.
26. Newman, D. J.; Cragg, G. M.; Snader, K. M., Natural products as sources of new drugs over the period 1981-2002. *Journal of natural products* **2003,** 66, (7), 1022-37.
27. Cragg, G. M.; Newman, D. J., Plants as a source of anti-cancer agents. *Journal of ethnopharmacology* **2005,** 100, (1-2), 72-9.

28. Quijia, C. R.; Chorilli, M. J. C. R. i. A. C., Characteristics, biological properties and analytical methods of piperine: A review. **2020,** 50, (1), 62-77.
29. Quijia, C. R.; Chorilli, M. J. P. R., Piperine for treating breast cancer: A review of molecular mechanisms, combination with anticancer drugs, and nanosystems. **2021**.
30. Tang, X.; Loc, W. S.; Dong, C.; Matters, G. L.; Butler, P. J.; Kester, M.; Meyers, C.; Jiang, Y.; Adair, J. H. J. N., The use of nanoparticulates to treat breast cancer. **2017,** 12, (19), 2367-2388.
31. Burande, A. S.; Viswanadh, M. K.; Jha, A.; Mehata, A. K.; Shaik, A.; Agrawal, N.; Poddar, S.; Mahto, S. K.; Muthu, M. S. J. A. P., Correction to: EGFR Targeted Paclitaxel and Piperine Co-loaded Liposomes for the Treatment of Triple Negative Breast Cancer. **2020,** 21, (6), 207.
32. Katiyar, S. S.; Muntimadugu, E.; Rafeeqi, T. A.; Domb, A. J.; Khan, W. J. D. d., Co-delivery of rapamycin-and piperine-loaded polymeric nanoparticles for breast cancer treatment. **2016,** 23, (7), 2608-2616.
33. Pachauri, M.; Gupta, E. D.; Ghosh, P. C. J. J. o. d. d. s.; technology, Piperine loaded PEG-PLGA nanoparticles: preparation, characterization and targeted delivery for adjuvant breast cancer chemotherapy. **2015,** 29, 269-282.
34. Rad, J. G.; Hoskin, D. W., Delivery of Apoptosis-inducing Piperine to Triple-negative Breast Cancer Cells via Co-polymeric Nanoparticles. *Anticancer Research* **2020,** 40, (2), 689-694.
35. García Márquez, A.; Demessence, A.; Platero-Prats, A. E.; Heurtaux, D.; Horcajada, P.; Serre, C.; Chang, J. S.; Férey, G.; de la Peña-O'Shea, V. A.; Boissière, C. J. E. J. o. I. C., Green Microwave Synthesis of MIL-100 (Al, Cr, Fe) Nanoparticles for Thin-Film Elaboration. *European Journal of Inorganic Chemistry* **2012,** 2012, (32), 5165-5174.
36. Bhattacharjee, A.; Gumma, S.; Purkait, M. K., Fe3O4 promoted metal organic framework MIL-100(Fe) for the controlled release of doxorubicin hydrochloride. *Microporous and Mesoporous Materials* **2018,** 259, 203-210.
37. Makhov, P.; Golovine, K.; Canter, D.; Kutikov, A.; Simhan, J.; Corlew, M. M.; Uzzo, R. G.; Kolenko, V. M. J. T. p., Co-administration of piperine and docetaxel results in improved anti-tumor efficacy via inhibition of CYP3A4 activity. **2012,** 72, (6), 661-667.
38. Zhang, Y.; Huo, M.; Zhou, J.; Zou, A.; Li, W.; Yao, C.; Xie, S. J. T. A. j., DDSolver: an add-in program for modeling and comparison of drug dissolution profiles. **2010,** 12, (3), 263-271.
39. Reyes Solís, L. M.; Sánchez, R. A.; Restrepo, J. J. R. d. C., Encapsulation of the Piperine Present in Piper tuberculatum Species Using Multilamellar Vesicles and Determination of its Antioxidant Power. **2017,** 21, (2), 11-28.
40. Marcos-Almaraz, M. T.; Gref, R.; Agostoni, V.; Kreuz, C.; Clayette, P.; Serre, C.; Couvreur, P.; Horcajada, P., Towards improved HIV-microbicide activity through the co-encapsulation of NRTI drugs in biocompatible metal organic framework nanocarriers. *Journal of Materials Chemistry B* **2017,** 5, (43), 8563-8569.
41. Souza, B. E.; Tan, J.-C. J. C., Mechanochemical approaches towards the in situ confinement of 5-FU anti-cancer drug within MIL-100 (Fe) metal–organic framework. *CrystEngComm* **2020,** 22, (27), 4526-4530.
42. Cunha, D.; Ben Yahia, M.; Hall, S.; Miller, S. R.; Chevreau, H.; Elkaïm, E.; Maurin, G.; Horcajada, P.; Serre, C. J. C. o. M., Rationale of drug encapsulation and release from biocompatible porous metal–organic frameworks. *Chemistry of materials* **2013,** 25, (14), 2767-2776.

43. Chaturvedi, G.; Kaur, A.; Umar, A.; Khan, M. A.; Algarni, H.; Kansal, S. K. J. J. o. S. S. C., Removal of fluoroquinolone drug, levofloxacin, from aqueous phase over iron based MOFs, MIL-100 (Fe). *Journal of Solid State Chemistry* **2019**, 121029.
44. Gandara-Loe, J. s.; Ortuño-Lizarán, I.; Fernández-Sanchez, L.; Alió, J. L.; Cuenca, N. s.; Vega-Estrada, A.; Silvestre-Albero, J. J. A. a. m.; interfaces, Metal–Organic Frameworks as Drug Delivery Platforms for Ocular Therapeutics. *ACS applied materials & interfaces* **2018,** 11, (2), 1924-1931.
45. Guo, A. L.; Durymanov, M.; Permyakova, A.; Sene, S.; Serre, C.; Reineke, J., Metal Organic Framework (MOF) Particles as Potential Bacteria-Mimicking Delivery Systems for Infectious Diseases: Characterization and Cellular Internalization in Alveolar Macrophages. *Pharmaceutical Research* **2019,** 36, (4).
46. Hall, B.; Zanchet, D.; Ugarte, D. J. J. o. a. c., Estimating nanoparticle size from diffraction measurements. **2000,** 33, (6), 1335-1341.
47. Li, X.; Semiramoth, N.; Hall, S.; Tafani, V.; Josse, J.; Laurent, F.; Salzano, G.; Foulkes, D.; Brodin, P.; Majlessi, L.; Ghermani, N. E.; Maurin, G.; Couvreur, P.; Serre, C.; Bernet-Camard, M. F.; Zhang, J. W.; Gref, R., Compartmentalized Encapsulation of Two Antibiotics in Porous Nanoparticles: an Efficient Strategy to Treat Intracellular Infections. *Particle & Particle Systems Characterization* **2019,** 36, (3).
48. Huo, S.-H.; Yan, X.-P. J. J. o. M. C., Metal–organic framework MIL-100 (Fe) for the adsorption of malachite green from aqueous solution. **2012,** 22, (15), 7449-7455.
49. Horcajada, P.; Gref, R.; Baati, T.; Allan, P. K.; Maurin, G.; Couvreur, P.; Ferey, G.; Morris, R. E.; Serre, C. J. C. r., Metal–organic frameworks in biomedicine. **2012,** 112, (2), 1232-1268.
50. Raza, K.; Kumar, D.; Kiran, C.; Kumar, M.; Guru, S. K.; Kumar, P.; Arora, S.; Sharma, G.; Bhushan, S.; Katare, O. P., Conjugation of Docetaxel with Multiwalled Carbon Nanotubes and Codelivery with Piperine: Implications on Pharmacokinetic Profile and Anticancer Activity. *Molecular Pharmaceutics* **2016,** 13, (7), 2423-2432.
51. Abolhassani, H.; Safavi, M. S.; Handali, S.; Nosrati, M.; Shojaosadati, S. A., Synergistic Effect of Self-Assembled Curcumin and Piperine Co-Loaded Human Serum Albumin Nanoparticles on Suppressing Cancer Cells. *Drug Development and Industrial Pharmacy* **2020,** 46, (10), 1647-1655.
52. Wu, T.-C.; Lee, P.-Y.; Lai, C.-L.; Lai, C.-H. J. P., Synthesis of multi-functional nano-vectors for target-specific drug delivery. **2021,** 13, (3), 451.
53. Simon, M. A.; Anggraeni, E.; Soetaredjo, F. E.; Santoso, S. P.; Irawaty, W.; Thanh, T. C.; Hartono, S. B.; Yuliana, M.; Ismadji, S. J. S. r., Hydrothermal Synthesize of HF-Free MIL-100 (Fe) for Isoniazid-Drug Delivery. *Scientific reports* **2019,** 9, (1), 1-11.
54. Motakef-Kazemi, N.; Shojaosadati, S. A.; Morsali, A. J. M.; materials, m., In situ synthesis of a drug-loaded MOF at room temperature. **2014,** 186, 73-79.
55. Bi, J.; Zheng, Y.; Fang, L.; Guan, Y.; Ma, A.; Wu, J. J. J. o. I.; Polymers, O.; Materials, Nano-Sized MIL-100 (Fe) as a Carrier Material for Nitidine Chloride Reduces Toxicity and Enhances Anticancer Effects In Vitro. *Journal of Inorganic and Organometallic Polymers and Materials* **2020**, 1-8.

SUPPORTING INFORMATION

IN SITU SYNTHESIS OF PIPERINE-LOADED MIL-100 (Fe) IN MICROWAVE FOR BREAST CANCER TREATMENT

Christian Rafael Quijia [a], Marcela Tavares Luiz [b], Richard Perosa Fernandes [c], Rafael Miguel Sábio [a], Regina Frem [c] and Marlus Chorilli [a]

[a]School of Pharmaceutical Sciences, São Paulo State University (UNESP), Araraquara, São Paulo, Brazil

[b]School of Pharmaceutical Science of Ribeirão Preto, University of São Paulo (USP), Ribeirão Preto, SP, Brazil

[c]Institute of Chemistry, São Paulo State University (UNESP), Araraquara, São Paulo, Brazil

Encapsulate PIP ex situ (PIP@MIL-100 (Fe)), MIL-100 (Fe) (1 mg) was suspended in 1 ml of ethanol solution and various concentrations of PIP (1; 2; 3 mg) were evaluated. The reaction mixture was kept under stirring at room temperature for 24, 48, and 72 h. Subsequently, the nanosuspension were recovered by centrifugation at 10,000 rpm for 8 min. To determine the PIP entrapment efficiency (EE), the previously extracted supernatants were quantified in triplicate by HPLC method for determining the concentration of unencapsulated PIP.

Table S 1. PIP EE (%) detected in PIP@MIL-100 (Fe)

Concentration (w/w)		**Time**		
MIL-100(Fe)	**PIP**	**24 h**	**48 h**	**72 h**
1	1	15%	14%	0%
1	2	10%	5%	0%
1	3	4%	0%	0%

Table S2. Yields of PIP@MIL-100(Fe) as a function of the PIP concentration.

Nanosystems	**Yield (%)**
MIL-100(Fe) + PIP (1 mg)	96
MIL-100(Fe) + PIP (4 mg)	45
MIL-100(Fe) + PIP (18 mg)	5
MIL-100(Fe) + PIP (38 mg)	0

Table S3. Thermal decomposition analysis of MIL-100 (Fe) samples

	Initial decomposition temperature	**Final residue (at 600 ºC)**	**Weight loss (m_{loss})***
MIL-100(Fe)	120 ºC	48 %	20.09%
PIP@MIL-100(Fe)	120 ºC	55 %	22.58%

*The drug loading was measured in the temperature range corresponding to the decomposition of PIP (270–380 ºC).

HPLC assay for PIP

The calibration curve was linear by analyzing a series of PIP concentrations in ethanol from 6.25 to100 µg mL^{-1} with a correlation coefficient of R^2=0.990 (Figure S1). The limit of detection (LOD) and limit of quantification (LOQ) were found to be 0.25 and 0.77 µg mL^{-1}, respectively. Standard samples were prepared and injected in triplicates on three successive days.

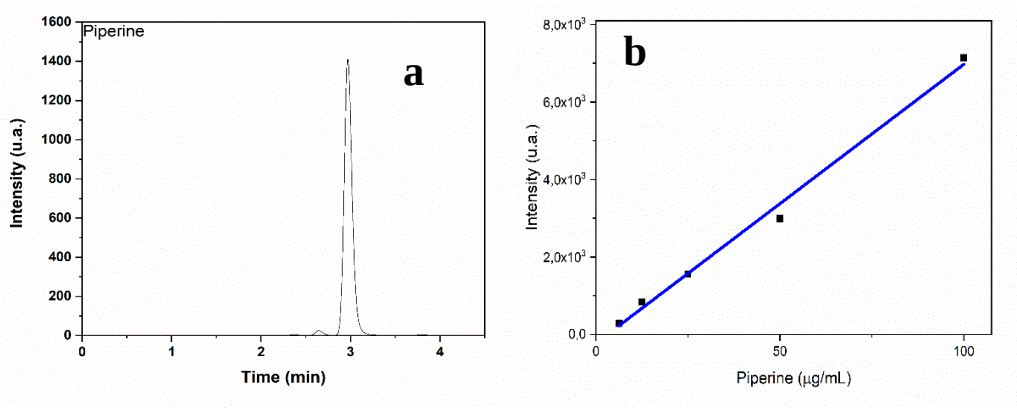

Figure S1. (a) Chromatogram of PIP (concentration = 6.25 to 100 µg mL^{-1}) in mobile phase (methanol/water (75:25)) and (b) calibration curve of PIP quantified by HPLC.

3 CAPÍTULO 3: Macrophage Cell Membrane Coating on Piperine-Loaded MIL-100(Fe) Nanoparticles for Breast Cancer Treatment

Artigo publicado em Junho 2023 no periódico Journal of Functional Biomaterials

DOI: 10.3390/jfb14060319

Macrophage Cell Membrane Coating on Piperine-Loaded MIL-100(Fe) Nanoparticles for Breast Cancer Treatment

Christian Rafael Quijia[1], Geovana Navegante[2], Rafael Miguel Sábio[1], Valeria Valente[2], Alberto Ocaña[3], Carlos Alonso-Moreno[4], Regina Célia Galvão Frem[5], and Marlus Chorilli[1*]

[1] Department of Drugs and Medicines, School of Pharmaceutical Sciences of São Paulo State University (UNESP), Rodovia Araraquara Jau, Km 01 – s/n – Campos Ville, 14800-903 Araraquara, Sao Paulo, Brazil. E-mail: christianqui@hotmail.com; rafael.m.sabio@unesp.br; marlus.chorilli@unesp.br

[2]Laboratory of Molecular and Cell Biology, School of Pharmaceutical Sciences, Department of Clinical Analysis, São Paulo State University (Unesp), Araraquara, Brazil. E-mail: geonavegante@gmail.com; valenteval@gmail.com

[3]Experimental Therapeutics Unit, Hospital Clínico San Carlos, IdISSC, Fundación Jiménez Díaz, START, 28040 Madrid, Spain. E-mail: alberto.ocana@salud.madrid.org

[4]Unidad NanoDrug, Facultad de Farmacia, Universidad de Castilla-La Mancha, 02008 Albacete, Spain. E-mail: Carlos.AMoreno@uclm.es

[5]Institute of Chemistry, São Paulo State University (UNESP), Prof. Francisco Degni 55, 14800-060 Araraquara, Sao Paulo, Brazil. E-mail: rcgfrem@gmail.com

[*]Corresponding author at Department of Drugs and Medicines, School of Pharmaceutical Sciences of São Paulo State University (UNESP), Rodovia Araraquara Jau, Km 01 – s/n – Campos Ville, 14800-903 Araraquara, Sao Paulo, Brazil. E-mail address: marlus.chorilli@unesp.br

Abstract:

Piperine (PIP), a compound found in Piper longum, has shown promise as a potential chemotherapeutic agent for breast cancer. However, its inherent toxicity has limited its application. To overcome this challenge, researchers have developed PIP@MIL-100(Fe), an organic metal-organic framework (MOF) that encapsulates PIP for breast cancer treatment. Nanotechnology offers further treatment options, including the modification of nanostructures with macrophage membranes (MM) to enhance evasion of the immune system. In this study, the researchers aimed to evaluate the potential of MM-coated MOFs encapsulated with PIP for breast cancer treatment. They successfully synthesized MM@PIP@MIL-100(Fe) through impregnation synthesis. The presence of MM coating on the MOF surface was confirmed through SDS-PAGE analysis, which revealed distinct protein bands. Transmission electron microscopy (TEM) images demonstrated the existence of a PIP@MIL-100(Fe) core with a diameter of around 50 nm, surrounded by an outer lipid bilayer layer measuring approximately 10 nm in thickness. Furthermore, the researchers evaluated the cytotoxicity indices of the nanoparticles against various breast cancer cell lines, including MCF-7, BT-549, SKBR-3, and MDA. The results demonstrated that the MOFs exhibited between 4- and

17-times higher cytotoxicity (IC_{50}) in all four cell lines compared to free PIP (IC_{50}=193.67 ± 0.30 μM). These findings suggest that MM@PIP@MIL-100(Fe) holds potential as an effective treatment for breast cancer. The study's outcomes highlight the potential of utilizing MM-coated MOFs encapsulated with PIP as an innovative approach for breast cancer therapy, offering improved cytotoxicity compared to free PIP alone. Further research and development are warranted to explore the clinical translation and optimize the efficacy and safety of this treatment strategy.

Keywords: metal-organic framework; vesicle; cytotoxicity; nanostructures.

Introduction

Nanotechnology is a rapidly developing field that brings promising opportunities to human cancer diagnosis and treatment. Nanoparticles can play a significant role as a drug delivery system for cancer treatment [1]. This system can be classified into three groups: inorganic nanomaterials (including iron oxide, gold nanoparticles, and zeolites), organic nanomaterials (such as polymeric nanoparticles, micelles, dendrimers, and liposomes), and a third type known as metal-organic frameworks or porous coordination polymers (MOFs) [2]. MOFs are porous materials composed of metal ions or clusters of higher nuclearity and multifunctional organic ligands, enabling them to overcome the limitations of other nanostructured systems, such as low drug loading and release capacity [3]. MOFs can be synthesized using various methods that allow them to control their chemical and physical properties. The assembly of inorganic subunits and organic ligands through strong covalent ion bonds creates MOFs with high and regular porosities and adaptable porosity structures that can host molecules of different shapes [4].

Piperine (PIP) is an alkaloid extracted from seeds of plants in the Piperaceae family that has been used as an antimicrobial, antiparasitic, and antidepressant agent, and as a modulator of oxidative stress-induced carcinogen [5]. Piperine has been demonstrated to inhibit the growth and survival of numerous different cancer cell types as well as to cause cell cycle arrest and apoptosis. It is especially potent against breast cancer and can target a variety of signaling pathways, oxidative stress, autophagy, and the activation of detoxifying enzymes [6, 7]. However, its use presents difficulties related to its hydrophobic nature and high concentration requirement [8, 9]. The incorporation of PIP into a nanostructured release system may help to overcome these difficulties. Various PIP-loaded nanostructures have been reported, such as carbon nanotubes, liposomes, and polymeric nanoparticles [10-12].

In a recent study conducted by Quijia et al. (2022) [13] PIP was encapsulated in MIL-100 (Fe). This MOF is a polycrystalline powder composed of iron (III) ions and 1,3,5-benzenetricarboxylic acid [14]. The main characteristics of this MOF (PIP@MIL-100 (Fe)) include particles measuring up to 120 nm in size and having a rhombohedral shape. It has a low polydispersity index of 0.03 and a hydrodynamic diameter of 98± 27.83 nm. Its zeta potential is +7± 0.6 mV. The nanosystem has a high loading capacity for PIP of 11.02% by weight (0.12 g g^{-1}) and a high encapsulation efficiency of 95± 3%. MCF-7 and 4T1 breast cancer cell lines were used in cytotoxicity tests, which revealed that PIP@MIL-100 (Fe) had roughly three times the cytotoxicity (IC_{50}) of free PIP.

The surface modification strategies of MOF nanoparticles and materials engineering, such as the use of macrophage membranes, have the potential to improve the efficiency and selectivity of delivering chemotherapeutic agents and other biomedical applications. The functionalization of MOF nanoparticles improves their chemical and colloidal stability and offers the possibility of intravenous administration and interaction with specific receptors [15]. Moreover, the camouflaging of nanostructures with macrophage membranes can increase their blood circulation and reduce their clearance by mononuclear phagocyte systems, which can be useful in combating cancer and other diseases. These surface modification and materials engineering strategies are promising research areas in the search for more effective and selective therapies for various diseases [16-18].

Here, we present a comprehensive study involving the preparation and characterization of membrane vesicles and proteins extracted from macrophage cells (RAW 264.7 strain). Our objective was to develop a novel strategy for coating MIL-100 (Fe) with these biomolecules to achieve controlled release of PIP, a potent anti-cancer agent, against breast cancer. Previous studies have employed PIP for encapsulating these MOFs, as documented in published research [13]. To assess the efficacy and properties of our nanostructures, we employed a range of analytical techniques. The characterization included measurements of hydrodynamic diameter, polydispersity index (PdI), zeta potential, stability (evaluated on the first and tenth day after synthesis using dynamic light scattering), size (dry diameter), shape (observed through transmission electron microscopy [TEM] and scanning electron microscopy [SEM]), chemical behavior (infrared vibration spectroscopy [IR]), SDS-PAGE analysis, thermogravimetric analysis (TGA), and in vitro release kinetics of PIP.

Furthermore, to evaluate the effectiveness of our nanostructured systems, in vitro efficacy trials were conducted using breast cancer cells. These trials were intended to investigate the

potential benefits of employing these innovative nanosystems for targeted drug delivery and therapy against breast cancer.

Materials and Methods

Materials

Piperine, Trimesic acid (BTC), Iron (III) chloride hexahydrate, 99% ethanol, Methanol HPLC grade, and MTT (3-(4,5-dimethylthiazol-2-yl)-2,5-diphenyltetrazolium bromide) were purchased from Sigma Aldrich (St. Louis, MO, USA). The cell culture medium used was RPMI-1640 supplemented with 10% fetal bovine serum (FBS) and 1% antibiotic (10,000 UI penicillin and 10 mg/mL streptomycin solution) from Sigma Aldrich.

Methods

Encapsulation of Piperine in MIL-100(Fe)

The PIP encapsulation process in MIL-100(Fe) was improved in comparison with the method described by Quijia et al. in 2022 [13], resulting in a drug encapsulation efficiency of 95 ± 3%. Additionally, the nanostructure was stored in absolute ethanol at 4 °C until use. In this study, we used the encapsulation percentage previously reported by our group, with an encapsulation efficiency of piperine in the MOFs of 95%, representing 0.025 mg/mg, which means mg of piperine per mg of MIL-100(Fe).

A detailed description of the encapsulation method can be found in Annex 1. This section outlines step-by-step instructions, including the preparation of the encapsulation solution, incubation conditions, purification techniques, and any additional modifications or considerations involved in the process.

Preparation of Macrophage Membrane Vesicles (MM)

To obtain MM vesicles from RAW 264.7 cells, the method described by Gao et al. (2016) and Rao et al. (2017) [19, 20]. was employed. Macrophage cells were grown in culture flasks until they produced approximately 1 x 10^8 cells mL^{-1}. The cells were then extracted with 0.05% Trypsin-EDTA and centrifuged for 5 min at 1015 rpm at 4 °C. The resulting cells were homogenized using a portable Dounce homogenizer (20 passes on ice) and suspended in a 10 mL hypotonic lysis buffer composed of 20 mM Tris-HCl, 10 mM KCl, and 2 mM MgCl (and a mini-protease inhibitor without EDTA) at 4 °C. The cell suspension was centrifuged at 5427 rpm for 5 min at 4 °C, and then the supernatant was collected and centrifuged again for 30 min at 11,750 rpm (**Figure 1A**). The isolated membranes were dispersed in PBS (pH 7.4) at 4 °C for subsequent assays.

Preparation of MM@PIP@MIL-100(Fe)

The MM@PIP@MIL-100(Fe) was prepared by the impregnation method, based on previous research [21-25], with modifications. PIP@MIL-100 (Fe) (5.0 mg) was dispersed in 10 mL of PBS (pH=7.4) and stirred for 30 min at 4 °C with previously extracted MM vesicles (approximately 4 mg/mL). The functionalized MOFs were centrifuged at 10,000 rpm for 10 min, the supernatant was removed, and the nanoparticles were kept at 4 °C in PBS (pH=7.4) (**Figure 1B**) [23, 26].

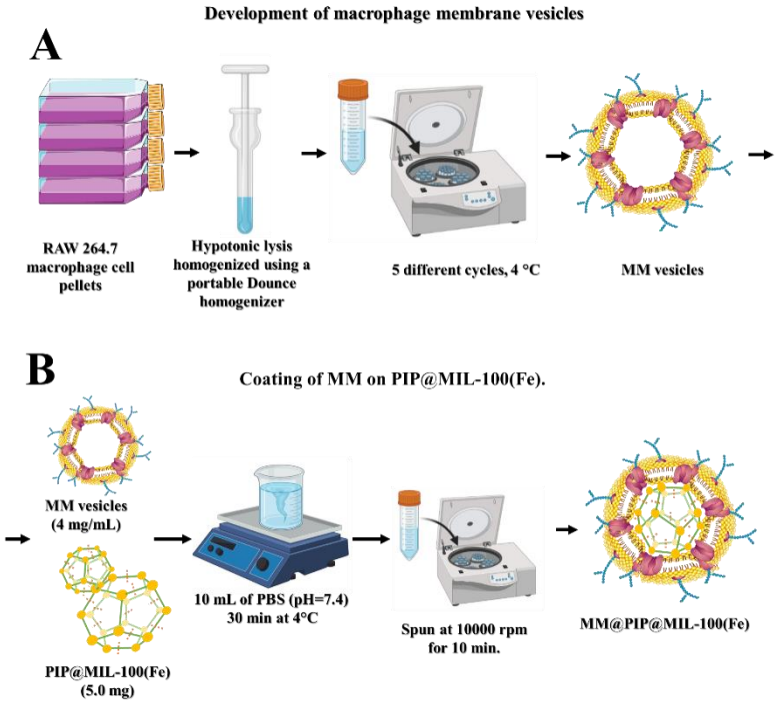

Figure 1. A. Development of macrophage membrane vesicles. B. Development of MM@PIP@MIL-100(Fe) nanostructures.

Photon Correlation Spectroscopy and Zeta Potential

The hydrodynamic diameter and zeta potential of nanoparticles dispersed in water at a concentration of 0.1 mg mL^{-1} were measured using an ultrasonic tip and the Zetasizer Nano series, a product from the UK. Three readings were taken during the measurements, which were carried out at room temperature and under light scattering detection at an angle of 173°. The z-average size was determined using cumulant analysis with a repeatability of 1.6% using the Zetasizer Nano-ZS. The Nano software was used to convert the intensity distribution into volume using theoretical plots of the log of the relative scattering intensity versus particle size at angles of 173° [27, 28].

Infrared Vibrational Spectroscopy Analysis

A Perkin-Elmer 400 IR spectrometer was used to perform the vibrational spectroscopy analysis in the infrared region (IR) of the electromagnetic spectrum. An agate mortar was used to combine the samples with potassium bromide (KBr), and the mixture was then added to pellets for reading with a resolution of 2 cm^{-1}. The method uses the molecules' characteristic infrared radiation absorption to figure out the structures of the molecules.

High-Resolution Transmission Electron Microscopy (HR-TEM) and High-Resolution Scanning Electron Microscopy (HR-SEM)

The samples were coated with a thin layer of gold and mounted on a holder before HR-SEM was carried out on them with the TOPCON SM-300 microscope at 10-20 kV. Using a PHILIPS CM 200 SUPER TWIN transmission electron microscope (TEM), the morphology of purified nanosolids was examined, and photomicrographs were taken at various magnifications. The JEOL JEM-2100 (LaB6) at 100 kV, available from LME IQSC-USP in Sao Carlos, Brazil, was used for the TEM analyses. The samples were made by depositing 3 µL of diluted nanosuspensions on a copper grid, draining the excess liquid, drying it, and staining it for 3 min with 3 µL of 2% w/v aqueous uranyl acetate. The samples were dried after the excess stain was removed, and the staining process was then repeated. The grids were analyzed after drying at room temperature.

Thermogravimetric Analysis (TGA)

TA Instruments' TGA-Q500 instrument was used to perform the TGA analysis. A platinum pan with a maximum volume of 50 L was loaded with 5 mg of each sample and heated at a rate of 10 °C/min from 30 to 600 °C. For the analysis, a dry nitrogen flow of 40 mL/min was used to aid in the decomposition of MM@PIP@MIL-100(Fe) and PIP@MIL-100(Fe) [29].

SDS-PAGE Characterization of MM@PIP@MIL-100(Fe)

The proteins were examined using sodium dodecyl sulfate-polyacrylamide gel electrophoresis (SDS-PAGE) [30]. Purified macrophage membrane vesicles (MM) and MM@PIP@MIL-100(Fe) were created in SDS sample buffer and measured with the BCA kit. Then 20 g of the sample was loaded onto each well of a 10% SDS-PAGE after samples were heated at 95 °C for 5 min. The samples were then run at 120 V for 2 h, and the resulting PAGE was stained for 2 h with Coomassie Blue and then washed overnight in preparation for visualization the next day on a gel documentation system [31].

In vitro Release Kinetics of PIP

Phosphate-buffered saline (PBS, pH=7.4 or pH=5) with 5% v/v Tween 20 and 5% v/v ethanol as the receptor medium was used to study the release kinetics of PIP under 37 °C two-

dimensional agitation (agitation frequency = 150 rpm) [32]. The MM@PIP@MIL-100(Fe) nanosystem was first dissolved in 5 mL of the receptor medium at a concentration of 10 mg/mL. The samples were centrifuged and a 1 mL sample of the supernatant was taken for PIP content analysis at predetermined time intervals (1–180 h). The medium was then replenished with 1 mL of new receptor medium. To determine the amount of PIP released, the collected samples were analyzed using high-performance liquid chromatography (**Figure S1**). The add-in (DDSolver) for Microsoft Excel that offers statistical criteria to assess the model's fitting quality was used to analyze the drug release model. To determine the best release model, two parameters—adjusted R^2 and Akaike information criterion (AIC)—were evaluated while accounting for the volume of data, the number of data points, and statistical analysis [33].

Cell Viability Assay

MCF-7, MDA, SKBR-3, BT-549, and HaCaT cancer cells were put in 96-well plates at a density of 4,000 cells/well and left there overnight. Dimethyl sulfoxide (DMSO) concentration in the study samples was kept under 0.25% (v/v) to prevent any negative effects on cell viability [34]. PIP was dissolved in DMSO at a concentration of 5% (w/v). DMEM medium was used to either disperse or dissolve MM@PIP@MIL-100 (Fe), which was then incubated for 48 h. In order to rule out any potential interference with the assay, nanoparticles in culture medium and culture medium alone were also tested along with the treatments, which were prepared at a 3 times higher concentration and added to the cells in a final volume of 200 µL per well.

Statistical Analysis

The experiments were carried out three times (n=3), and the mean SEM of the outcomes was obtained. Data comparison techniques included ANOVA with post-test or t-student tests, with significance set at $p< 0.05$. GraphPad Prism® version 7.0 was used to conduct these statistical analyses. ANOVA divides observed variance data into various components for use in further tests. By obtaining the diameter distribution of the nanostructures and choosing the best fit for polydispersion based on a log-normal distribution, the modal diameter of the nanostructures was ascertained. The linear regression model based on the dose-response curve was used to calculate the inhibitory concentration (IC_{50}) and its 95% confidence intervals.

Results and Discussion

Analysis of Average Hydrodynamic Diameter and Zeta Potential

After coating the PIP@MIL-100(Fe) material with macrophage-derived vesicles (MM-vesicles) using the impregnation method (MM@PIP@MIL-100(Fe) material), DLS

measurements were also performed. As expected, the results showed an increase in the average hydrodynamic diameter of the nanoparticles from 98 ± 27.83 to 150 ± 24.16 nm (**Table 1**), as well as a change in the zeta potential of the nanoparticles from +7 ± 0.6 to -32 ± 2.36 mV, suggesting that the membrane coating was successful. It is important to note that, under these circumstances, the acidic nature of the PIP@MIL-100(Fe) suspension (pH ~ 2.9-3.8) confers a positive charge to the material due to the protonation reaction of carboxylate groups. While coating with the macrophage membrane vesicle (MM) has a pH ~ 7.4, the surface of MOFs acquires a negative charge that is due to electrostatic interactions between the positive ζ potential of PIP@MIL-100(Fe) and the negative ζ potential of MM (**Table 1**), due to the charge of phospholipids and proteins constituting the cell membrane. Therefore, the acidic carboxylic groups of the MOF ligand help in the conjugation of primary amines or macromolecular groups, such as peptides and proteins from MM, ensuring the correct topological orientation of cell membranes in the MM@PIP@MIL-100(Fe) platform [26, 35-41]. **Table 1** summarizes the obtained results using the dynamic light scattering (DLS) technique on the Zetasizer Nano ZS equipment, including the average hydrodynamic diameter, polydispersity index (PdI), and zeta potential of the nanoparticles.

Table 1.- Zeta potential (ζ) analysis, hydrodynamic diameter, and polydispersity index of different nanostructures.

	PIP@MIL-100 (Fe)	**Vesicle (MM)**	**MM@PIP@MIL-100(Fe)**
Zeta Potential (mV)	+ 7 ± 0.6	- 14 ± 1.50	- 32 ± 2.36
Hydrodynamic diameter (nm)	98 ± 27.83	88 ± 0.81	150 ± 24.16
Polydispersity index	0.03 ± 0.006	0.4 ± 0.09	0.4 ± 0.05

Analysis of Nanostructured Systems by Vibrational Spectroscopy in the Infrared Region (FT-IR)

The coating with MM on the MOF exhibited absorption bands similar to those of the cell membrane vesicles previously reported, such as the 1800-1350 cm^{-1} lipid ester groups and amide I and II protein bands (**Figure 2**) [42]. The vibrational spectrum between 1100-800 cm^{-1} and the stretching and bending of phosphate groups provide some information about the stretching and bending bands of the phosphate groups. The strong band ν_1 (PO_4) typically belongs to the region of 1000-1100 cm^{-1}, while the bending mode ν_2 (PO_4) usually appears as a medium to strong band in the range of 600-900 cm^{-1}. Additionally, the symmetric stretching

(v_1) of the phosphate groups (PO_4^{3-}) typically exhibits around 1050-1100 cm^{-1}. [43] This confirms the presence of vesicles in the MOFs, including both protein and lipid molecules.

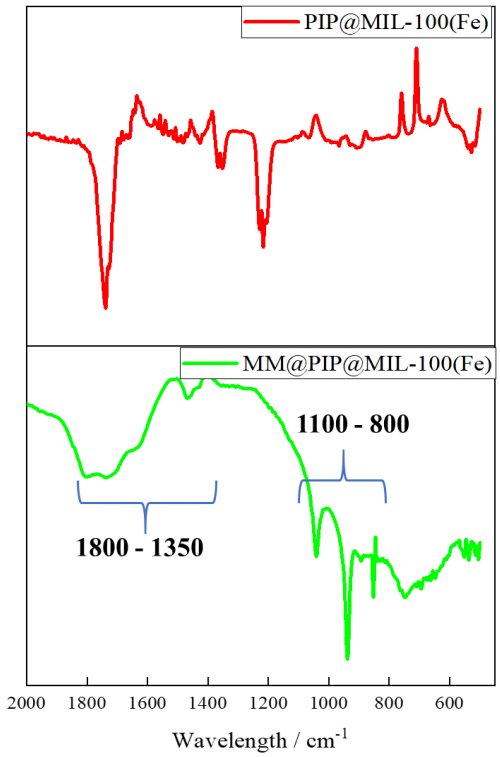

Figure 2. Fourier-transform infrared (FT-IR) spectrum analysis of nanoparticles: PIP@MIL-100(Fe) (red line); MM@PIP@MIL-100(Fe) (green line).

Morphology Analysis of Nanomaterials

In this study, the morphology and particle size of materials based on MOF were prepared and analyzed using scanning electron microscopy (SEM) and transmission electron microscopy (TEM) techniques. Uranyl acetate was used to negatively stain the MM@PIP@MIL-100(Fe) material's particles, which were then visualized using TEM. The images produced by the technique clearly displayed a PIP@MIL-100(Fe) core with a diameter of about 50 nm. As shown in **Figure 3-D**, there was an additional lipid bilayer outer layer that was 10 nm thick. This demonstrated that the cell membrane had successfully been coated onto the PIP@MIL-100(Fe) composite. Additionally, **Figures 3-A and 3-C** show the SEM images for the materials PIP@MIL-100(Fe) and MM@PIP@MIL-100(Fe), respectively.

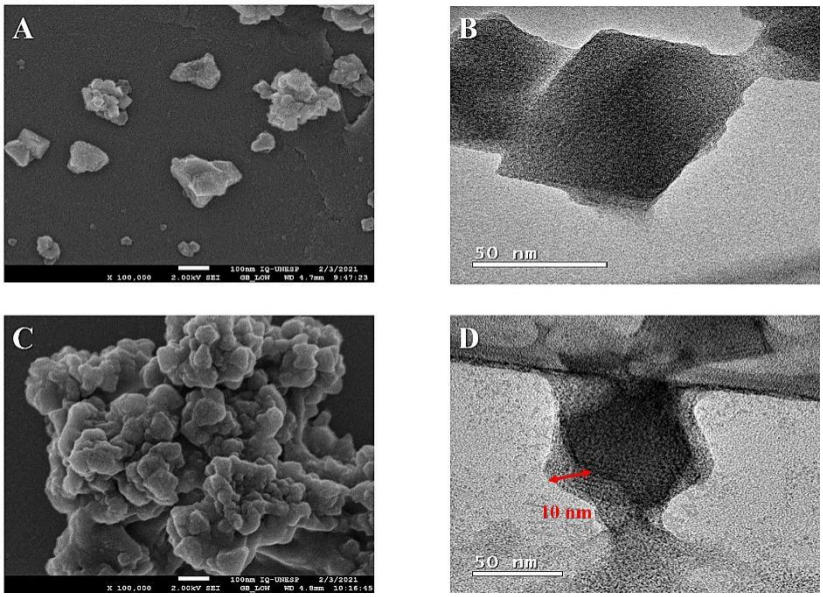

Figure 3. Morphology analysis using scanning electron microscopy (SEM): (A) PIP@MIL-100 (Fe); (C) MM@PIP@MIL-100 (Fe); and (B) PIP@MIL-100(Fe) and (D) MM@PIP@MIL-100(Fe) using transmission electron microscopy (TEM). Note: Figures 3-A and 3-B are from a previous article by Quijia et al. (2022)[13]

Thermogravimetric Analysis

The thermal behavior of PIP@MIL-100(Fe) and MM@PIP@MIL-100(Fe) materials was studied using thermogravimetric analysis (TGA). The analysis was conducted with a heating rate of 10 °C/min, and the temperatures ranged from 30 °C to 600 °C. The thermogravimetric curves of the materials used in this study are illustrated in **Figure 4**.

In the thermal decomposition of the MM coating in MOFs (**red line in Figure 4**), the sample in the region between 25 and 73 °C showed a mass loss of 19.4% associated with the coating of macrophage membrane vesicles (MM) of MM@PIP@MIL-100(Fe). These values are likely due to the release of moisture mainly from the cellular vesicle or the heating of organic matter [44].

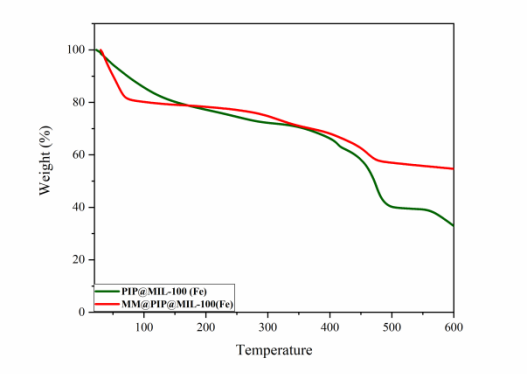

Figure 4. Thermogravimetric curves of the compounds: PIP@MIL-100(Fe) (green line); MM@PIP@MIL-100(Fe) (red line)

Characterization and stability of the MM@PIP@MIL-100(Fe) platform

SDS-PAGE was used to analyze the proteins from MM-vesicles and the purified MM@PIP@MIL-100(Fe) materials. Compared to natural MM-vesicles, the proteins were successfully coated onto MM@PIP@MIL-100(Fe) after the impregnation treatment, according to the results shown in **Fig. 5A**. This suggests that proteins were successfully transferred from the macrophage's natural membrane to the PIP@MIL-100(Fe) composite. MM@PIP@MIL-100(Fe) stability was also examined, and samples kept in 1 PBS (4 °C) for 10 days revealed no discernible size change (p-value > 0.05) (**Fig. 5B**). This finding indicates that the nanoparticles may still maintain their stable structure, which is important for upcoming biomedical research.

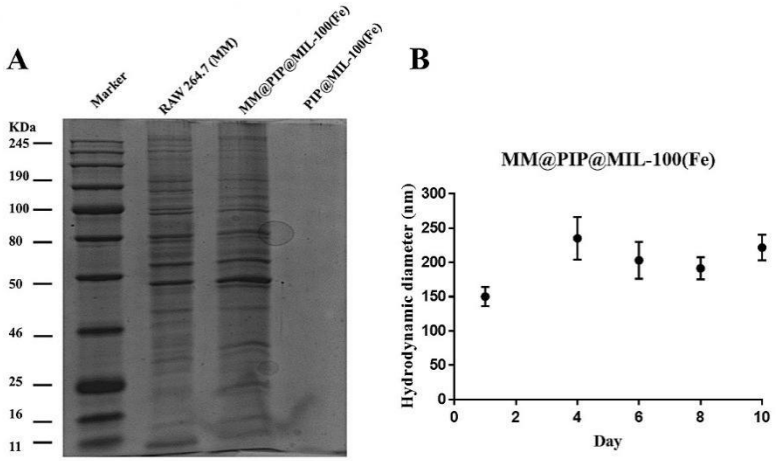

Figure 5. A. SDS-PAGE analyses of proteins extracted from the membrane of RAW 264.7 cell line and MM@PIP@MIL-100(Fe). B. Verification of the average hydrodynamic diameter of MM@PIP@MIL-100(Fe) sample stored in 1× PBS (4ºC) for 10 days. Data with standard deviation (n = 3), ANOVA with Tukey's post-test, $p<0.05$.

In Vitro Release Assay of PIP

To examine the release profile of PIP, a study was carried out under physiologically relevant conditions in a phosphate-buffered saline (PBS) solution at both pH 7.4 and 5.0, with the addition of 5% v/v Tween 20 and 5% v/v ethanol, at a temperature of 37 °C. These conditions were selected to simulate both the blood circulation and the acidic microenvironments present in tumor regions [45]. Because most nanostructures tend to be internalized by endocytosis in cancer cells and become trapped in endosomal and lysosomal compartments, which typically range in pH from 4.5 to 5.5, pH 5.0 was chosen. [46].

Table 2 shows that the release of PIP from MM@PIP@MIL-100(Fe) followed the simplified Korsmeyer-Peppas model with a high R^2 (> 0.95) and n values > 0.43, indicating that the release mechanism was governed by diffusion. The release curve exhibited a slow stage with

only about 25% (0.15 mg mL^{-1}) of PIP released at pH=5 after 14 days. For pH=7.4, the release was even slower with only 7.2% (0.014 mg mL^{-1}) released (**Figure 6**).

Table 2.- Fitting of the release profile equation, where M is the cumulative release (%) and t is the release time (h).

	MM@PIP@MIL-100(Fe)	
	pH=7.4	pH=5.0
Korsmeyer-Peppas Model	$M = k_{KP} * t^{n}$	
Equation	$M=2.17\ t^{0.21}$	$M=7.51\ t^{0.22}$
Rsqr	**0.97221752**	**0.972872357**
AIC	00.000	00.027
Weibull Model	$M = 100\left[e^{-\frac{(t-Ti)^{\beta}}{\alpha}}\right]$	
Equation	$M = 100\left[e^{-\frac{(t-0.8)^{0.20}}{42.18}}\right]$	$M = 100\left[e^{-\frac{(t-0.8)^{0.22}}{11.93}}\right]$
Rsqr	0.96896075	0.967943034
AIC	00.003	00.031
Gompertz Model	$M = 100 * e^{-\alpha * e^{-\beta * \log(t)}}$	
Equation	$M = 100 * e^{-0.004 * e^{-0,000 * \log(t)}}$	$M = 100 * e^{-0.003 * e^{-0.000 * \log(t)}}$
Rsqr	0.96557946	0.96128035
AIC	00.002	00.031

According to Palanikumar et al. (2022) [47], the presence of MM vesicles impedes drug release from the PIP@MIL-100(Fe) material, although it does not entirely eliminate it. As a result, the MM@PIP@MIL-100(Fe) platform has a highly stable encapsulation, which is essential in preventing premature release and guaranteeing that loaded drugs eventually reach target cancer cells. Additionally, the decrease in release at pH=7.4 is likely attributed to the safeguarding function of MM vesicles on the nanomaterial. This finding indicates the potential for PIP to have a controlled release from pH-sensitive MM-MIL-100(Fe), which is loaded with PIP in acidic solutions. This feature is important as it minimizes side effects while increasing PIP accumulation at the tumor sites [48].

On the other hand, the release of PIP at pH 7.4 (7%) is much lower compared to the amount released at pH 5.0 (25%) after 120 hours of analysis (**Figure 6**), which is likely due to cell membrane vesicles. The vesicles have relatively alkaline pH values (pH 7.4-7.1); in acidic

pH, there are changes in the electrical charge of the membrane from groups present in the lipid molecule and peptides, causing degradation or rupture of the membrane [49-52].

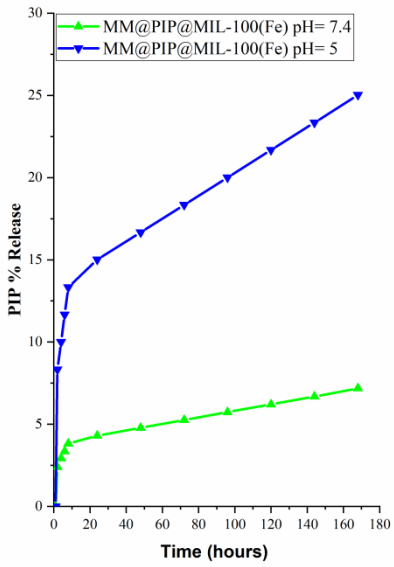

Figure 6. Release profile of MM@PIP@MIL-100(Fe) at pH values 7.4 and 5.0.

Cytotoxicity

Table 3 and Figure S2, in parentheses, present the number of times that the nanostructures exceeded the IC_{50} in relation to the drug (PIP). MM@PIP@MIL-100 (Fe) exhibits high cytotoxicity (IC_{50}) in the four cell lines compared to free piperine. All PIP-loaded nanosystems have a more significant toxic effect ($p < 0.05$) on tumor cells than free PIP, according to the statistical analysis using Tukey's ANOVA test in comparison with the IC_{50} (**Figure 7**). Lysosomal enzymes with an acidic pH are probably the cause of this cytotoxic effect because they can significantly increase drug release in the cytoplasm and cause cell death [53].

Table 3.- Cytotoxicity index of nanoparticles and piperine against breast cancer cells

	Cytotoxicity index (IC_{50}) expressed in µM			
	MCF-7	**MDA**	**SKBR-3**	**BT-549**
PIP	193.67 ± 0.30	139.60 ± 1.17	72.62 ± 1.08	96.38 ± 1.10
MM@PIP@MIL-100 (Fe)	11.45 ± 1.18 **(17)**	16.32 ± 1.12 **(8)**	18.51 ± 1.29 **(4)**	8.71 ± 1.12 **(12)**

Note: Piperine (PIP), Macrophage Membranes (MM). The results represented in the table refer to the averages of three independent experiments (mean ± standard deviation). IC_{50} corresponds to the minimum concentration to inhibit 50% of cancer cells. Cells were treated with 6.25 to 100 µM and incubated for 48 h. The number of times the nanostructures exceeded the IC_{50} in relation to the drug (PIP) is shown in parentheses.

It is important to acknowledge that the coating of MM-vesicles onto MOFs exhibited higher toxicity in certain cell lines. A study by Wuttke et al. (2015) demonstrated that the coating of nanoMOFs with lipid bilayers can enhance their uptake by cancer cells [23]. Additionally, previous research has indicated that macrophage membranes possess the ability to actively bind to cancer cells due to the high expression of α4 and β1 integrins in RAW 264.7 cells, providing them with specific metastasis-targeting capabilities [54]. Consequently, the presence of these proteins in MOFs contributed to improved absorption and increased toxicity in cancer cells.

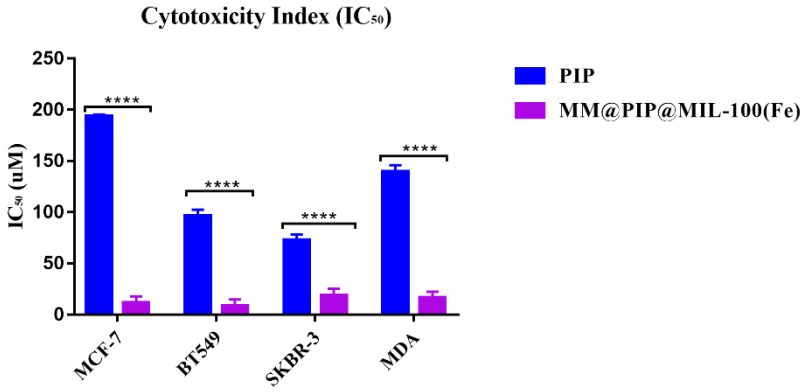

Figure 7. Indices of nanoparticle cytotoxicity against breast cancer cells (MCF-7; BT-549; SKBR-3; MDA)

Conclusion

In this study, the researchers successfully coated PIP@MIL-100(Fe) with MM-vesicles, resulting in the creation of a new material called MM@PIP@MIL-100(Fe). The coating process was confirmed through various analyses and measurements. DLS measurements indicated an increase in the average hydrodynamic diameter of the nanoparticles, along with a change in their zeta potential, providing evidence of successful coating. TEM imaging revealed the presence of a PIP@MIL-100(Fe) core with a diameter of approximately 50 nm, surrounded by an outer layer of lipid bilayer measuring about 10 nm in thickness, indicating successful cell membrane coating. TGA was conducted to investigate the thermal behavior of the materials, while SDS-PAGE analysis was utilized to analyze the proteins coated onto MM@PIP@MIL-100(Fe) following the impregnation treatment. Stability assays demonstrated that the nanoparticles maintained a stable structure. The release of PIP from MM@PIP@MIL-100(Fe) was characterized and found to exhibit a high correlation with the simplified Korsmeyer-Peppas model, suggesting controlled and predictable release kinetics. Overall, these findings indicate that MM@PIP@MIL-100(Fe) has potential applications in future biomedical analyses, highlighting its suitability for further research in the field.

Moreover, additional research is needed to explore these potential applications in more detail and to conduct in vivo studies to validate the efficacy and safety of MM@PIP@MIL-100(Fe) for various biomedical applications. These future directions will contribute to the advancement of nanomedicine and the development of innovative therapeutic and diagnostic strategies.

Supplementary Materials: The following supporting information can be downloaded fromwww.mdpi.com/xxx/s1, **Figure S1.** (a) Chromatogram of PIP (concentration = 6.25 to 100 µg mL^{-1}) in the mobile phase (methanol/water [75:25]) and (b) calibration curve of PIP quantified by HPLC. **Figure S2**. Cytotoxic activity of piperine. **Figure S3.** Fourier-transform infrared (FT-IR). **Figure S4.** PIP@MIL-100(Fe) in situ

Author Contributions: C.R.Q; C.A.M.; R.C.G.F, and M.C.; methodology: C.R.Q; G.N. C.A.M.; R.C.G.F, and M.C.; formal analysis: C.R.Q; R.C.G.F, and M.C.; investigation: C.R.Q; R.M.S; C.A.M.; R.C.G.F, and M.C.; resources: C.R.Q; C.A.M.; V.V.; A.O; R.C.G.F, and M.C.; data curation, C.R.Q; and G.N.; writing C.R.Q; R.C.G.F, and M.C.; writing—reviewing and editing: R.C.G.F, and M.C.; supervision: A.O; R.C.G.F, and M.C.; project administration: R.C.G.F, and M.C. All authors have read and agreed to the published version of the manuscript.

Acknowledgments: The authors acknowledge FAPESP (process 2018/21119–0) and grant CPP2021-008597 funded by MICIN/AEI/10.13039/501100011033 and European Union Next Generation EU/PRTR, and SBPLY/21/180501/000050 funded by JCCM and by EU through Fondo Europeo de Desarrollo Regional for the financial support given for the development of this work.

Conflicts of Interest: The authors declare no conflict of interest.

References

[1] A. T. Alshareeda, M. N. Khatijah, and B. S. J. A. J. o. S. Al-Sowayan, "Nanotechnology: A revolutionary approach to prevent breast cancer recurrence," vol. 46, no. 1, pp. 13-17, 2023.

[2] M. Rezaei, A. Abbasi, R. Varshochian, R. Dinarvand, and M. Jeddi-Tehrani, "NanoMIL-100(Fe) containing docetaxel for breast cancer therapy," Artificial Cells Nanomedicine and Biotechnology, vol. 46, no. 7, pp. 1390-1401, 2018.

[3] M. X. Wu and Y. W. Yang, "Metal-Organic Framework (MOF)-Based Drug/Cargo Delivery and Cancer Therapy," (in eng), Adv Mater, Review vol. 29, no. 23, Jun 2017.

[4] G. Férey and C. Serre, "Large breathing effects in three-dimensional porous hybrid matter: facts, analyses, rules and consequences," Chem Soc Rev, vol. 38, no. 5, pp. 1380-1399, 2009.

[5] K. Srinivasan, "Black pepper and its pungent principle-piperine: a review of diverse physiological effects," (in eng), Crit Rev Food Sci Nutr, Review vol. 47, no. 8, pp. 735-48, 2007.

[6] L. H. Lai et al., "Piperine suppresses tumor growth and metastasis in vitro and in vivo in a 4T1 murine breast cancer model," (in eng), Acta Pharmacol Sin, Research Support, Non-U.S. Gov't vol. 33, no. 4, pp. 523-30, Apr 2012.

[7] D. P. Bezerra et al., "In vivo growth-inhibition of Sarcoma 180 by piplartine and piperine, two alkaloid amides from Piper," (in eng), Braz J Med Biol Res, Research Support, Non-U.S. Gov't vol. 39, no. 6, pp. 801-7, Jun 2006.

[8] S. Chuchawankul, N. Khorana, and Y. Poovorawan, "Piperine inhibits cytokine production by human peripheral blood mononuclear cells," (in eng), Genet Mol Res, Research Support, Non-U.S. Gov't vol. 11, no. 1, pp. 617-27, Mar 14 2012.

[9] M. B. Daware, A. M. Mujumdar, and S. Ghaskadbi, "Reproductive toxicity of piperine in Swiss albino mice," (in eng), Planta Med, vol. 66, no. 3, pp. 231-6, Apr 2000.

[10] M. Pachauri, E. D. Gupta, P. C. J. J. o. d. d. s. Ghosh, and technology, "Piperine loaded PEG-PLGA nanoparticles: Preparation, characterization and targeted delivery for adjuvant breast cancer chemotherapy," vol. 29, pp. 269-282, 2015.

[11] S. S. Imam et al., "Formulation of piperine–chitosan-coated liposomes: characterization and In Vitro Cytotoxic Evaluation," vol. 26, no. 11, p. 3281, 2021.

[12] K. Raza et al., "Conjugation of docetaxel with multiwalled carbon nanotubes and codelivery with piperine: implications on pharmacokinetic profile and anticancer activity," vol. 13, no. 7, pp. 2423-2432, 2016.

[13] C. R. Quijia et al., "In situ synthesis of piperine-loaded MIL-100 (Fe) in microwave for breast cancer treatment," vol. 75, p. 103718, 2022.

[14] P. Horcajada et al., "Synthesis and catalytic properties of MIL-100(Fe), an iron(III) carboxylate with large pores," (in eng), Chem Commun (Camb), no. 27, pp. 2820-2, Jul 19 2007.

[15] R. A. Meyer, J. C. Sunshine, and J. J. Green, "Biomimetic particles as therapeutics," Trends in biotechnology, vol. 33, no. 9, pp. 514-524, 2015.

[16] L. Rao et al., "Effective cancer targeting and imaging using macrophage membrane-camouflaged upconversion nanoparticles," Journal of Biomedical Materials Research Part A, vol. 105, no. 2, pp. 521-530, Feb 2017.

[17] M. Xuan, J. Shao, L. Dai, Q. He, and J. Li, "Macrophage cell membrane camouflaged mesoporous silica nanocapsules for in vivo cancer therapy," Advanced healthcare materials, vol. 4, no. 11, pp. 1645-1652, 2015.

[18] M. J. Xuan, J. X. Shao, L. R. Dai, J. B. Li, and Q. He, "Macrophage Cell Membrane Camouflaged Au Nanoshells for in Vivo Prolonged Circulation Life and Enhanced Cancer Photothermal Therapy," Acs Applied Materials & Interfaces, vol. 8, no. 15, pp. 9610-9618, Apr 2016.

[19] C. Gao, Z. Lin, B. Jurado-Sánchez, X. Lin, Z. Wu, and Q. J. S. He, "Stem cell membrane-coated nanogels for highly efficient in vivo tumor targeted drug delivery," vol. 12, no. 30, pp. 4056-4062, 2016.

[20] L. Rao et al., "Effective cancer targeting and imaging using macrophage membrane-camouflaged upconversion nanoparticles," vol. 105, no. 2, pp. 521-530, 2017.

[21] M. Barjasteh, M. Vossoughi, M. Bagherzadeh, and K. P. J. I. J. o. P. Bagheri, "Green synthesis of PEG-coated MIL-100 (Fe) for controlled release of dacarbazine and its anticancer potential against human melanoma cells," vol. 618, p. 121647, 2022.

[22] X. Li et al., "Drug-Loaded Lipid-Coated Hybrid Organic-Inorganic “Stealth” Nanoparticles for Cancer Therapy," vol. 8, p. 1027, 2020.

[23] S. Wuttke et al., "MOF nanoparticles coated by lipid bilayers and their uptake by cancer cells," Chemical Communications, vol. 51, no. 87, pp. 15752-15755, 2015.

[24] T. Hidalgo et al., "Chitosan-coated mesoporous MIL-100 (Fe) nanoparticles as improved bio-compatible oral nanocarriers," Scientific reports, vol. 7, p. 43099, 2017 2017.

[25] E. Bellido et al., "Heparin-Engineered Mesoporous Iron Metal-Organic Framework Nanoparticles: Toward Stealth Drug Nanocarriers," Advanced Healthcare Materials, vol. 4, no. 8, pp. 1246-1257, Jun 2015.

[26] A. Zimpel et al., "Imparting functionality to MOF nanoparticles by external surface selective covalent attachment of polymers," vol. 28, no. 10, pp. 3318-3326, 2016.

[27] R. Grall, T. Hidalgo, J. Delic, A. Garcia-Marquez, S. Chevillard, and P. Horcajada, "In vitro biocompatibility of mesoporous metal (III; Fe, Al, Cr) trimesate MOF nanocarriers," Journal of Materials Chemistry B, vol. 3, no. 42, pp. 8279-8292, 2015.

[28] T. Simon-Yarza et al., "A smart metal–organic framework nanomaterial for lung targeting," Angewandte Chemie International Edition, vol. 56, no. 49, pp. 15565-15569, 2017.

[29] B. E. Souza and J.-C. J. C. Tan, "Mechanochemical approaches towards the in situ confinement of 5-FU anti-cancer drug within MIL-100 (Fe) metal–organic framework," CrystEngComm, vol. 22, no. 27, pp. 4526-4530, 2020.

[30] L. L. Bu et al., "STAT3 blockade enhances the efficacy of conventional chemotherapeutic agents by eradicating head neck stemloid cancer cell," (in eng), Oncotarget, Research Support, Non-U.S. Gov't vol. 6, no. 39, pp. 41944-58, Dec 8 2015.

[31] L. Rao et al., "Effective cancer targeting and imaging using macrophage membrane-camouflaged upconversion nanoparticles," (in eng), J Biomed Mater Res A, Research Support, Non-U.S. Gov't vol. 105, no. 2, pp. 521-530, Feb 2017.

[32] P. Makhov et al., "Co-administration of piperine and docetaxel results in improved anti-tumor efficacy via inhibition of CYP3A4 activity," vol. 72, no. 6, pp. 661-667, 2012.

[33] Y. Zhang et al., "DDSolver: an add-in program for modeling and comparison of drug dissolution profiles," vol. 12, no. 3, pp. 263-271, 2010.

[34] T. Hidalgo, R. Simón-Vázquez, A. González-Fernández, and P. J. C. s. Horcajada, "Cracking the immune fingerprint of metal–organic frameworks," vol. 13, no. 4, pp. 934-944, 2022.

[35] E. Bellido, M. Guillevic, T. Hidalgo, M. J. Santander-Ortega, C. Serre, and P. J. L. Horcajada, "Understanding the colloidal stability of the mesoporous MIL-100 (Fe) nanoparticles in physiological media," Langmuir, vol. 30, no. 20, pp. 5911-5920, 2014.

[36] Q. Xia, Y. Zhang, Z. Li, X. Hou, and N. Feng, "Red blood cell membrane-camouflaged nanoparticles: A novel drug delivery system for antitumor application," Acta Pharmaceutica Sinica B, 2019.

[37] M. Rezaei, A. Abbasi, R. Varshochian, R. Dinarvand, and M. Jeddi-Tehrani, "NanoMIL-100 (Fe) containing docetaxel for breast cancer therapy," Artificial cells, nanomedicine, and biotechnology, vol. 46, no. 7, pp. 1390-1401, 2018.

[38] G. Chaturvedi, A. Kaur, A. Umar, M. A. Khan, H. Algarni, and S. K. J. J. o. S. S. C. Kansal, "Removal of fluoroquinolone drug, levofloxacin, from aqueous phase over iron based MOFs, MIL-100 (Fe)," Journal of Solid State Chemistry, p. 121029, 2019.

[39] S. Jung, Y. Kim, S.-J. Kim, T.-H. Kwon, S. Huh, and S. J. C. C. Park, "Bio-functionalization of metal–organic frameworks by covalent protein conjugation," vol. 47, no. 10, pp. 2904-2906, 2011.

[40] A. Guo, M. Durymanov, A. Permyakova, S. Sene, C. Serre, and J. J. P. r. Reineke, "Metal organic framework (MOF) particles as potential bacteria-mimicking delivery Systems for Infectious Diseases: characterization and cellular internalization in alveolar macrophages," vol. 36, no. 4, p. 53, 2019.

[41] Y. Ding et al., "Development and evaluation of a novel drug delivery: Soluplus®/TPGS mixed micelles loaded with piperine in vitro and in vivo," vol. 44, no. 9, pp. 1409-1416, 2018.

[42] J. Mihály, R. Deák, I. C. Szigyártó, A. Bóta, T. Beke-Somfai, and Z. J. B. e. B. A.-B. Varga, "Characterization of extracellular vesicles by IR spectroscopy: fast and simple classification based on amide and CH stretching vibrations," vol. 1859, no. 3, pp. 459-466, 2017.

[43] K. Yagi, K. Yamada, C. Kobayashi, Y. J. J. o. C. T. Sugita, and Computation, "Anharmonic vibrational analysis of biomolecules and solvated molecules using hybrid QM/MM computations," vol. 15, no. 3, pp. 1924-1938, 2019.

[44] E. Alcázar, M. Rocha-Leão, J. J. J. o. t. a. Dweck, and calorimetry, "Yeast intracellular water determination by thermogravimetry," vol. 59, no. 3, pp. 643-648, 2000.

[45] M. A. Simon et al., "Hydrothermal Synthesize of HF-Free MIL-100 (Fe) for Isoniazid-Drug Delivery," Scientific reports, vol. 9, no. 1, pp. 1-11, 2019.

[46] Y. Yan and H. J. N. Ding, "pH-responsive nanoparticles for cancer immunotherapy: a brief review," vol. 10, no. 8, p. 1613, 2020.

[47] L. Palanikumar et al., "pH-responsive high stability polymeric nanoparticles for targeted delivery of anticancer therapeutics," vol. 3, no. 1, pp. 1-17, 2020.

[48] Y. Yang, Z. Wang, Y. Peng, J. Ding, and W. J. F. i. p. Zhou, "A smart pH-sensitive delivery system for enhanced anticancer efficacy via paclitaxel endosomal escape," vol. 10, p. 10, 2019.

[49] Z. Mao, X. Zhou, and C. J. B. S. Gao, "Influence of structure and properties of colloidal biomaterials on cellular uptake and cell functions," vol. 1, no. 9, pp. 896-911, 2013.

[50] D. Maouyo, S. Chu, and M. H. J. A. J. o. P.-C. P. Montrose, "pH heterogeneity at intracellular and extracellular plasma membrane sites in HT29-C1 cell monolayers," vol. 278, no. 5, pp. C973-C981, 2000.

[51] J. Misiewicz, S. Afonin, and A. S. J. B. e. B. A.-B. Ulrich, "Control and role of pH in peptide–lipid interactions in oriented membrane samples," vol. 1848, no. 3, pp. 833-841, 2015.

[52] A. D. Petelska and Z. A. J. B. J. Figaszewski, "Effect of pH on the interfacial tension of lipid bilayer membrane," vol. 78, no. 2, pp. 812-817, 2000.

[53] S. R. Bonam, F. Wang, and S. J. N. R. D. D. Muller, "Lysosomes as a therapeutic target," vol. 18, no. 12, pp. 923-948, 2019.

[54] C. Gong et al., "Macrophage-cancer hybrid membrane-coated nanoparticles for targeting lung metastasis in breast cancer therapy," vol. 18, pp. 1-17, 2020.

SUPPORTING INFORMATION

Macrophage Cell Membrane Coating on Piperine-Loaded MIL-100(Fe) Nanoparticles for Breast Cancer Treatment

Christian Rafael Quijia[1], Geovana Navegante[2], Rafael Miguel Sábio[1], Valeria Valente[2], Alberto Ocaña[3], Carlos Alonso-Moreno[4], Regina Célia Galvão Frem[5], and Marlus Chorilli[1*]

[1] Department of Drugs and Medicines, School of Pharmaceutical Sciences of São Paulo State University (UNESP), Rodovia Araraquara Jau, Km 01 – s/n – Campos Ville, 14800-903 Araraquara, Sao Paulo, Brazil. E-mail: christianqui@hotmail.com; rafael.m.sabio@unesp.br; marlus.chorilli@unesp.br

[2]Laboratory of Molecular and Cell Biology, School of Pharmaceutical Sciences, Department of Clinical Analysis, São Paulo State University (Unesp), Araraquara, Brazil. E-mail: geonavegante@gmail.com; valenteval@gmail.com

[3]Experimental Therapeutics Unit, Hospital Clínico San Carlos, IdISSC, Fundación Jiménez Díaz, START, 28040 Madrid, Spain. E-mail: alberto.ocana@salud.madrid.org

[4]Unidad NanoDrug, Facultad de Farmacia, Universidad de Castilla-La Mancha, 02008 Albacete, Spain. E-mail: Carlos.AMoreno@uclm.es

[5]Institute of Chemistry, São Paulo State University (UNESP), Prof. Francisco Degni 55, 14800-060 Araraquara, Sao Paulo, Brazil. E-mail: rcgfrem@gmail.com

[*]Corresponding author at Department of Drugs and Medicines, School of Pharmaceutical Sciences of São Paulo State University (UNESP), Rodovia Araraquara Jau, Km 01 – s/n – Campos Ville, 14800-903 Araraquara, Sao Paulo, Brazil. E-mail address: marlus.chorilli@unesp.br

HPLC assay for PIP

The calibration curve was linear by analyzing a series of PIP concentrations in ethanol from 6.25 to100 µg mL^{-1} with a correlation coefficient of R^2=0.990 (**Figure S1**). The limit of detection (LOD) and limit of quantification (LOQ) were found to be 0.25 and 0.77 µg mL^{-1}, respectively. Standard samples were prepared and injected in triplicates on three successive days.

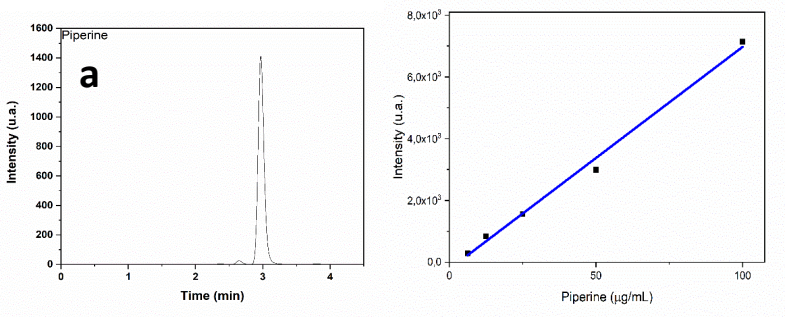

Figure S1. (a) Chromatogram of PIP (concentration = 6.25 to 100 µg mL^{-1}) in mobile phase (methanol/water (75:25)) and (b) calibration curve of PIP quantified by HPLC.

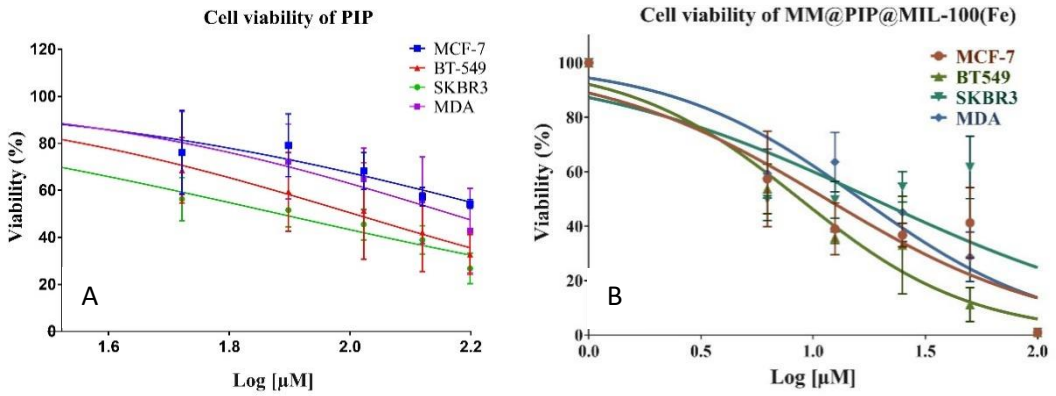

Figure S2. Cytotoxic activity of piperine (A) and MM@PIP@MIL-100 (Fe)- (B). The results represented cell viability and refer to the averages of three independent experiments (mean ± standard deviation). Cells were treated with 6.25 to 100 µM and incubated for 48 h. Viability was analyzed by nonlinear regression in GraphPad Prism version 7.0 (GraphPad Software, San Diego, CA, USA).

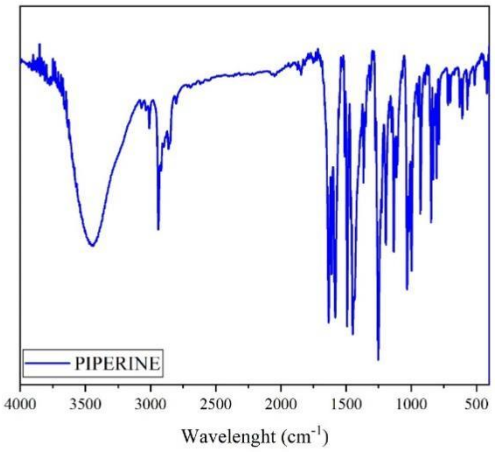

Figure S3. Fourier-transform infrared (FT-IR) spectrum analysis of PIP (blue line).

ANNEX 1

Synthesis of MIL-100(Fe)

The synthesis of MIL-100(Fe) was performed using a previously established method. [1] In this method, iron (III) chloride hexahydrate (0.081 g; 0.29 mmol) and BTC (0.028 g; 0.13 mmol) were dissolved in distilled water (1 mL). The resulting mixture was heated to 130 °C for 30 seconds and maintained at this temperature for 7 minutes (300 W) using a Mars-5 microwave reactor (CEM, US) with a maximum power output of 300 W and a frequency of 60 Hz. The MIL-100(Fe) product was obtained by centrifugation at 5600g for 8 minutes. To activate the solid, it was redispersed in absolute ethanol (1 mL) and subjected to centrifugation at 5600 g for 8 minutes. This process was repeated for a total of 4 cycles. The resulting orange solid was recovered with a yield of 98% (40 mg). Finally, the nanostructure was stored in pure ethanol at 4 °C for preservation.

PIP@MIL-100(Fe) in situ

We conducted the microwave synthesis of PIP@MIL-100(Fe) on-site following a previously described method, but with a variation. In this case, we introduced different concentrations of PIP (1, 4, 18, and 38 mg) into the initial synthesis solution. After the synthesis, the resulting PIP@MIL-100(Fe) was separated by centrifugation at 5600g for 8 minutes, and the sample with the most favorable chemical properties was chosen for further investigation. To continue the research, the recovered PIP@MIL-100(Fe) was then dispersed again in absolute ethanol (1 mL), subjected to centrifugation at 5600g for 8 minutes, and this process was repeated four times. As a result, an orange solid (40 mg, 96% yield) was obtained. To maintain the integrity of the nanostructure, it was stored in absolute ethanol at a temperature of 4 °C until it was ready to be used (see Fig. S4).

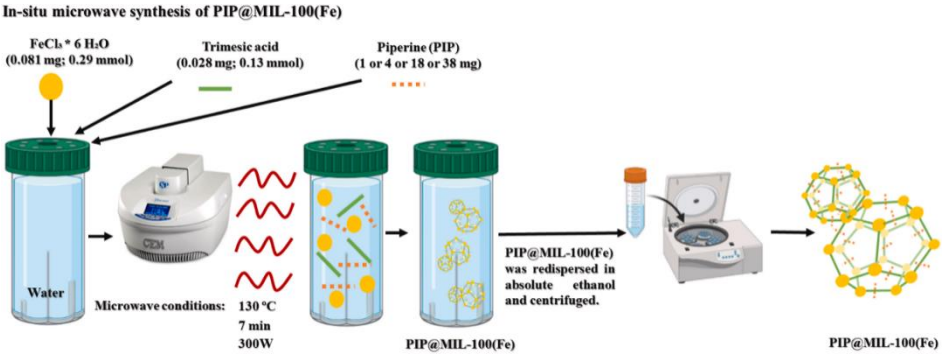

Figure S4. We performed the in-situ microwave synthesis of PIP@MIL-100(Fe) by dissolving BTC (0.028 mg; 0.13 mmol), iron (III) chloride hexahydrate (0.081 mg; 0.29 mmol), and various concentrations of PIP (1; 4; 18; and 38 mg) in 1 mL of distilled water. The reaction mixture was then subjected to microwave irradiation at 300 W, heating it to 130 °C for 30 seconds, and maintaining this temperature for 7 minutes. Next, the obtained PIP@MIL-100(Fe) was dispersed again in 1 mL of absolute ethanol, followed by centrifugation at 5600 g for 8 minutes. This centrifugation and redispersion process was repeated four times. As a result, an orange solid (40 mg, 96% yield) was recovered.

REFERENCE BIBLIOGRAPHIC

[1] C. R. Quijia *et al.*, "In situ synthesis of piperine-loaded MIL-100 (Fe) in microwave for breast cancer treatment," vol. 75, p. 103718, 2022.

4 CAPÍTULO 4: Piperine-loaded Chitosan-Coated MIL-100(Fe) Nanoparticles For Potential Application In Breast Cancer Treatment

Artigo científico que será submetido ao periódico Microporous and Mesoporous Materials.

Chitosan-Coated MIL-100(Fe) Nanoparticles for Enhanced Piperine Release in Breast Cancer Treatment

Christian Rafael Quijia[1*], Alberto Ocaña [2], Carlos Alonso-Moreno [3], Regina Célia Galvão Frem[4], and Marlus Chorilli[1]

[1] Department of Drugs and Medicines, School of Pharmaceutical Sciences of São Paulo State University (UNESP), Rodovia Araraquara Jau, Km 01 – s/n – Campos Ville, 14800-903 Araraquara, Sao Paulo, Brazil

[2]Experimental Therapeutics Unit, Hospital Clínico San Carlos, IdISSC, Fundación Jiménez Díaz, START, 28040 Madrid, Spain.

[3]Unidad NanoDrug, Facultad de Farmacia, Universidad de Castilla-La Mancha, 02008 Albacete, Spain.

[4]Institute of Chemistry, São Paulo State University (UNESP), Prof. Francisco Degni 55, 14800-060 Araraquara, Sao Paulo, Brazil

[*]Corresponding author at Department of Drugs and Medicines, School of Pharmaceutical Sciences of São Paulo State University (UNESP), Rodovia Araraquara Jau, Km 01 – s/n – Campos Ville, 14800-903 Araraquara, Sao Paulo, Brazil
E-mail address: christianqui@hotmail.com

ABSTRACT:

Breast cancer is one of the leading causes of death among women with cancer worldwide. Piperine (PIP) is a promising compound with potential chemotherapeutic activity for the treatment of breast cancer due to its antitumor activity, but its toxicity has limited its introduction in preclinical studies. An attractive platform for the treatment of breast cancer is represented by PIP@MIL-100(Fe), a metal-organic framework (MOF) network encapsulated with PIP and used as a release system. An engineering strategy in nanotechnology is the surface modification of nanosystems, such as chitosan (CHI), which is used to increase resistance to degradation and enable controlled drug release. Based on these scientific and technological advances, the aim of this study is to evaluate the therapeutic potential of PIP encapsulated in metal-organic frameworks coated with CHI in the treatment of breast cancer. The CHI@PIP@MIL-100(Fe) was successfully synthesized, which consists of MIL-100(Fe) containing PIP and coated with CHI, using the impregnation method. The infrared spectroscopy analysis showed major absorption bands such as the saccharide structure (1042, 1092, and 1164cm^{-1}), confirming the presence of CHI in the MOFs. The cytotoxicity tests conducted on breast cancer cells, including SKBR3, MCF-7, MDA-MB-231, and BT549, using CHI@PIP@MIL-100(Fe), exhibited lower cytotoxicity indices in comparison to free PIP, which showed an index that was three to four times higher. Therefore, these nanostructures show potential as PIP-based therapies for breast cancer.

Keywords: metal-organic framework; vesicle; cytotoxicity; nanostructures.

1. INTRODUCTION

Piperine (PIP) is a naturally occurring alkaloid derived from seeds of plants in the Piperaceae family. It exhibits a wide range of applications, including antimicrobial, antiparasitic, antidepressant, and modulation of oxidative stress-induced carcinogenesis [1]. Notably, PIP has demonstrated promising anti-cancer properties in various cancer types, including breast cancer. Its mechanisms of action against cancer involve inhibiting cell proliferation, inducing apoptosis, suppressing angiogenesis, and modulating signaling pathways [2]. Given these properties, PIP holds significant potential for the development of novel therapeutic interventions in breast cancer.

To further harness the therapeutic potential of PIP in a controlled and targeted manner, encapsulating it within nanoparticles has emerged as a valuable approach. Among the various types of nanoparticles explored for PIP encapsulation, liposomes and solid lipid nanoparticles have garnered considerable attention due to their biocompatibility, stability, and ability to encapsulate hydrophobic drugs. These lipid-based carriers protect PIP from enzymatic degradation, promote absorption, and enable sustained release within the target tissue. Additionally, polymeric nanoparticles such as poly(lactic-co-glycolic acid) (PLGA) nanoparticles have shown promise in encapsulating PIP and facilitating controlled drug release over time [1].

In the realm of cancer research, MIL-100(Fe), a metal-organic framework (MOF), has garnered significant interest. MOFs are crystalline materials composed of metal ions coordinated with organic ligands, exhibiting exceptional porosity and tunable properties. MIL-100(Fe) stands out due to its large pore volume and high surface area, allowing for efficient drug loading and delivery [3]. Numerous preclinical studies in breast cancer models have demonstrated the efficacy of utilizing MIL-100(Fe) for drug delivery. For instance, chemotherapeutic agents like doxorubicin have been successfully loaded into MIL-100(Fe) and coated with lipid-based nanoparticles, resulting in improved stability and targeted drug delivery, thereby enhancing therapeutic efficacy while reducing systemic toxicity. Furthermore, employing MIL-100(Fe) as a carrier for piperine has shown improved anti-cancer activity and increased drug accumulation in breast tumor cells [4].

Various coating strategies have been explored to enhance the functionality and performance of MIL-100(Fe) nanoparticles. Polymer coatings offer numerous benefits, including improved stability, prolonged circulation time, and controlled drug release. Polymers such as polyethylene glycol (PEG), poly (lactic-co-glycolic acid) (PLGA), and polyethyleneimine (PEI) have been utilized to coat MIL-100(Fe) nanoparticles, leading to

improved colloidal stability, stealth properties, and drug encapsulation[5-10]. Liposome coating has also proven effective in modifying MIL-100(Fe) nanoparticles. Liposomes are lipid-based vesicles capable of encapsulating both hydrophobic and hydrophilic drugs. By coating MIL-100(Fe) nanoparticles with liposomes, a hybrid system is formed that combines the advantages of both platforms [5, 11]. Furthermore, functionalizing liposomes with ligands specific to tumor cells or tissues enables liposome-coated MIL-100(Fe) nanoparticles to offer improved drug loading capacity, prolonged circulation time, and targeted drug delivery [5].

Chitosan (CHI), a natural polysaccharide derived from chitin, has been explored as a coating material for MIL-100(Fe) nanoparticles. CHI exhibits desirable properties for biomedical applications, such as biocompatibility, biodegradability, and mucoadhesiveness. Coating MIL-100(Fe) nanoparticles with CHI enhances their stability, facilitates cellular uptake, and enables sustained release of encapsulated therapeutics [8].

Motivated by recent advancements in science and technology, this present study focuses on utilizing chitosan polymer for the coating of MIL-100(Fe) nanoparticles and encapsulation of (PIP). In vitro tests were conducted to assess the efficacy of these nanostructures against breast cancer cells. The primary objective of this research is to develop a robust aqueous system that enhances the bioavailability of PIP while mitigating its non-specific toxicity. By exploring novel approaches such as nanoparticle encapsulation and MOF-based drug delivery, this study aims to contribute to the development of more effective and targeted therapeutic interventions for breast cancer treatment.

2. EXPERIMENTAL SECTION

2.1. MATERIALS

These chemicals were used as received without any additional treatment or processing. Specifically, iron (III) chloride hexahydrate (97%) and 1,3,5-benzene tricarboxylic acid (trimesic acid, BTC; 95%) were obtained from Sigma-Aldrich. Ethanol (96%) and methanol (99.5%) were acquired from Sigma Aldrich, St. Louis, MO, USA, and Neon, Brazil. RPMI 1640 medium supplemented with glutamax-1 from Gibco Life Technologies, L-glutamine (2 mM), and Tris/EDTA (10 mM, pH 7.4) were purchased from Life Technologies. Heat-inactivated fetal bovine serum (FBS), dimethylsulfoxide (DMSO; ≥99.7%), and penicillin/streptomycin (100 U/mL) were provided by Fischer.

2.2. Encapsulation of piperine in MIL-100(Fe)

The synthesis of PIP@MIL-100(Fe) involved following a previously established procedure. In this method, iron (III) chloride hexahydrate (0.081 g; 0.29 mmol), 1,3,5-benzenetricarboxylic acid (0.028 g; 0.13 mmol) as the ligand, and piperine (1 mg; 3.5 mmol)

were dissolved in distilled water. The reaction mixture was then heated at 130 °C for 30 seconds, followed by 7 minutes at the same temperature. The resulting PIP@MIL-100(Fe) product was obtained through centrifugation. To activate the solid, it was redispersed in absolute ethanol and subjected to multiple cycles of centrifugation. An orange solid with a yield of 98% was achieved, and it was stored in ethanol at 4 °C. The encapsulation efficiency was measured at 95 ± 3%, which is consistent with findings reported by Quijia C. et al., 2022. [4] The process is illustrated in (**Fig. S1**).

2.3. Preparation of CHI@PIP@MIL-100(Fe)

The technique described by Hidalgo et al. 2017 was used to prepare CHI@PIP@MIL-100(Fe), with a few modifications [8]. 10 mg of PIP@MIL-100(Fe) nanoparticles were dispersed in 5 ml of ethanol using an ultrasonic tip. It is important to note that the nanoparticles were used in their wet form, and the wet-to-dry ratio was previously determined from nanoparticles dried at 100 °C overnight. In another container, 10 mg of chitosan (CHI) were suspended in 5 ml of water. Then, the two suspensions were mixed and stirred for 30 minutes. The molar ratio between PIP@MIL-100 nanoparticles and CHI in the reaction mixture was 31.3:0.4, with MIL-100(Fe) and CHI concentrations of 1.0 and 1 $mg \cdot mL^{-1}$, respectively. The CHI-coated nanoparticles were collected by centrifugation and washed with aliquots of 15 ml of 1% (v/v) acetic acid (once) and water (five times). Finally, the product was stored in a wet state using water and 0.5% polyvinyl acetate (PVA). as the storage medium (**Figure 1**).

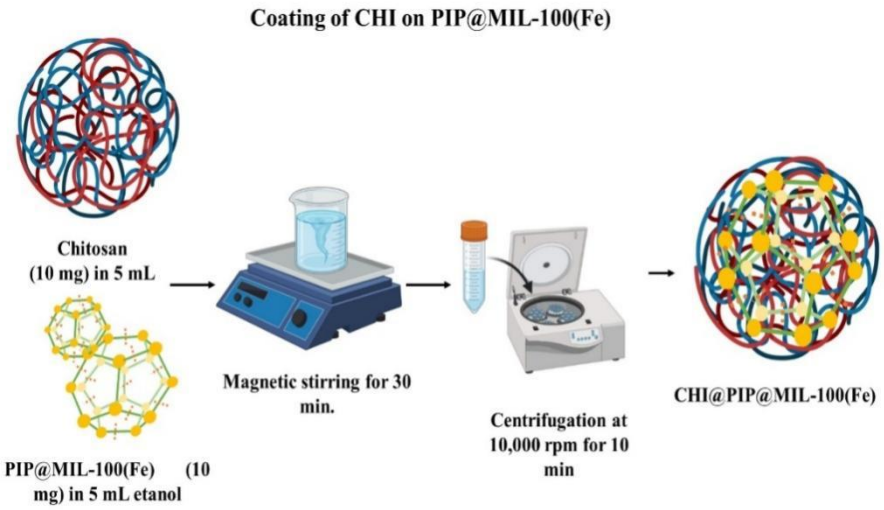

Figure 1. Development of CHI@PIP@MIL-100(Fe) nanostructures.

2.4. CHARACTERIZATION OF MOFS

Various analytical techniques were employed to characterize the samples in this study. Powder X-ray diffraction (XRD) was conducted using a Rigaku Rint 2000 diffractometer. The XRD measurements utilized Cu-Kα radiation (wavelength of 1.5406 Å) and covered an angle range of 2θ from 2º to 30º, with a step size of 0.02˚ and a duration of 2.5 s per step at room temperature. Photon correlation spectroscopy and zeta potential were performed using the Malvern Nano-ZS instrument and Zetasizer (Nano series; UK) to determine the hydrodynamic diameter and zeta potential of nanoparticles dispersed in water. Dynamic light scattering (DLS) was carried out at a concentration of 0.1 mg mL^{-1}, and three measurements were taken at room temperature with light scattering detection at a 173º angle. Vibrational spectroscopy analysis (infrared - IR) was conducted using a Perkin-Elmer model 400 IR spectrometer to analyze the infrared spectra (4000-400 cm^-1) after the samples were mixed with potassium bromide (KBr) and scanned with a resolution of 2 cm^-1. High-resolution scanning electron microscopy (HR-SEM) and high-resolution transmission electron microscopy (HR-TEM) were used to examine the morphology of the purified nanosolids. Images were captured using a TOPCON SM-300 microscope at 10–20 kV for HR-SEM, while the JEOL JEM-2100 (LaB6) at 100 kV was used for HR-TEM. For HR-TEM analysis, nanosuspensions were applied to a copper grid, dried, and stained with aqueous uranyl acetate. Thermogravimetric analysis (TGA) was performed using a TGA-Q500 instrument from TA Instruments. The samples, weighing approximately 5 mg, were heated from 30°C to 600°C at a rate of 10°C/min under a dry nitrogen flow of 40 mL/min. Adsorption porosity analysis of MIL-100(Fe) was carried out using N_2 adsorption-desorption with the ASAP 2020-Micrometrics equipment, covering a relative pressure range from 0.002 to 0.998. Gasification at 100°C for 24 hours was also conducted, and the MOFs were activated prior to the measurements to remove any solvent molecules in the pores. Elemental analysis was performed using a CHNS/O 2400 series II Elemental Analyzer (Perkin Elmer), allowing the determination of carbon, hydrogen, and nitrogen percentages with an accuracy of ±0.5 [12, 13].

2.4.1. *In vitro* release kinetics of PIP

As stated in Makhov, et al.,2012, [14] the PIP release experiments were carried out at 37°C using a receptor medium of phosphate-buffered saline (PBS) with 5% v/v Tween 20 and 5% v/v ethanol, with pH values of 7.4 or 5. In the beginning, 5 mL of the receptor medium were used to dissolve 10 mg of the CHI@PIP@MIL-100(Fe) nanosystem. The samples were centrifuged at predetermined intervals between 1 and 180 hours, and a 1 mL aliquot of the supernatant was taken to ascertain the PIP content. The extracted volume was then replaced

with 1 mL of the receptor medium, which was then added to the medium. The amount of PIP released from the removed aliquots was then measured using high-performance liquid chromatography (**Figure S2**). An add-in for Microsoft Excel called DDSolver was used to analyze the drug release modeling. It uses statistical criteria like adjusted R2 and Akaike information criterion (AIC) in its calculations and considers variables like data size, the number of data points, and statistical analysis, as described in Zhang et al., 2010, [15] to select the best release model.

2.4.2. Cell viability assay

Breast cancer cell lines, specifically MCF-7, MDA, SKBR-3, BT-549, and HaCaT, were seeded in 96-well plates with 4,000 cells per well and allowed to incubate overnight. PIP was dissolved in DMSO to form a 5% (w/v) solution, with the DMSO concentration in the experiments restricted to 0.25% (v/v) to avoid any adverse effects on cell viability. The MM@PIP@MIL-100 (Fe) (at concentrations of 100-6.25 µM) was dispersed or dissolved in DMEM medium and incubated for 48 hours. The treatments were prepared at a 3 times higher concentration to account for a direct 1/3 dilution in the well, with 50 µL of MOF solution added to achieve a final volume of 200 µL per well [16]. Nanoparticles in culture medium and medium alone were also tested to exclude any interference with the assay. Subsequently, the treatments were replaced with fresh medium (100 µL), and cytotoxicity was measured using the MTT reagent (10 µL of 5 $mg \cdot mL^{-1}$ in PBS), followed by incubation at 37°C for 4 hours, a wash with 200 µL of PBS, and the addition of 100 µL of DMSO to each well. The absorbance was measured at λ= 555 nm in a plate reader after shaking. The cytotoxicity index was built from a dose-response curve using the data obtained from cell viability as a function of different concentrations of the substance. The concentration at which a 50% reduction in cell viability occurs is defined as the IC_{50}.

2.4.3. Statistical analysis

The experiments were performed thrice (n=3), and the average values ± SEM were reported. ANOVA with post-test or t-student was used to compare the data, and statistical significance was determined at $p<0.05$. The statistical software GraphPad Prism® version 7.0 was used for all the statistical analyses. For other analyses, appropriate statistical tests were employed as follows: determination of the modal diameter of the nanostructures involved obtaining the diameter distribution, and the best fit for polydispersion was determined based on a log-normal distribution. The inhibitory concentration (IC_{50}) values and their 95% confidence intervals were determined from a linear regression model of the dose-response curve.

3. RESULTS AND DISCUSSIONS

3.1. XRD analysis

According to Guo et al., 2019; Cortés et al., 2021; Michailidou et al., 2020 [6, 17-19], the XRD analysis of crystallinity exhibited crystalline planes in both the synthesized MIL-100(Fe) and PIP@MIL-100(Fe), as well as the simulated material, with a consistent pattern of diffraction intensity at six specific angles (2θ= 3.34°, 3.94°, 4.72°, 6.2°, 10.26°, and 10.9°) **(Figure 2).** The crystallinity of the CHI@PIP@MIL-100(Fe) material remained nearly unchanged despite a typical peak broadening due to the reduced size of the crystallite resulting from a surface modification. These results align with the findings reported by Hidalgo et al. in 2017 [8].

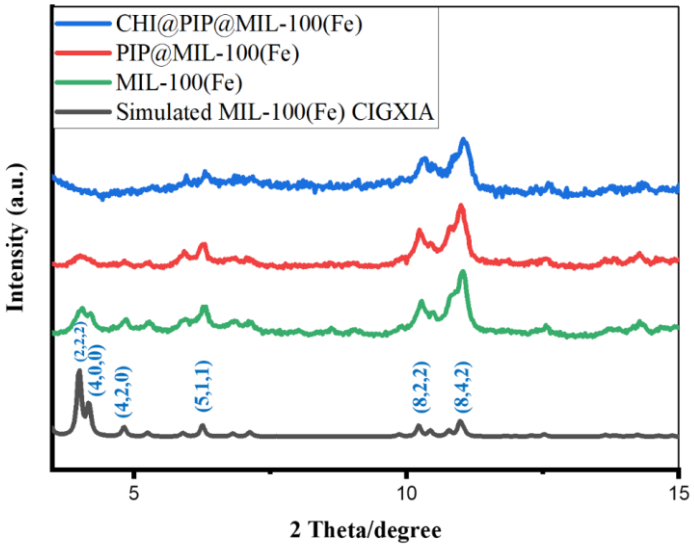

Figure 2. XRD of the simulated pattern (black); MIL-100(Fe) synthesized (green); PIP@MIL-100(Fe) (red), and CHI@PIP@MIL-100(Fe). Angle (2θ) 2-30º.

3.2. Analysis of average hydrodynamic diameter and zeta potential.

The average chitosan coating size was 177 ± 1.74 nm. The NPs' hydrodynamic diameter increased by about 80 nm after the CHI functionalization. This indicates the presence of an outer corona. The change in ζ before and after external functionalization (as shown in **Table 1**) clearly confirms that the MOF's surface is coated with CHI residues. This corresponds to the presence of CHI's protonated amino groups with a positive ζ potential. Previous research by Hidalgo *et al.* (2017) has suggested that the hydroxyl groups of CHI polymer and Fe species on the surface of MIL-100(Fe) are the primary interaction points between CHI and MOFs. Fe III can also indirectly interact by forming a hydrogen bond between the oxygen of its coordinated OH group and the HO-C6 proton of the D-glucosamine

unit [8]. Additionally, the presence of a PVA surfactant prevented MOF aggregation, while a ζ potential of over +30 mV maintained its colloidal stability and made it a stable colloidal system [20]. However, the stability of the nanoparticles, analyzed solely by hydrodynamic diameter, was found to be stable only for 10 days. This can be attributed to the interaction with PBS, a physiological saline solution, where ionic interactions and aggregate formation can occur due to the dependence on the concentration of ions present. These interactions affect the stability of MOF nanoparticles.

Table 1.- Zeta potential (ζ) analysis, hydrodynamic diameter, and polydispersity index of different nanostructures.

	PIP@MIL-100 (Fe)	**CHI@PIIP@MIL-100(Fe)**
Zeta Potential (mV)	+ 7 ± 0,6	+35,7 ± 3,34
Hydrodynamic diameter (nm)	98 ± 27,83	177 ± 1,74
Polydispersity index	0,03 ± 0,006	0,18 ± 0,012

3.3. Analysis of nanostructured systems by vibrational spectroscopy in the infrared region (FT-IR)

Figure 3 compares the Fourier-transform infrared (FT-IR) spectra of CHI and CHI-coated MIL-100(Fe) materials. The presence of CHI in the MOFs is demonstrated by the absorption bands of the carboxylate groups in PIP@MIL-100(Fe) (1374 and 1632 cm^{-1}) and the saccharide structure (1042, 1092, and 1164 cm^{-1}) in the coated material. But CHI's amide band (1393cm^{-1}) cannot be seen, possibly because they overlap with MIL-100(Fe)'s carboxylate bands [8].

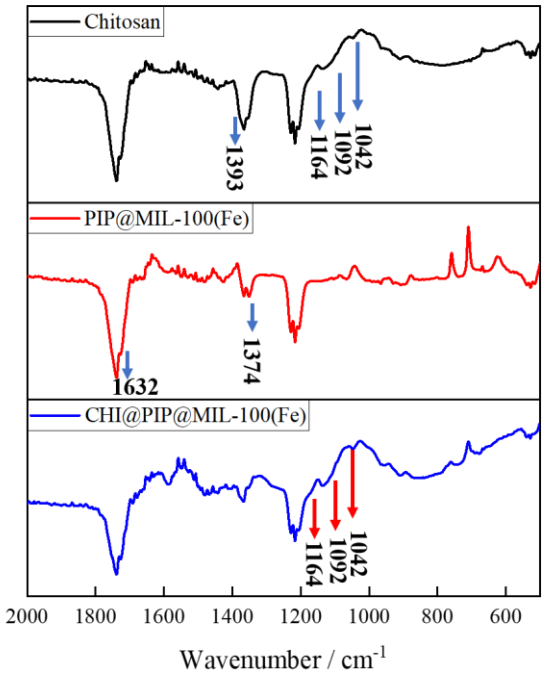

Figure 3. Fourier-transform infrared (FT-IR) spectrum analysis of nanoparticles: Chitosan (black line); PIP@MIL-100(Fe) (red line); CHI@PIP@MIL-100(Fe) (blue line). Note: Figures 3-A and 3-B from the previous article by Quijia et al., 2022. [4]

3.4. Elemental analysis of MOF and chitosan using a CHNS

Once the FT-IR of CHI@PIP@MIL-100(Fe) was analyzed, elemental analysis was carried out to evaluate the carbon, hydrogen, and nitrogen content and compare the presence of CHI in the MOF. Based on the analytical results shown in **Table 2**, it can be verified that the carbon content of CHI@PIP@MIL-100(Fe) increases by approximately 7% compared to PIP@MIL-100(Fe), suggesting that there was a change in composition, corroborating the presence of CHI in the MOFs.

Table 2.- Elemental analysis of MOF and chitosan using a CHNS

RESULTS	% OF ELEMENTS			
	C	H	N	S
Chitosan	42,16	8,56	8,06	1,79
PIP@MIL-100(Fe)	**27,1**	**6,4**	0,78	1,42
CHI@PIP@MIL-100(Fe)	**34,2**	**6,7**	**5,7**	1,5

3.5. Morphology analysis of nanomaterials

In the study on MOF composite material, the SEM images in **Figures 4-C and 4-D** revealed a 10 nm outer layer that was distinguishable from the inner layer. This outer layer was found to be a dried layer of CHI due to its highly carbonaceous composition, which is more than 20 times greater than that of the inner layer. These findings are consistent with another study by Hidalgo et al. 2017, [8] indicating the successful coating of CHI on the

PIP@MIL-100(Fe) composite. The SEM images of PIP@MIL-100(Fe) and CHI@PIP@MIL-100(Fe) materials were presented in **Figures 4-A and 4-C**, respectively.

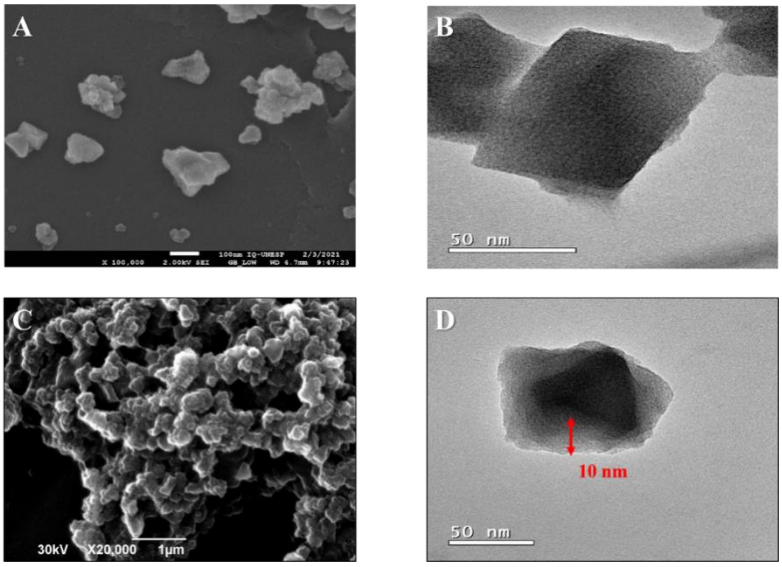

Figure 4. Morphology analysis by scanning electron microscopy (SEM): (A) PIP@MIL-100 (Fe), and (C) CHI@PIP@MIL-100 (Fe); Morphology analysis by transmission electron microscopy (TEM) (B) PIP@MIL-100(Fe), and (D)CHI@PIP@MIL-100(Fe).

3.6. Thermal Analysis

Thermogravimetric analysis (TGA) was used to investigate the thermal characteristics of MIL-100(Fe), PIP@MIL-100(Fe) and CHI@PIP@MIL-100(Fe) materials over a temperature range of 30°C to 600°C, with a heating rate of 10°C.min^{-1}. The thermogravimetric curves of these materials, which were the focus of this study, are shown in **Figure 5**.

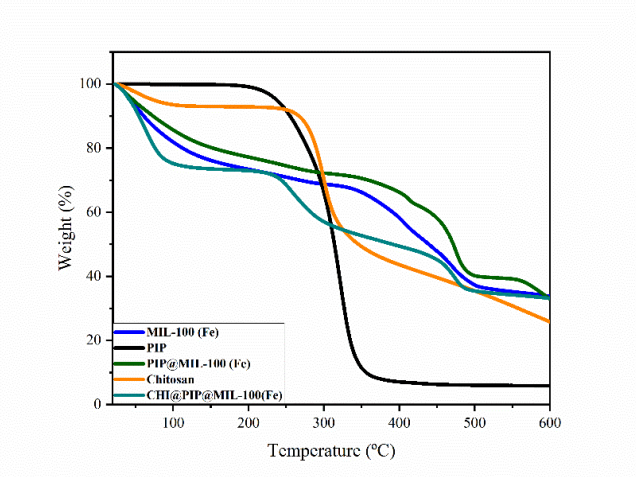

Figure 5. Thermogravimetric curves of the compounds: PIP@MIL-100(Fe) (green line); CHI@PIP@MIL-100(Fe) (light blue line); Chitosan (orange line).

The PIP@MIL-100(Fe) sample exhibits a total weight loss mainly divided into four sections. As seen in Figure 5, initially, the mass loss is 22% below 270 °C, which has been attributed to the release of trapped water molecules. However, the decomposition of PIP (270-380 °C) accounts for an additional 22% weight loss. Furthermore, a weight loss of approximately 25% was recorded between 380-490 °C, attributed to the collapse of the structure due to the removal of tricarboxylic acid benzene. A total weight loss of 13% was observed at 525 °C, which could be due to the decomposition of the ligand to form iron oxide, and finally, a weight loss of 13% was reported at the same temperature for PIP@MIL-100(Fe) [4, 21].

The study found that the chitosan coating in MOFs (shown as a light blue line in **Figure 5)** experiences two weight loss stages between 50 to 600°C. The first stage takes place from 50–267°C and involves an approximate 11% loss of water molecules. The primary degradation of pure chitosan, on the other hand, begins at 300°C and is completely degraded at about 450°C with a weight loss of approximately 44% [22]. The amount of CHI coating in MOFs was indirectly estimated by comparing the CHI concentration in the initial reaction mixture (1 mg mL^{-1}) with 5 mg of PIP@MIL-100(Fe). The region that showed a weight loss of 16.56% between 241 and 300°C corresponded to the CHI coating.

3.7. Nitrogen adsorption-desorption isotherms

The textural properties of MIL-100(Fe), PIP@MIL-100(Fe) and CHI@PIP@MIL-100(Fe), including specific surface area and pore structure, were confirmed through nitrogen adsorption-desorption measurements, as shown in Figure 6. After coating with chitosan on PIP@MIL-100(Fe), the surface areas and pore volumes decreased to 400 m^2 g^{-1} and 0.17 cm^3g^{-1}, respectively, due to the presence of a nonporous organic material on the external surface. This reduction was attributed to pore blockage under dry and cold measurement conditions, which resulted in the collapse and freezing of the polymeric chains on the surface of the nanoparticles and is consistent with findings from Zimpel et al. (2016) [11]. (**Table 3 and Figure 6**).

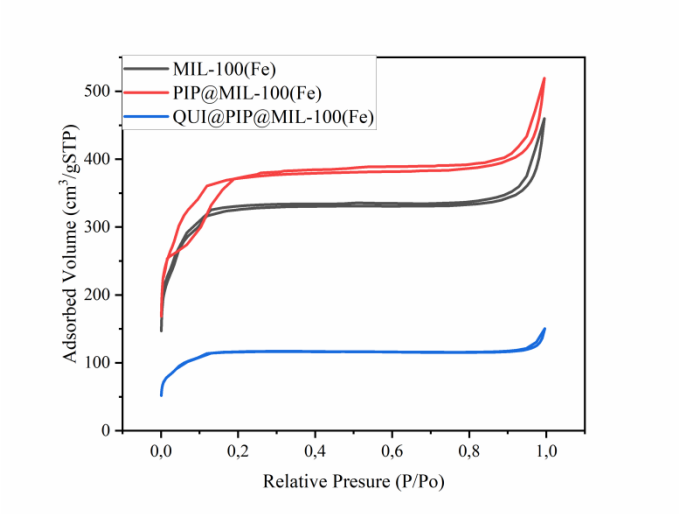

Figure 6. a.- N_2 adsorption/desorption curves of PIP@MIL-100(Fe) encapsulated material (in red) and chitosan-coated MOFs (in blue).

Table 3.- Specific area and pore volume of materials.

	S_{BET} (m^2g^{-1})	**Total pore volume (cm^3g^{-1})**
MIL-100(Fe)	1122,069	0,52
PIP@MIL-100(Fe)	1280,341	0,60
CHI@PIP@MIL-100(Fe)	400,376	0,17

3.8. In vitro release assay of PIP

3.8.1. Study of PIP release in PBS at pH 7.4 and 5.0

To simulate physiological conditions such as those found in blood circulation or acidic microenvironments of tumor regions, researchers performed an experiment using phosphate-buffered saline (PBS) solution containing 5% v/v Tween 20 and 5% v/v ethanol, at 37°C and at pH levels of 7.4 and 5.0. The pH of 5.0 was chosen because endocytosis in cancer cells typically captures most nanostructures, which become trapped in the endosomal and lysosomal compartments that normally have a pH range of 4.5 to 5.5 [23].

Table 4.- Results of table fitting of the release profile equation. where M, t represents the cumulative release (%) and release time (h), respectively

	CHI@PIP@MIL-100(Fe)	
	pH=7	pH=5
Korsmeyer-Peppas Model	$M = k_{KP} * t^{n}$	
Equation	M=33,88 $t^{0,24}$	M=31,14 $t^{0,26}$
Rsqr	0,74275327	0,617251416
AIC	00.086	00.092
Weibull Model	$M = 100\left[e^{-\frac{(t-Ti)^{\beta}}{\alpha}}\right]$	
Equation	$M = 100\left[e^{-\frac{(t-0,8)^{0,7}}{2,88}}\right]$	$M = 100\left[e^{-\frac{(t-1,2)^{0,57}}{2,86}}\right]$
Rsqr	**0,97286139**	**0,928738602**
AIC	00.063	00.075
Gompertz Model	$M = 100 * e^{-\alpha * e^{-\beta * \log(t)}}$	
Equation	$M = 100 * e^{-0,004 * e^{-0,003 * \log(t)}}$	$M = 100 * e^{-0,005 * e^{-0,003 * \log(t)}}$
Rsqr	0,97907157	0,958888871
AIC	00.058	00.067

Note: Adjusted R^2 (Rsqr) and the Akaike Information Criterion (AIC)

The Weibull model was used to adjust the release profile of PIP in CHI@PIP@MIL-100(Fe) at pH levels of 7.4 and 5 (**Table 4**). The b values obtained from this model were 0.7, indicating Fickian diffusion where b ≤ 0.75 [24]. The release at pH 7.4 was 5% lower at 0.01 mg mL^{-1} (**Figure 7**), while at pH 5, it was 18% lower at 0.036 mg mL^{-1}, after 160 hours. This indicates that the release rate of PIP in these nanosystems is pH-dependent and is faster at a lower pH than near neutral pH. This finding is in agreement with previous studies on chitosan nanoparticles, which have demonstrated that the solubility of CHI is higher at a lower pH due to the ionization of D-glucosamine residues, resulting in increased polymer swelling and faster drug release [25].

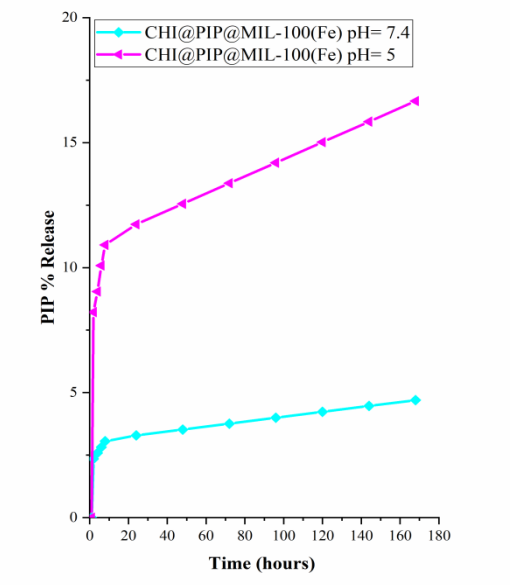

Figure 7. Release profile of CHI@PIP@MIL-100(Fe) at pH values 7,4 and 5.

3.9. Assay cytotoxicity

In **Table 5**, in parentheses, the number of times that the nanostructures exceeded the IC_{50} with respect to the drug (PIP) is presented. This variability in cytotoxicity may be attributed to their different phagocytic activities, which are related to cellular uptake of MOFs. A study conducted by Tamames-Tabar et al., 2014, analyzed the cell lineage dependency, concluding that some cell lines can uptake more rapidly, such as J774 and HeLa cells [26].

Table 5.- Cytotoxicity index of nanoparticles and piperine against breast cancer cells

	MCF-7	**MDA**	**SKBR-3**	**BT-549**
PIP	193,67 ± 0,30	139,60 ± 1,17	72,62 ± 1,08	96,38 ± 1,10
CHI@PIP@MIL-100 (Fe)	59,49 ± 1,18 **(3)**	32,02 ± 1,19 **(4)**	46,87 ± 1,11 **(2)**	31,35 ± 1,05 **(3)**

Note: Piperine (PIP), Chitosan (CHI). The results represented in the table refer to the averages of three independent experiments (mean ± standard deviation). a. IC_{50} corresponds to the minimum concentration to inhibit 50% of cancer cells. Cells were treated with 6.25 to 100 µM and incubated for 48 h. The number of times the nanostructures exceed the IC_{50} in relation to the drug (PIP) is shown in parentheses.

Statistical analysis using Tukey's ANOVA test, compared with the IC_{50}, indicates that all PIP-loaded nanosystems have a notably more toxic effect ($p<0.05$) on tumor cells than PIP alone (**Figure 8**). This cytotoxic impact is likely due to the acidic pH of lysosomal enzymes,

which can significantly enhance drug release into the cytoplasm, resulting in comparable cell death compared to free drugs [27].

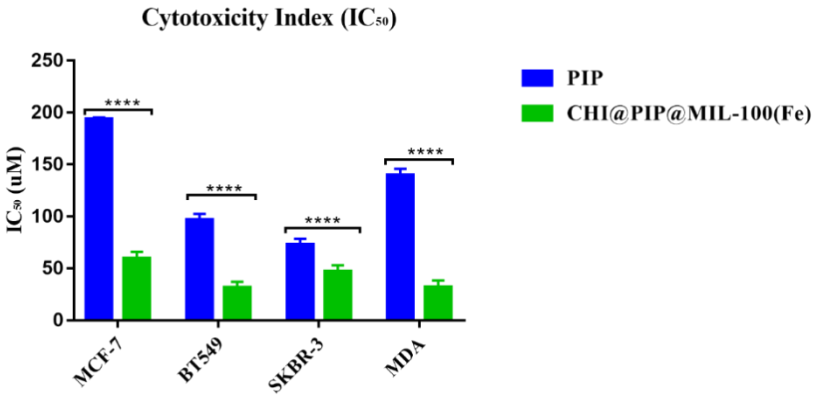

Figure 8. Indices of cytotoxicity of nanoparticles against breast cancer cells (MCF-7; BT-549; SKBR-3; MDA)

The CHI@PIP@MIL-100(Fe) nanoparticle exhibited high cytotoxicity compared to PIP (**Table 5**). This cytotoxicity can be attributed to CHI's characteristics, such as its bioadhesive capacity, which is associated with increased cellular penetration of nanoparticles. Additionally, the positive charge of this nanoparticle, as shown in **Table 1**, promotes an electrostatic interaction with negatively charged cell membranes [28]. Therefore, it is predicted that coating the nanoparticle with CHI allows it to be absorbed by cancer cells before releasing MOFs. On the other hand, CHI has been shown to be capable of inhibiting the growth of various cancer cells and inducing cell cycle arrest and apoptosis [29].

4. CONCLUSION

In summary, the study investigated CHI@PIP@MIL-100(Fe) nanosystems for the treatment of breast cancer. The analysis revealed successful surface modification of the nanosystems with chitosan (CHI), maintaining crystallinity and colloidal stability. The nanosystems exhibited pH-dependent drug release, with faster release at lower pH values. Moreover, they demonstrated higher cytotoxicity against tumor cells compared to free PIP, potentially due to enhanced cellular penetration and improved drug release in acidic tumor microenvironments. The findings suggest that CHI@PIP@MIL-100(Fe) nanosystems have the potential to be utilized for targeted and controlled drug delivery in breast cancer treatment, with opportunities for further optimization and combination therapies. However, additional preclinical studies are needed to assess long-term toxicity, biodistribution, and therapeutic efficacy before clinical translation.

In conclusion, CHI@PIP@MIL-100(Fe) nanosystems offer promising prospects for the treatment of breast cancer. These nanosystems possess controlled drug release properties,

enhanced cytotoxicity, and stability in the tumor microenvironment. Future research should focus on optimizing the nanosystems, investigating their *in vivo* behavior, and exploring potential combination therapies. Before clinical translation, comprehensive studies are required to evaluate their safety and efficacy.

5. ACKNOWLEDGEMENTS

The authors acknowledge FAPESP (process 2018/21119–0) and grant CPP2021-008597 funded by MICIN/AEI/10.13039/501100011033 end European Union Next Generation EU/PRTR, and SBPLY/21/180501/000050 funded by JCCM and by EU through Fondo Europeo de Desarrollo Regionalfor the financial support given for the development of this work.

6. REFERENCE BIBLIOGRAPHIC

[1] C.R. Quijia, V.H. Araujo, M.J.A.P. Chorilli, Piperine: Chemical, biological and nanotechnological applications, 71 (2021) 185-213.
[2] R.A. Rather, M.J.F.i.c. Bhagat, d. biology, Cancer chemoprevention and piperine: molecular mechanisms and therapeutic opportunities, 6 (2018) 10.
[3] C.R. Quijia, C. Lima, C. Silva, R.C. Alves, R. Frem, M.J.J.o.D.D.S. Chorilli, Technology, Application of MIL-100 (Fe) in drug delivery and biomedicine, 61 (2021) 102217.
[4] C.R. Quijia, M.T. Luiz, R.P. Fernandes, R.M. Sabio, R. Frem, M.J.J.o.D.D.S. Chorilli, Technology, In situ synthesis of piperine-loaded MIL-100 (Fe) in microwave for breast cancer treatment, 75 (2022) 103718.
[5] S. Wuttke, S. Braig, T. Preiß, A. Zimpel, J. Sicklinger, C. Bellomo, J.O. Rädler, A.M. Vollmar, T.J.C.C. Bein, MOF nanoparticles coated by lipid bilayers and their uptake by cancer cells, Chemical Communications, 51 (2015) 15752-15755.
[6] A.L. Guo, M. Durymanov, A. Permyakova, S. Sene, C. Serre, J. Reineke, Metal Organic Framework (MOF) Particles as Potential Bacteria-Mimicking Delivery Systems for Infectious Diseases: Characterization and Cellular Internalization in Alveolar Macrophages, Pharmaceutical Research, 36 (2019).
[7] S. Rojas, I. Colinet, D. Cunha, T. Hidalgo, F. Salles, C. Serre, N. Guillou, P.J.A.o. Horcajada, Toward Understanding Drug Incorporation and Delivery from Biocompatible Metal–Organic Frameworks in View of Cutaneous Administration, ACS omega, 3 (2018) 2994-3003.
[8] T. Hidalgo, M. Giménez-Marqués, E. Bellido, J. Avila, M. Asensio, F. Salles, M. Lozano, M. Guillevic, R. Simón-Vázquez, A.J.S.r. González-Fernández, Chitosan-coated mesoporous MIL-100 (Fe) nanoparticles as improved bio-compatible oral nanocarriers, Scientific reports, 7 (2017) 43099.
[9] T. Hidalgo, M. Alonso-Nocelo, B. Bouzo, S. Reimondez-Troitiño, C. Abuin-Redondo, M. de la Fuente, P.J.N. Horcajada, Biocompatible iron (iii) carboxylate metal–organic frameworks as promising RNA nanocarriers, 12 (2020) 4839-4845.
[10] Y.-K. Seo, S.K. Chitale, U. Lee, P. Patil, J.-S. Chang, Y.K.J.J.o.n. Hwang, nanotechnology, Formation of Polyaniline-MOF Nanocomposites Using Nano-Sized Fe (III)-MOF for Humidity Sensing Application, 19 (2019) 8157-8162.
[11] A. Zimpel, T. Preiß, R. Röder, H. Engelke, M. Ingrisch, M. Peller, J.O. Rädler, E. Wagner, T. Bein, U.J.C.o.M. Lächelt, Imparting functionality to MOF nanoparticles by external surface selective covalent attachment of polymers, 28 (2016) 3318-3326.

[12] M.T. Marcos-Almaraz, R. Gref, V. Agostoni, C. Kreuz, P. Clayette, C. Serre, P. Couvreur, P. Horcajada, Towards improved HIV-microbicide activity through the co-encapsulation of NRTI drugs in biocompatible metal organic framework nanocarriers, Journal of Materials Chemistry B, 5 (2017) 8563-8569.
[13] B.E. Souza, J.-C.J.C. Tan, Mechanochemical approaches towards the in situ confinement of 5-FU anti-cancer drug within MIL-100 (Fe) metal–organic framework, CrystEngComm, 22 (2020) 4526-4530.
[14] P. Makhov, K. Golovine, D. Canter, A. Kutikov, J. Simhan, M.M. Corlew, R.G. Uzzo, V.M.J.T.p. Kolenko, Co-administration of piperine and docetaxel results in improved anti-tumor efficacy via inhibition of CYP3A4 activity, 72 (2012) 661-667.
[15] Y. Zhang, M. Huo, J. Zhou, A. Zou, W. Li, C. Yao, S.J.T.A.j. Xie, DDSolver: an add-in program for modeling and comparison of drug dissolution profiles, 12 (2010) 263-271.
[16] T. Hidalgo, R. Simón-Vázquez, A. González-Fernández, P.J.C.s. Horcajada, Cracking the immune fingerprint of metal–organic frameworks, 13 (2022) 934-944.
[17] G. Chaturvedi, A. Kaur, A. Umar, M.A. Khan, H. Algarni, S.K.J.J.o.S.S.C. Kansal, Removal of fluoroquinolone drug, levofloxacin, from aqueous phase over iron based MOFs, MIL-100 (Fe), Journal of Solid State Chemistry, (2019) 121029.
[18] D. Cunha, M. Ben Yahia, S. Hall, S.R. Miller, H. Chevreau, E. Elkaïm, G. Maurin, P. Horcajada, C.J.C.o.M. Serre, Rationale of drug encapsulation and release from biocompatible porous metal–organic frameworks, Chemistry of materials, 25 (2013) 2767-2776.
[19] J.s. Gandara-Loe, I. Ortuño-Lizarán, L. Fernández-Sanchez, J.L. Alió, N.s. Cuenca, A. Vega-Estrada, J.J.A.a.m. Silvestre-Albero, interfaces, Metal–Organic Frameworks as Drug Delivery Platforms for Ocular Therapeutics, ACS applied materials & interfaces, 11 (2018) 1924-1931.
[20] G. Michailidou, N.M. Ainali, E. Xanthopoulou, S. Nanaki, M. Kostoglou, E.N. Koukaras, D.N.J.P. Bikiaris, Effect of poly (vinyl alcohol) on nanoencapsulation of budesonide in chitosan nanoparticles via ionic gelation and its improved bioavailability, 12 (2020) 1101.
[21] P. Horcajada, S. Surblé, C. Serre, D.-Y. Hong, Y.-K. Seo, J.-S. Chang, J.-M. Greneche, I. Margiolaki, G.J.C.C. Férey, Synthesis and catalytic properties of MIL-100 (Fe), an iron (III) carboxylate with large pores, Chemical Communications, (2007) 2820-2822.
[22] S. Kumar, J.J.I.J.o.M.S. Koh, Physiochemical, optical and biological activity of chitosan-chromone derivative for biomedical applications, 13 (2012) 6102-6116.
[23] Y. Yan, H.J.N. Ding, pH-responsive nanoparticles for cancer immunotherapy: a brief review, 10 (2020) 1613.
[24] Y. Herdiana, N. Wathoni, S. Shamsuddin, M.J.H. Muchtaridi, Drug release study of the chitosan-based nanoparticles, (2021) e08674.
[25] B.K. Patel, R.H. Parikh, P.S.J.J.o.d.d. Aboti, Development of oral sustained release rifampicin loaded chitosan nanoparticles by design of experiment, 2013 (2013).
[26] C. Tamames-Tabar, D. Cunha, E. Imbuluzqueta, F. Ragon, C. Serre, M.J. Blanco-Prieto, P.J.J.o.M.C.B. Horcajada, Cytotoxicity of nanoscaled metal–organic frameworks, Journal of Materials Chemistry B, 2 (2014) 262-271.
[27] S.R. Bonam, F. Wang, S.J.N.R.D.D. Muller, Lysosomes as a therapeutic target, 18 (2019) 923-948.
[28] Y. Herdiana, N. Wathoni, D. Gozali, S. Shamsuddin, M.J.P. Muchtaridi, Chitosan-Based Nano-Smart Drug Delivery System in Breast Cancer Therapy, 15 (2023) 879.
[29] J. Ding, Y.J.F.i.P. Guo, Recent advances in chitosan and its derivatives in cancer treatment, 13 (2022).

5 CONCLUSÕES

Em resumo, esse trabalho demonstra que a estratégia de preparação e de encapsulação *in situ* de fármacos em sistemas de liberação controlada baseados em MOFs oferece novas oportunidades para a encapsulação da piperina (PIP) no MIL-100 (Fe). Foi possível encapsular PIP a uma porcentagem > do 90 %, comparado com o método tradicional (impregnação) que encapsulou menos do que 15 % (**Anexo 1**). Por outro lado, foram desenvolvidas ainda duas novas nanoestruturas de MOFs revestidas com membrana de macrófago (MM) e quitosana (QUI), os quais foram aplicados em linhagens celulares de câncer de mama (ver a seguir). As MOFs que foram revestidas com MM e QUI mostraram exitosamente a modificação de superfície mediante diversas técnicas, sendo as mais importantes microscopia eletrônica de transmissão que sugeriu o sucesso do recobrimento das membranas de macrófago ou quitosana, que formaram uma camada externa de ~ 10 nm de espessura. Por espectroscopia vibracional no infravermelho puderam ser identificadas as principais bandas de absorção, incluindo aqueles referentes à estrutura de sacarídeos (1164, 1092 e 1042 cm^{-1}), sugerindo, portanto, a presença da quitosana no MOF. Já o sucesso na preparação da nanosistema MM@PIP@MIL-100(Fe) pode ser verificado através das bandas de massa molecular das proteínas nos ensaios de eletroforese. Foi verificado também que os materiais exibem uma liberação controlada do fármaco piperina, em meio PBS a dois diferentes valores de pH (5,0 e 7,4), a 37 °C. De um modo geral, a liberação da PIP ocorre por um modelo cinético tipo difusão *Fickiana*. Por outro lado, as modificações realizadas na superfície das MOFs resultaram em porcentagens menores de liberação (< 25 %, 7 dias), quando comparado com a matriz PIP@MIL-100(Fe). Os resultados da avaliação de citotoxicidade frente a quatro diferentes linhagens celular de câncer de mama (MCF-7, SKBR3, MDA -MB-231 e BT549) indicaram que as nanoestruturas MOFs carregadas com PIP são mais tóxicas do que o próprio fármaco. Com base nesses resultados, este trabalho demonstrou que os materiais baseados na MOF porosa MIL-100(Fe) contendo piperina e revestimentos de membrana de macrófago ou quitosana apresentaram um padrão de liberação sustentado (~ 7 dias) e controlado, demonstrando potencialidade de ser uma estrutura promissora em terapias baseadas em piperina contra o câncer de mama.

6 CONSIDERAÇÕES FINAIS

Embora a piperina tenha sido encapsulada com sucesso nos materiais aqui propostos, estudos *in vivo* ainda precisam ser realizados, fato esse que não foi ainda possível, pois uma quantidade maior de fármaco dentro das matrizes seria necessária. Este teste foi realizado colocando uma quantidade maior de PIP durante a síntese; todavia, este teste demonstrou que infelizmente os nanocompostos tiveram uma modificação em sua estrutura, conforme analisado em DRX e MEV. Por exemplo, ao colocar 4 mg de PIP, os resultados de cristalografia revelaram uma perda de cristalinidade pela diminuição de picos do difratômetro em 2θ= 4,72º; 6,2º; 10,26º e 10, 9º (**Anexo 1**). Quando 20 mg do fármaco foi adicionado no meio reacional, (ver **Artigo 1**), apenas 14 % de rendimento foi obtido e os produtos formados são um material amorfo e partículas na forma de agulhas (**Anexo 2**).

Para a análise de citômetro de fluxo deste tipo de material, é necessário otimizar o encapsulamento da piperina por outro tipo de metodologia (método mecanoquímico ou método de alta pressão, por exemplo), conforme argumentado no parágrafo anterior, já que para atingir as análises dentro do citômetro é necessário que os MOFs contenham 20 mg de PIP, e isso não foi possível de realizar.

A análise de internalização no nível intracelular tem sido amplamente relatada. No entanto, para o nosso estudo é necessário realizar modificações de superfície contendo fluoróforos nas matrizes tanto na vesícula da membrana do macrófago quanto na quitosana.

Finalmente, a estratégia de síntese e encapsulamento da piperina realizados *in situ* nos materiais desenvolvidos neste trabalho poderia ser amplamente utilizada para outros tipos de fármacos ou outros tipos de doenças, uma vez que esta metodologia é inovadora e não há nenhum outro estudo relatado anteriormente.

7 ANEXOS

7.1 Anexo 1. - Analise XRD.

É observado no XRD que PIP@MIL-100(Fe) = 4 mg, tem uma perda de cristalinidade pela diminuição de intensidade de difração em 2θ= 4,72º; 6,2º; 10,26º e 10, 9º.

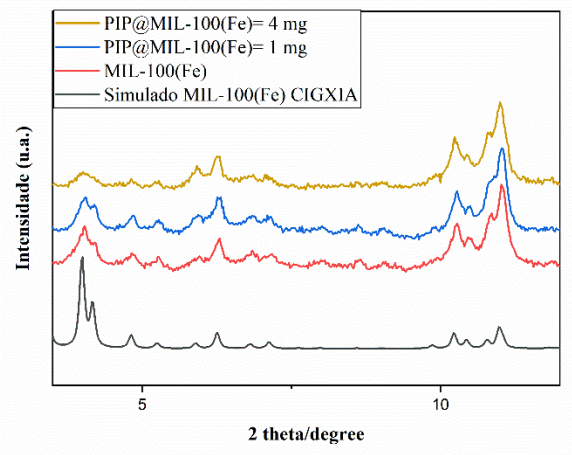

XRD do padrão simulado (preto); sintetizado do MIL-100(Fe) (Vermelho); PIP@MIL-100(FE)= 1 mg (Azul), e PIP@MIL-100(Fe) = 4 mg. Ângulo (2 θ) 2-30º.

7.2 Anexo 2. - Analise MEV.

Análise da morfologia por microscópio eletrônico de varredura (MEV): PIP@MIL-100 (Fe). É observado que a PIP@MIL-100(Fe) = 20 mg, a morfologia em forma de agulha e amorfas.

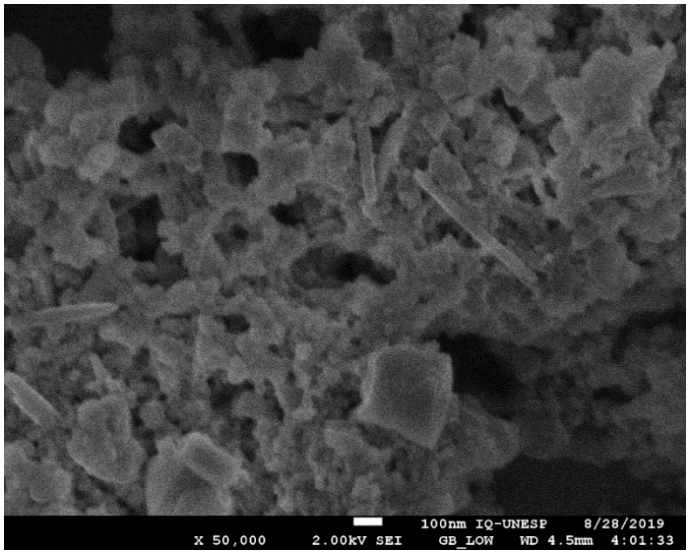

7.3 Anexo 3. – Viabilidade celular em diferentes linhas celulares usando piperina

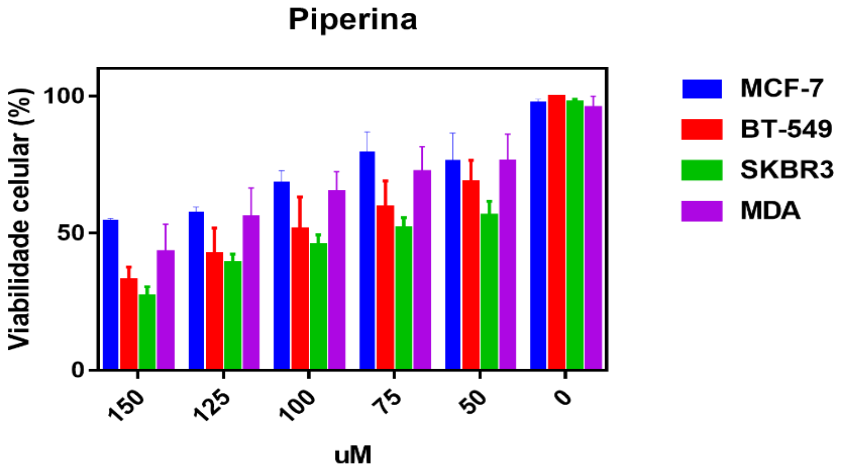

7.4 Anexo 4. – Viabilidade celular em diferentes linhas celulares usando PIP@MIL-100(Fe)

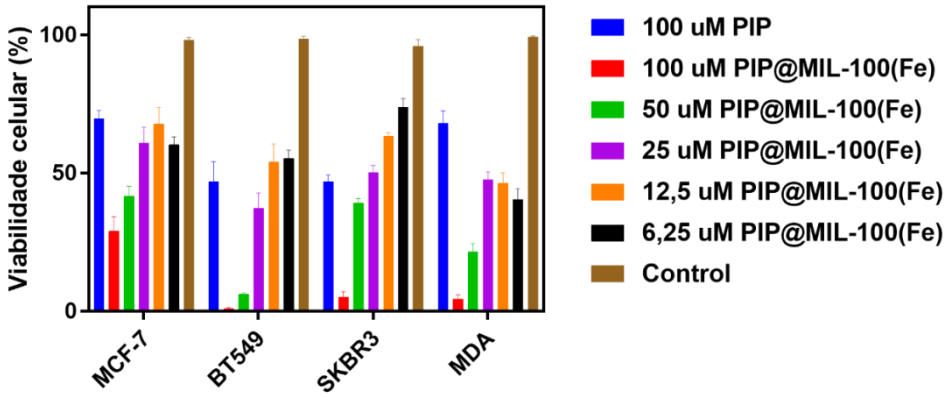

7.5 Anexo 5. – Viabilidade celular em diferentes linhas celulares usando QUI@PIP@MIL-100(Fe)

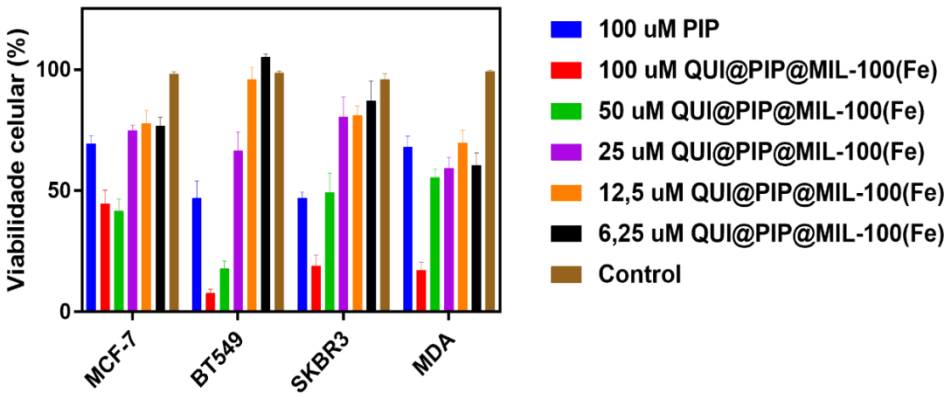

7.6 Anexo 6. – Viabilidade celular em diferentes linhas celulares usando MM@PIP@MIL-100(Fe)

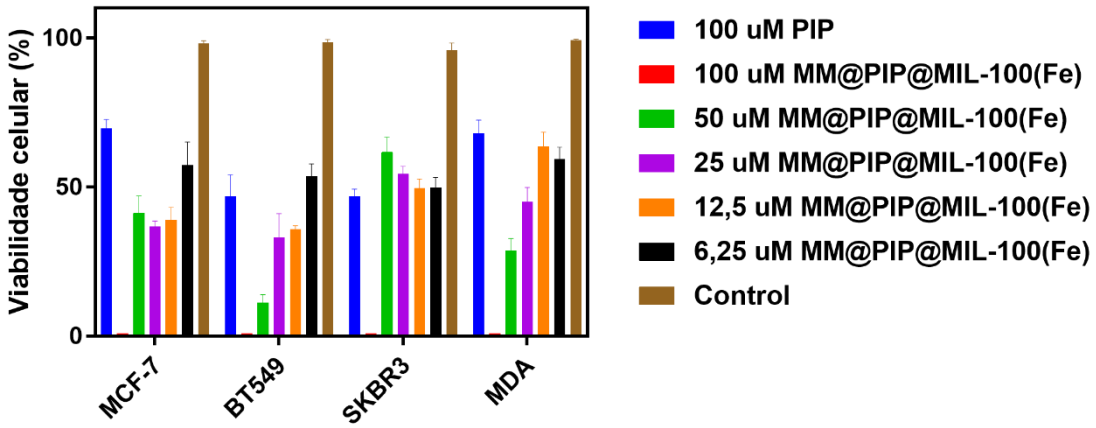

7.7 Anexo 7. – Validação do método de quantificação

7.7.1 Desenvolvimento do método analítico para quantificação de PIP por cromatografia líquida de alta eficiência com detector de arranjos de diodos (CLAE-DAD)

Antes de realizar a quantificação da piperina, ela foi dissolvida em etanol com 99,9% de pureza. Em seguida, um método eficiente foi desenvolvido para atender aos requisitos mínimos para aplicação em análises por cromatografia líquida de alta eficiência com detector de arranjo de diodos (CLAE-DAD). Foram realizadas avaliações dos parâmetros de linearidade, precisão, exatidão, robustez, limite de detecção (LD) e limite de quantificação (LQ) de acordo com as diretrizes da Conferência Internacional de Harmonização e da RDC 166/2017. (55). O método utilizado para a quantificação da PIP por CLAE foi adaptado do trabalho de Reyes Solís, Sánchez (56) para a detecção de piperina em vesículas.

7.7.1.1 Parâmetros para testar a metodologia analítica

Os experimentos foram realizados em cromatógrafo a líquido de alta eficiência (Perkin Elmer, Brasil), equipado com detector de arranjo de diodos (DAD), detecção em 340 nm, com bomba LC-20A, instalado no laboratório de Farmacotécnica na Faculdade de Ciência Farmacêuticas de Araraquara – UNESP. A separação foi realizada em coluna C18 (Zorbax Extend 150 x 4.6 mm; 5 µm). A fase móvel foi constituída de metanol e água deionizada (75:25 v/v), com fluxo de fase móvel de 0.8 $mL.min^{-1}$ e volume de injeção de 10 µL.

7.7.1.2 Seletividade

Devido ao método de encapsulação *in situ* por micro-onda, a seletividade consiste primeiramente em colocar em solução etanólica partículas do MIL-100(Fe) e a PIP. Uma alíquota de 1 mL de sobrenadante foi recuperada por centrifugação (10000 rpm por 8 min)

(**Fig. 3**). A seletividade foi determinada comparando os cromatogramas obtidos do sobrenadante recuperado da PIP e do MIL-100(Fe) em solução etanólica (37, 57-59).

Figura 3.- Procedimento de analises da piperina no MIL-100(Fe) por CLAE

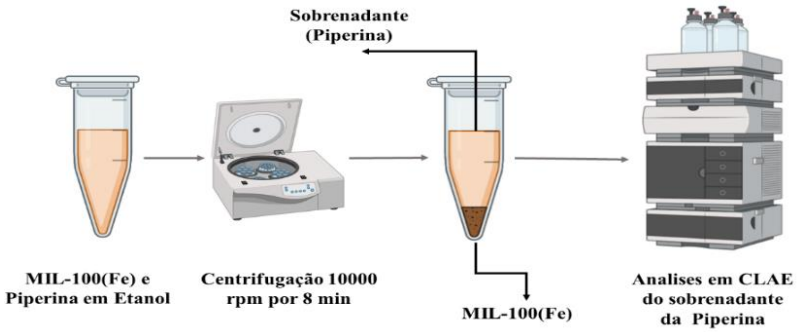

Analises de encapsulação da piperina no MIL-100(Fe) por CLAE. Uma alíquota de 1 mL é centrifugada (10000 rpm por 8 min); O sobrenadante é recuperado, para logo ser analisado por CLAE e analisar os cromatogramas.

Fonte: Autor

7.7.1.3 Linearidade

A avaliação da linearidade foi realizada por meio da média de três curvas analíticas da piperina (PIP). A partir de uma solução-mãe com concentração de 1 mg/mL, foram preparadas cinco diluições com concentrações variando de 6,25 a 100 µg/mL. Cada curva padrão foi lida em triplicata para os cinco níveis de concentração. Para avaliar a linearidade, utilizou-se a análise de regressão linear com ajuste dos dados pelo método dos mínimos quadrados. A qualidade do ajuste do modelo foi verificada por meio de análise de variância (ANOVA) com um nível de significância de $p < 0,05\%$.

7.7.1.4 Análise residual

Uma análise residual foi realizada para verificar a linearidade. Essa análise permite verificar se o modelo de regressão é verdadeiro, ou seja, se a relação entre as variáveis dos eixos X e Y é linear, por meio da avaliação do erro em cada ponto do modelo; se houver variância constante (homocedasticidade), o modelo linear está correto. A análise pode ser realizada de forma gráfica ou analítica através de testes de hipóteses (F).

7.7.1.5 Precisão

No estudo de precisão, concentrações de 6,25, 50 e 100 µg/mL da piperina (PIP) foram analisadas em triplicata em dois dias distintos e não consecutivos. A média dos resultados obtidos foi avaliada pelo teste t de Student (bilateral, com nível de significância de $p < 0,05$).

7.7.1.6 Exatidão

A exatidão foi avaliada pelo método de recuperação do analito para as concentrações de 6,25; 50 e 100 µg. mL^{-1}, em triplicata em etanol. Este foi adaptado da metodologia de Reyes Solís, Sánchez (56). A piperina foi colocada nas soluções das partículas de MIL-100(Fe), as quais foram centrifugadas em 10.000 rpm por 8 min. O sobrenadante (PIP) extraído da centrifugação foi analisado nas concentrações de 6,25; 50 e 100 µg. mL^{-1}. O coeficiente de variação e a porcentagem de recuperação foram utilizados para avaliar a exatidão, conforme a equação 1:

$$Exatidão\ (\%) = \frac{Concentração\ experimental}{Concentração\ teórica}\ x\ 100$$

Equação 1 : Exatidão

7.7.1.7 Limite de Detecção (LD) e Limite de Quantificação (LQ)

Os valores de limite de detecção (LD) e limite de quantificação (LQ) foram obtidos matematicamente a partir da média das três curvas analíticas. Para calcular os valores de LD (**Equação 2**) e LQ (**Equação 3**), utilizou-se o desvio padrão (DP) do resíduo da linha de regressão e sua relação com a inclinação da curva analítica (IC), também conhecida como coeficiente angular.

$$LD = \frac{DP}{IC} x\ 3{,}3$$

Equação 2: Limite de detecção

$$LQ = \frac{DP}{IC} x\ 10{,}0$$

Equação 3: Limite de quantificação

7.8 Desenvolvimento do método analítico para quantificação de PIP por cromatografia líquida de alta eficiência com detector de arranjos de diodos (CLAE-DAD)

O cromatograma obtido para uma solução etanólica de piperina (100 µg/mL) via método cromatográfico está apresentado na **Figura 4** e mostrou um tempo de retenção igual a 3,03 minutos. A diferença do método adaptado e do método original se baseia nas constituições da fase móvel, sendo que no método proposto por Reyes Solís, Sánchez (56), a fase móvel foi metanol e água deionizada em uma porcentagem de 75:25, apresentando tempo de corrida de 5 min. Desta forma, para o fármaco eludir mais rapidamente, com a mesma fase

móvel (metanol e água 75:25) , fluxo de 0,8 mL.min^{-1} e o tempo de corrida foi de fato menor do que 5 min.

Figura 4. Cromatograma típico da PIP (100 µg/mL) obtido pelo método cromatográfico em solução etanólica.

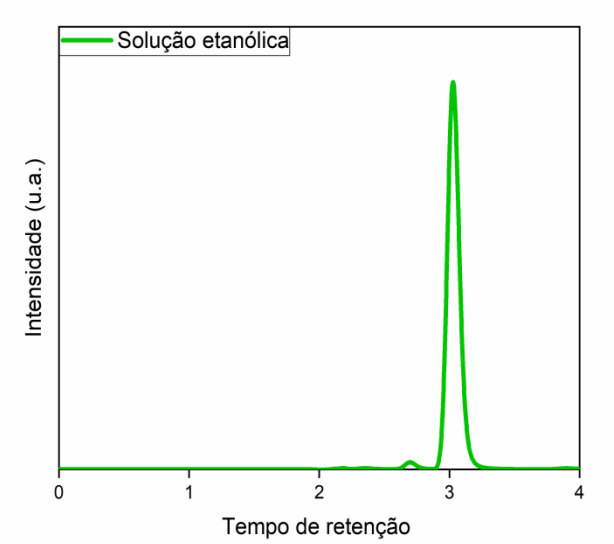

Fonte: Autor

7.8.1 Conformidade do sistema cromatográfico

O número de pratos da coluna ficou abaixo do limite requerido de 2000 e as médias dos valores de assimetria e fator de cauda estão abaixo do valor preconizado de 2. Além disso, verificou-se que os valores da área do pico e tempo de retenção apresentaram precisão, com desvio padrão relativo (DPR) menor que 5%, conforme apresentado na **Tabela 2** (55, 60) . Com base nesses resultados, pode-se afirmar que o método e o equipamento utilizados para as análises são adequados e confiáveis.

Tabela 2. Parâmetros estudados para avaliar a conformidade do sistema cromatográfico empregado para análise da piperina (PIP).

Injeções	TR	Área	Assimetria	Fator de cauda	Número de pratos
1	2,99	7137	1,26	0,97	1892
2	2,99	7140	1,25	0,98	1910
3	2,99	7131	1,27	0,98	1895
4	2,99	7134	1,27	0,96	1883
5	2,99	7148	1,27	0,97	1897
6	2,99	7149	1,27	0,98	1881
Média	**2,99**	**7139,833**	**1,265**	**0,973333**	**1893**
DP	0	7,359801	0,008367	0,008165	10,52616
D.P.R	0	0,103081	0,661391	0,838866	0,556057

TR: tempo de retenção (min); DP: desvio padrão, D.P.R: desvio padrão relativo

Fonte: Autor

7.8.2 Seletividade

Para avaliar a seletividade do MIL-100 (Fe) encapsulado com a PIP em solução etanólica, foi realizada inicialmente a centrifugação para quantificar o sobrenadante (PIP em estudo), o qual foi analisado no cromatógrafo. Os resultados mostraram que o MIL-100(Fe), sem ou com a piperina, não apresentaram picos cromatográficos coincidentes com o tempo de retenção específico do mesmo, como demonstra a **Figura 5**.

Figura 5.- Cromatogramas da PIP (100 µg. mL^{-1}) (verde) e do material PIP@MIL-100(Fe) (preto), em etanol.

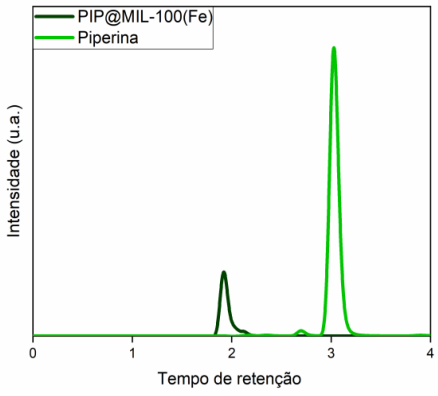

Fonte: Autor

7.8.3 Linearidade

A curva de calibração da piperina (PIP) apresentou uma relação linear dentro da faixa proposta de 6,25 a 100 µg/mL, comprovada pelo coeficiente de regressão linear (r^2 = 0,9932) para o composto analisado. Isso indica um ajuste satisfatório dos dados para a linha de regressão (y = 71,95x - 222,44), conforme apresentado na figura.na **Figura 6**.

Figura 6. Curva padrão da PIP em etanol com intervalo de concentração compreendido entre 6,25-100 µg. mL^{-1} obtido por CLAE.

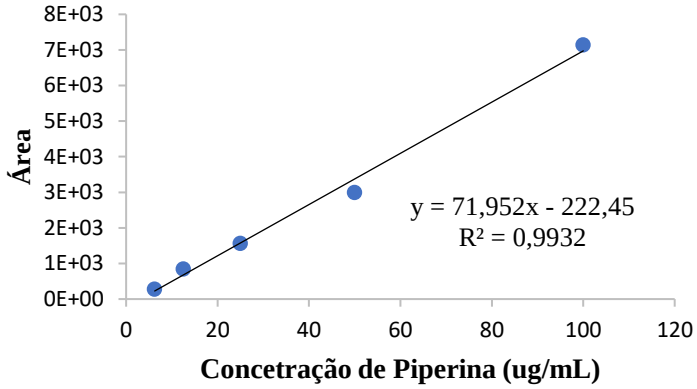

Fonte: Autor

A análise estatística de regressão linear a partir do método dos mínimos quadrados evidenciou em ANOVA uma significância ($F_{calculado} > F_{tabulado}$) e que não há diferença significativa entre as curvas analíticas ($F_{calculado} < F_{tabulado}$) a partir dos dados obtidos no intervalo de 95% de confiança (ver **Tabela 3**).

Tabela 3. Análise de variância dos valores das áreas determinados na obtenção da curva analítica da PIP.

Fontes de variação	Graus de liberdade	Soma Quadrática	Variância	$F_{calculado}$	$F_{tabulado}$
Entre concentrações	4	91049963	22762490	563,894*	3,48
Regressão Linear	1	91021678	91021678	2255,38*	4,96
Desvio da Linearidade	3	28284	9428	0,065	3,71
Dentro (resíduos)	10	3860	386	-	-
Total	14	91053824	-	-	-

* Significativo para p<00.5%

Fonte: Autor

7.8.4 Análise residual

Foi realizada uma análise de homocedasticidade para verificar se a variabilidade do erro é constante em todo o intervalo linear e, portanto, se a previsão da concentração (produto da aplicação da equação de regressão) é válida. A **tabela 4** apresentam os resultados da análise residual realizada. Ao comparar o valor de F calculado com o F crítico, observa-se que há homoscedasticidade.

Tabela 4.- Analise de Variância

	Grados de liberdade	Suma de quadrados	Media dos quadrados	F	Valor crítico de F
Regressão	1	69436,1638	69436,1638	2876,24623	1,21061E-16
Resíduos	13	313,83618	24,1412446		
Total	14	69750			

7.8.5 Precisão

A fim de garantir a confiabilidade das análises do fármaco, é necessário que o método seja preciso, ou seja, que os resultados de uma série de leituras da mesma amostra sejam próximos entre si (61). Os dados apresentados nas **Tabelas 5 e 6** sugerem que o método é preciso, já que a diferença entre os valores de precisão intra-corrida e inter-corrida foi menor que 5%, conforme exigido pela legislação em vigor.

Tabela 5. Precisão intracorrida do método analítico para análise da PIP.

N	**Concentração teórica**	**Concentração real**	**Áreas**
1	100	100,1132	7724
2	100	100,2239	7744
3	100	100,2101	7752
4	100	100,2101	7764
5	100	100,1409	7771
6	100	100,2101	7725
Media	-	106,8629	7746,667
D.P.R%	-	0,25	0,25

Fonte: Autor

Tabela 6. Precisão intermediaria do método analítico para análise da PIP.

N	**Concentração**	**Analista e dia**	**Médias**	**D.P.R %**
6	100	1	7747	4,68
		2	7264	4,55

Fonte: Autor

7.8.6 Exatidão

A exatidão de um método analítico se refere ao grau de concordância entre os resultados obtidos em um mesmo ensaio e um valor de referência considerado verdadeiro (62).A faixa aceitável de variação na concentração do analito é de 80-120% de acordo com a RDC nº 166/2017, mas valores próximos a 100% são preferíveis (61). Os resultados

apresentados na **Tabela 7** estão dentro dos limites recomendados, o que sugere que o método empregado é acurado.

Tabela 7. Exatidão do método analítico para análise da PIP.

Padrão µg/mL	Média	Exatidão (%)	D.P.R %
12,5	5,82071511	93,1	0,07
50	49,00825836	98,0	2,52
200	99,24585928	99,2	1,25

Fonte: Autor

7.8.7 Limite de detecção e Limite de quantificação

A capacidade do método para detectar e quantificar baixas concentrações da piperina foi avaliada através dos valores de LQ e LD, que foram determinados matematicamente a partir da inclinação da curva analítica. Os resultados obtidos mostraram que os valores de LQ e LD foram de 0,774 µg. mL^{-1} e 0,255 µg. mL^{-1}, respectivamente, indicando que o método utilizado é sensível o suficiente para detectar e quantificar baixas concentrações da piperina.

7.8.8 Robustez

Os resultados encontrados na **Tabela 8** indicam que o método analítico proposto é robusto, já que o mesmo permaneceu preciso mesmo diante de pequenas variações na composição e vazão ($mL.min^{-1}$) da fase móvel, evidenciando a estabilidade do método diante dessas mudanças.

Tabela 8. Robustez do método analítico para análise da PIP.

Condições cromatográficas	**Concentração teórica**	**Concentração experimental (µg/mL)**	**Exatidão (%)**
Vazão (mL/min)			
0,7	100	112,56	112,6
0,75	100	104,99	105,0
Fase Móvel			
75%Metanol:25%Água	100	98,41	98,4
76%Metanol:24%Água	100	98,39	98,4
74%Metanol:26%Água	100	98,71	98,7

Fonte: Autor

7.8.9 Avaliação do método de quantificação de PIP liberada por CLAE-DAD

A avaliação da liberação da PIP em PBS, nos pHs 7.4 ou pH 5.0, com Tween 20 (5% v/v) e etanol (5% v/v) foi adaptada pelo método proposto por Reyes Solís, Sánchez (56). O cromatograma mostrou um tempo de retenção de 3,00 e 3,50 min para PIP em pHs 7.4 ou pH 5.0, respectivamente (**Fig. 7**.). A fase móvel foi metanol e água deionizada em uma porcentagem de 75:25 e o tempo de corrida foi menor do que 5 min.

Figura 7. Cromatogramas típicos da PIP em PBS, pH 7,4 (em azul) ou pH 5,0 (em vermelho) com Tween 20 (5% v/v) e etanol (5% v/v) (100 µg/mL) obtidos pelo método cromatográfico.

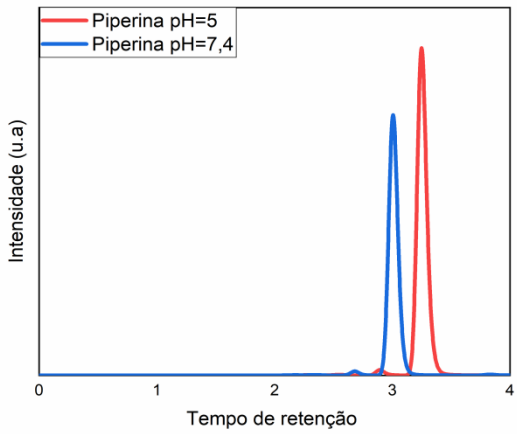

Fonte: Autor

7.8.10 Conformidade do sistema cromatográfico

A quantidade de pratos da coluna excedeu o mínimo necessário de 2000 e as médias dos valores de assimetria e fator de cauda ficaram abaixo do limite de 2. Além disso, como apresentado na **Tabela 9**, a precisão dos valores obtidos para a área do pico e o tempo de retenção foram verificados, com um D.P.R. de menos de 5%, o que mostra que o método e o equipamento utilizados nas análises são adequados. (55, 60). Isso garante a confiabilidade dos resultados em diferentes valores de pH.

7.8.11 Seletividade

Para avaliar a seletividade da liberação da PIP pelo nanomaterial nos dois diferentes valores de pH, foi realizada inicialmente a centrifugação para quantificar o sobrenadante (PIP em estudo), o qual foi analisado no cromatógrafo. Os resultados mostraram que em PBS, pH 7,4 ou pH 5 com Tween 20 (5% v/v) e etanol (5% v/v) sem ou com a PIP não apresentaram picos cromatográficos coincidentes com o tempo de retenção específico da mesma, como demonstra a **Figura 8**.

Figura 8.- Cromatogramas da PIP em PBS, pH 7,4 (azul) ou pH 5,0 (vermelho) com Tween 20 (5% v/v) e etanol (5% v/v) (100 µg. mL^{-1}), e PIP@MIL-100(Fe) (preto).

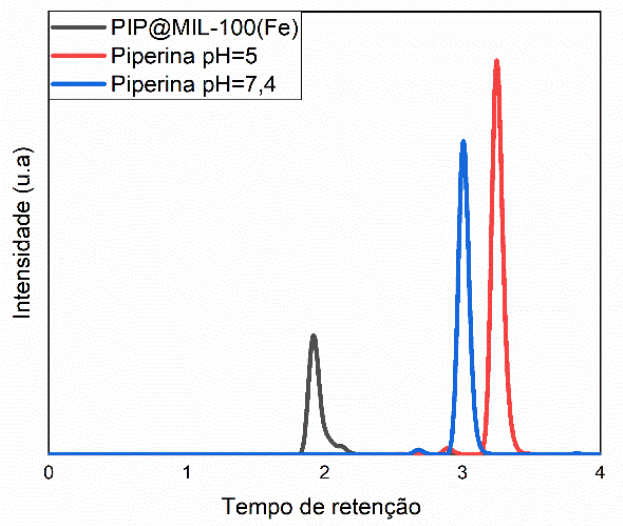

Fonte: Autor

Tabela 9. Parâmetros estudados para avaliar a conformidade do sistema cromatográfico empregado para análise da liberação da PIP em PBS, pH 7,4 ou pH 5,0 com Tween 20 (5% v/v) e etanol (5% v/v).

pH =5,0						**pH=7,4**					
Injeções	TR	Área	Assimetria	Fator de cauda	Números pratos	**Injeções**	TR	Área	Assimetria	Fator de cauda	Números pratos
1	3	8844	1,02	1,13	3615	1	3	7423	1,04	1,13	2974
2	3	8815	1,01	1,12	3623	2	3	7412	1,04	1,12	2989
3	3	8822	1,01	1,14	3626	3	3	7412	1,05	1,1	3035
4	3	8913	1,01	1,12	3652	4	3	6608	1,05	1,1	3070
5	3	8881	1,02	1,14	3664	5	3	6597	1,05	1,1	3091
6	3	8828	1,02	1,14	3681	6	3	6584	1,05	1,1	3010
Média	**3**	**8850,5**	**1,015**	**1,131667**	**3643,5**	Média	**3**	**7006**	**1,046667**	**1,108333**	**3028,167**
DP	0	38,61994	0,005477	0,009832	26,22022	DP	0	448,8496	0,005164	0,013292	45,91913
D.P.R	0	0,436359	0,539628	0,8688	0,719644	D.P.R	0	6,406646	0,493374	1,199242	1,5164

TR: tempo de retenção (min); DP: desvio padrão e D.P.R: desvio padrão relativo

Fonte: Autor

7.8.12 Linearidade

A linearidade da curva de calibração para a liberação da PIP nos diferentes valores de pH foi comprovada no intervalo proposto de 25-200 µg. mL^{-1}, conforme evidenciado pelos coeficientes de regressão linear obtidos para pH=5,0 (r^2 =0,979) e pH=7,4 (r^2 =0,993) para o composto estudado. Os valores obtidos demonstraram um ajuste satisfatório dos dados para a linha de regressão pH:5,0 (y = 81,43x -262,88) e pH:7,4 (y = 71,95x -222,44), como ilustrado na **Figura 9**.

Figura 9. Curvas padrão da PIP em PBS, pH 7,4 ou pH 5,0 com Tween 20 (5% v/v) e etanol (5% v/v) com intervalo de concentração compreendido entre 25-200 µg. mL^{-1} obtido por CLAE.

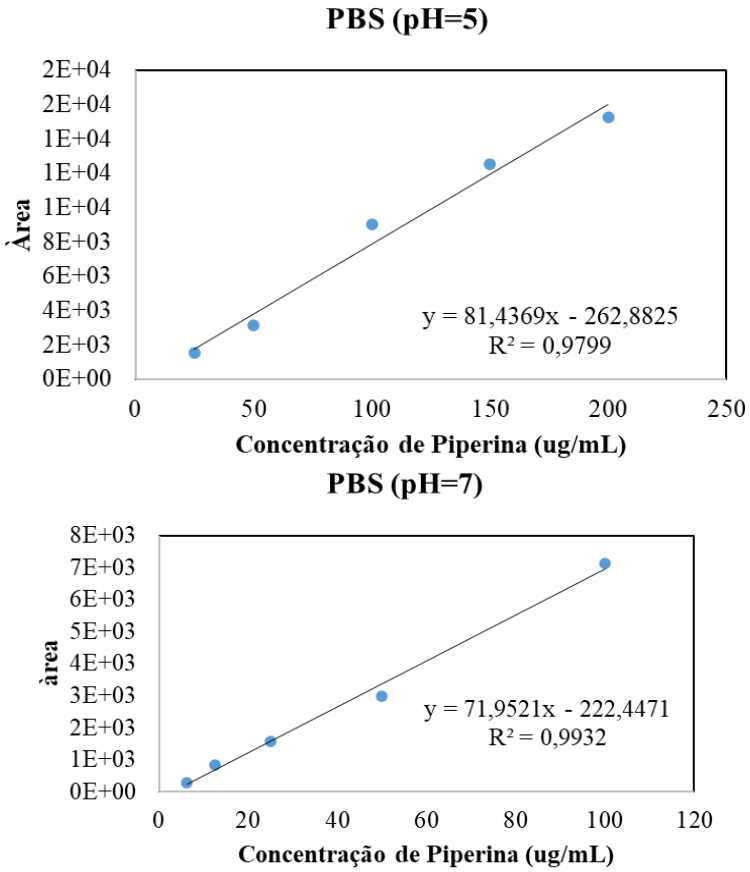

Fonte: Autor

Através da análise estatística de regressão linear utilizando o método dos mínimos quadrados, foi possível evidenciar uma significância estatística na ANOVA ($F_{calculado} > F_{tabulado}$), além de não haver diferença significativa entre as curvas analíticas ($F_{calculado} < F_{tabulado}$), com um intervalo de confiança de 95%, conforme apresentado na **Tabela 10**.

Tabela 10. Análise de variância dos valores das áreas determinados na obtenção da curva analítica da liberação da droga em diferentes valores de pH.

pH=5,0						**pH=7,4**					
Fontes de variação	Graus de liberdade	Soma Quadrática	Variância	$F_{calculado}$	$F_{tabulado}$	Fontes de variação	Graus de liberdade	Soma Quadrática	Variância	$F_{calculado}$	$F_{tabulado}$
Entre concentrações	4	416264889	104066222	404,808*	3,48	Entre concentrações	4	90894675,067	22723668,767	427,873*	3,48
Regressão Linear	1	344825493	344825493	1341,339*	4,96	Regressão Linear	1	90273101,800	90273101,800	1699*	4,96
Desvio da Linearidade	3	71439395	23813131	92,631	3,71	Desvio da Linearidade	3	621573,267	207191,089	3,901	3,71
Dentro (resíduos)	10	2570755	257075	-	-	Dentro (resíduos)	10	531084,223	53108,422	-	-
Total	14	418835644	-	-	-	Total	14	91425759,289	-	-	-

* Significativo para p<00.5%

7.8.13 Análise residual

Foi realizada uma análise de homocedasticidade para a liberação da PIP em pH 5 e pH 7,4. A **tabela 11 e 12** apresentam os resultados da análise residual realizada. Ao comparar o valor de F calculado com o F crítico, observa-se que há homoscedasticidade.

Tabela 11.- Analise de Variância a pH= 5

	Grados de liberdade	Suma de quadrados	Media dos quadrados	F	Valor crítico de F
Regressão	1	344812779	344812779	60,573339	3,0183E-06
Resíduos	13	74002295,3	5692484,25		
Total	14	418815074			

Tabela 12.- Analise de Variância a pH= 7,4

	Grados de liberdade	Suma de quadrados	Media dos quadrados	F	Valor crítico de F
Regressão	1	3,819E+13	3,819E+13	2876,24623	1,2106E-16
Resíduos	13	1,7261E+11	1,3278E+10		
Total	14	3,8363E+13			

7.8.14 Precisão

De acordo com os resultados apresentados nas **Tabelas 13 e 14**, é possível inferir que o método analítico utilizado para a análise de PIP em PBS, pH 7,4 ou pH 5,0 com Tween 20 (5% v/v) e etanol (5% v/v) é preciso. Isso pode ser comprovado pela diferença inferior a 5% entre os valores de precisão intracorrida e precisão intercorrida, o que está de acordo com as normas estabelecidas pela legislação vigente.

T**abela 13.** Precisão intracorrida do método analítico para análise da liberação da PIP em diferentes valores de pH.

	pH=5				**pH=7,4**		
N	Concentração Teórica	Concentração real	Áreas	N	Concentração Teórica	Concentração real	Áreas
1	100	108,3524	8561	1	100	92,73718	6450
2	100	108,3524	8561	2	100	90,80528	6311
3	100	108,512	8574	3	100	90,6524	6300
4	100	108,3401	8560	4	100	89,88798	6245
5	100	108,1928	8548	5	100	90,30493	6275
6	100	108,07	8538	6	100	90,55511	6293
Media	-	108,3033	8557	Media	-	90,82381	6312,333
D.P.R %	-	0,92	0,91	D.P.R %	-	0,92	0,91

Tabela 14. Precisão intermediaria do método analítico para da liberação da PIP em diferentes pHs.

		pH=5,0			**pH=7,4**		
N	Concentração	Analista e dia	Medias	D.P.R %	Analista e dia	Medias	D.P.R %
6	100	1	8557	4,79	1	6312	2,96
		2	8277	2,35	2	6448	1,50

7.8.15 Exatidão

A exatidão do método para a liberação da PIP nos diferentes valores de pH foi comprovada pelos valores obtidos, os quais se encontram dentro dos limites preconizados, como apresentado na **Tabela 15**. Isso evidencia a confiabilidade e precisão do método analítico empregado.

Tabela 15. Exatidão do método analítico para análise da liberação da PIP nos diferentes valores de pH.

pH=5,0				pH=7,4			
Padrão µg/mL	**Média**	**Exatidão (%)**	**D.P.R %**	**Padrão µg/mL**	**Média**	**Exatidão (%)**	**D.P.R %**
25	22,19	88,8	0,28	6,25	7,01	112,2	10,50
100	101,53	101,5	0,28	50	44,69	89,4	17,45
200	190,30	95,2	0,15	100	97,98	98,0	7,65

Fonte: Autor

7.8.16 Limite de detecção e Limite de quantificação

A sensibilidade do método para a liberação da PIP nos diferentes valores de pH foi expressa pela inclinação da curva analítica. Para PBS em pH=5.0, os valores do LQ e LD foram de 18,961 µg. mL^{-1} e 6,257 µg. mL^{-1}, respectivamente, e para PBS em pH=7,4 os valores do LQ e LD foram de 5,410 µg. mL^{-1} e 1,785 µg. mL^{-1}, respectivamente, demonstrando a capacidade do método de detectar e quantificar baixas concentrações de PIP em PBS nos dois valores de pH investigados.

7.8.17 Robustez

Os resultados da **Tabela 16** indicam que o método analítico proposto é robusto diante de variações leves na composição e vazão ($mL.min^{-1}$) da fase móvel, uma vez que o método permaneceu preciso em todas as condições testadas.

Tabela 16. Robustez do método analítico para análise da PIP.

	pH=5,0			pH=7,4	
Condições cromatográficas	**Concentração Teórica (µg/mL)**	**Concentração experimental (µg/mL)**	**Exatidão (%)**	**Concentração experimental (µg/mL)**	**Exatidão (%)**
Vazão (mL/min)					
0,7	100	111,62	112,6	97,98	98,0
0,75	100	112,20	112,2	98,63	98,6
Fase Móvel					
75% Metanol:25% Água	100	107,53	107,5	97,98	98,0
76% Metanol:24 % Água	100	106,00	106,0	91,62	91,6
74% Metanol:26 % Água	100	105,91	105,9	91,51	91,5

Fonte: Autor

8 LICENÇAS DO JORNAL PARA PUBLICAÇÃO

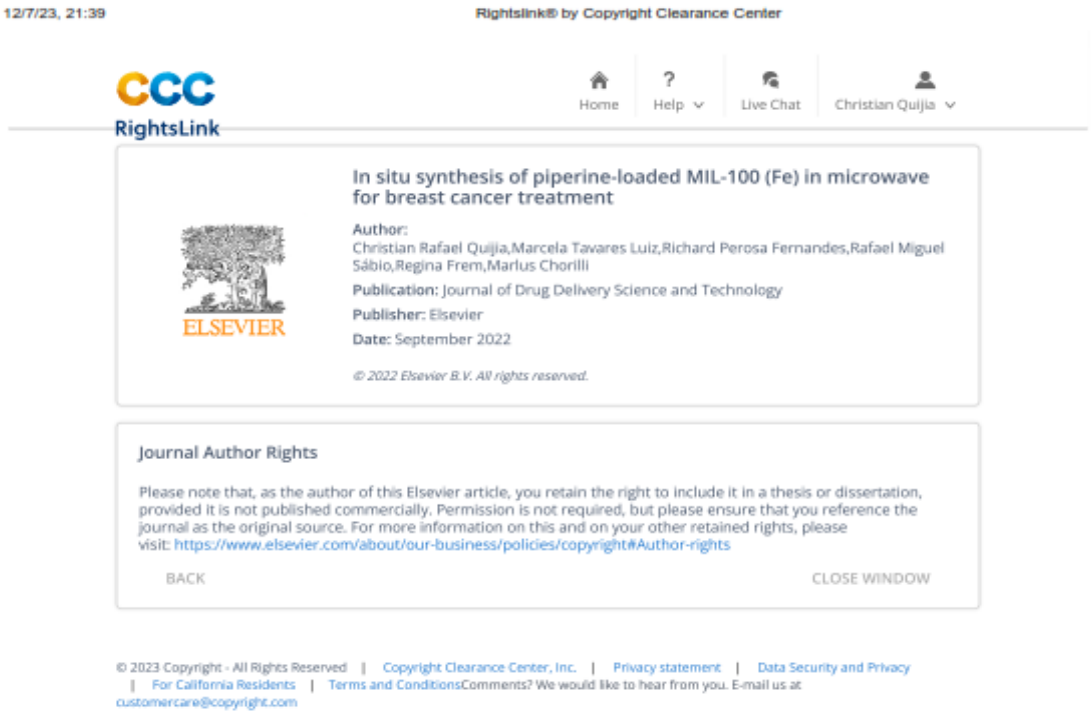

12/7/23, 21:39 Rightslink® by Copyright Clearance Center

CCC RightsLink

Home | Help | Live Chat | Christian Quijia

In situ synthesis of piperine-loaded MIL-100 (Fe) in microwave for breast cancer treatment

Author:
Christian Rafael Quijia,Marcela Tavares Luiz,Richard Perosa Fernandes,Rafael Miguel Sábio,Regina Frem,Marlus Chorilli

Publication: Journal of Drug Delivery Science and Technology

Publisher: Elsevier

Date: September 2022

© 2022 Elsevier B.V. All rights reserved.

Journal Author Rights

Please note that, as the author of this Elsevier article, you retain the right to include it in a thesis or dissertation, provided it is not published commercially. Permission is not required, but please ensure that you reference the journal as the original source. For more information on this and on your other retained rights, please visit: https://www.elsevier.com/about/our-business/policies/copyright#Author-rights

BACK CLOSE WINDOW

© 2023 Copyright - All Rights Reserved | Copyright Clearance Center, Inc. | Privacy statement | Data Security and Privacy | For California Residents | Terms and ConditionsComments? We would like to hear from you. E-mail us at customercare@copyright.com

https://s100.copyright.com/AppDispatchServlet 1/1

Terms of Use

§ 1
These Terms of Use govern the use of the MDPI websites or any other MDPI online services you access. This includes any updates or releases thereof. By using our online services, you are legally bound by and hereby consent to our Terms of Use and Privacy Policy. These Terms of Use form a contract between MDPI AG, registered at St. Alban-Anlage 66, 4052 Basel, Switzerland ("MDPI") and you as the user ("User"). These Terms of Use shall be governed by and construed in accordance with Swiss law, applicable at the place of jurisdiction of MDPI in Basel, Switzerland.

§ 2
Unless otherwise stated, the website and affiliated online services are the property of MDPI and the copyright of the website belongs to MDPI or its licensors. You may not copy, hack or modify the website or online services, or falsely claim that some other site is associated with MDPI. You agree not to use the website in any manner that violates any applicable laws, these Terms of Use or infringes the intellectual property of, or interferes with any other rights of, MDPI and third parties. Any use of this website in violation of these principles may give rise to civil claims, a claim for damages and/or result in criminal proceedings being taken against you. MDPI is a registered brand protected by the Swiss Federal Institute of Intellectual Property.

§ 3
Unless otherwise stated, articles published on the MDPI websites are labeled as "Open Access" and licensed by the respective authors in accordance with the Creative Commons Attribution (CC-BY) license. Within the limitations mentioned in §4 of these Terms of Use, the "Open Access" license allows for unlimited distribution and reuse as long as appropriate credit is given to the original source and any changes made compared to the original are indicated.

§ 4
Some articles published on this website (especially articles labeled as "Review" or similar) may make use of copyrighted material for which the author(s) have obtained a reprint permission from the copyright holder. Usually such reprint permissions do not allow author(s) and/or MDPI to further license the copyrighted material. The licensing described in §3 of these terms and conditions are therefore not applicable to such kind of material enclosed within articles. It is the user's responsibility to identify reusability of material provided on this website, for which he may take direct contact with the authors of the article.

§ 5
You may register or otherwise create a user account, user name or password (your "Registration") that allows you to access or receive certain content and/or to participate or utilize certain features of our online service, including features in which you interact with us or other users. You represent and warrant that the information provided in your registration is accurate to the best of your knowledge. You are responsible for the use of any password you create as part of your registration and for maintaining its confidentiality, and you agree that MDPI may use this password to identify you. We reserve the right to deny, terminate or restrict your access to any content or feature reached via such registration process for any reason, at our sole discretion. MDPI reserves the right to block or to terminate the user's access to the website at any time and without prior notice.

§ 6
The MDPI website and online services may provide links to other websites or external resources. As part of these Terms of Use, you acknowledge that MDPI is not responsible for the availability of such external sites or resources, and that MDPI is not liable for any content, services, advertising, or materials available from such external sites or resources.

§ 7
The website may contain advertising. MDPI does not endorse any responsibility of any kind for the content of the advertisement or sponsorship or the advertised product or service, which is the responsibility of the advertiser or sponsor, unless the advertised product or service is offered by MDPI.

§ 8
There is no warranty for the website and its content, to the extent permitted by applicable law. MDPI, the copyright holders and/or other parties provide the website and its content "as is" without representations or warranties of any kind, either expressed or implied, including, but not limited to, the implied warranties of merchantability, satisfactory quality and fitness for a particular purpose relating to this website, its content or any to which it is linked. No representations or warranties are given as to the accuracy or completeness of the information provided on this website, or any website to which it is linked. The content available on this website is for information purposes only. It does not constitute advice or a binding offer. Any liability for possible damages resulting from the use of the website or information available on it is excluded.

§ 9
In no event, unless required by applicable law shall MDPI, its employees, agents, suppliers, contractors or any other party, be liable to the user for any damages of any nature, including any general, special, incidental or consequential damages, loss, cost, claim or any expense of any kind arising out of the use, inability to access, or in connection with the use of the website, its content and information, even if the user has been advised of the possibility of such damages.

§ 10
MDPI reserves the right to change these Terms of Use at any time by posting changes to this page of the website without prior notice. Please check these Terms of Use periodically for any modifications. Your continued use of any Service following the posting of any changes will mean that you have accepted and agreed to the changes.

MDPI expressly reserves the right to amend, supplement, delete or temporarily or definitively cease publication of parts of the website or the entire website without prior notice.

§ 11
Basel, Switzerland shall be the place of jurisdiction for all legal disputes arising of these Terms of Use, even if the Customer has her/his domicile outside of Switzerland.

§ 12
Swiss law applicable at the place of jurisdiction of MDPI shall apply exclusively.

§ 13
If any provisions of the Terms of Use should be found invalid, this shall not affect the validity of the remaining provisions. In any such case, the contracting parties shall negotiate on the invalid clause to substitute by a valid arrangement as close as possible to the original provision

These Terms of Use were last updated on 15 March 2023

MDPI AG, St. Alban-Anlage 66, CH-4052 Basel, Switzerland